The Selective Production of Biomass Derived Chemicals using Heterogeneous Catalysts

by

Ricardo Alamillo Jr.

A dissertation submitted in partial fulfillment of the requirements for the degree of

Doctor of Philosophy

(Chemical Engineering)

at the UNIVERSITY OF WISCONSIN-MADISON 2016

Date of Final Oral Examination: January 4, 2016

The dissertation is approved by the following members of the Final Oral Committee:

James A. Dumesic, Professor, Chemical and Biological Engineering

George Huber, Professor, Chemical and Biological Engineering

Christos Maravelias, Professor, Chemical and Biological Engineering

Sean Palecek, Professor, Chemical and Biological Engineering

Troy Runge, Assistant Professor, Biological Systems Engineering

Ricardo Alamillo Jr.

Under the supervision of Professor James A. Dumesic at the University of Wisconsin-Madison

The development of heterogeneous catalytic technologies for the efficient and selective conversion of lignocellulosic biomass to platform molecules such as 5-hydroxymethylfurfural (HMF) and 2,5-dihydroxymethylfurfural (DHMTHF) has been studied. Supported metal catalysts were used for the selective hydrogenation of HMF to DHMTHF. Small trace amounts of acid in the aqueous solution with HMF feed was found to play an important role in determining the selectivity for the hydrogenation of HMF to DHMTHF. The acid was able to be neutralized by treating HMF feeds with an ion-exchange resin or using ruthenium deposited on a support with a high isoelectric point (e.g. ceria or magnesia-zirconia) to achieve high DHMTHF yields.

DHMTHF, tetrahydrofuran (THF), gamma valerolactone (GVL), and other aprotic miscible organic solvents were mixed with water to form a monophasic co-solvent. These co-solvents systems were found to be separation friendly solvents compared to dimethyl sulfoxide (DMSO) and other higher boiling organic solvents that are selective for HMF production. The monophasic co-solvents investigated were also selective for the production of HMF from fructose using Brønsted acid catalysts; additionally, an increase in the rate of reaction, compared to water, was observed. Using isotopically labeled fructose and ¹³C NMR, the fructose tautomer distribution in water and various co-solvents were quantified. Fructose tautomerization favors the furanose form in the mixed solvent, relative to water alone, explaining at least part of the rate enhancement.

The HMF selectivity depends on both the fructose conversion and the amount of DHMTHF present. With high levels of the co-solvent in water (e.g., ratios of 3:1 and 9:1), the HMF selectivity increases with fructose conversion.

The use of co-solvents and acid-functionalized ordered mesoporous silica catalysts show high selectivity for HMF from fructose. The synthesis to intercalate PVP on the catalyst surface was developed to achieve high selectivities previously achieved only with ionic liquids. The high concentration of pyrrolidone in the confined space of the pores favors the furanose tautomers which can be easily dehydrated to HMF. The solid acid catalyst is both easily recovered from the reaction mixture, and the product is readily isolated from the low-boiling, mono-phasic co-solvent system. Thus, the reaction environment within the catalyst has been designed to favor the desired product. Acid-functionalized ordered mesoporous carbons and supported bimetallics were also investigated for the continuous production of HMF from fructose.

Solvent reactivity studies for homogenous base, homogenous Lewis acid, solid bases, and solid Lewis acids for glucose isomerization to fructose were conducted. The small addition of miscible organic solvent led to a drop of reactivity compared to that of pure water. However, with increasing GVL concentration, the reactivity increased as well. Benzene-bridged PMOs doped with Lewis acidic Sn sites were readily and rapidly synthesized. These thermally robust, hydrophobic materials catalyze the selective isomerization of glucose to fructose in co-solvent systems. Brønsted acid sites were incorporated and a bifunctional PMO was synthesized for tandem conversion of glucose to fructose and its dehydration to HMF.

Acknowledgements

To begin, I would like to thank my advisor, Dr. James A. Dumesic, for his patience, guidance, humor, and knowledge and dedication to science and research. Working with him has been invaluable towards my development as a researcher and as a professional.

I am also thankful to have known the members of the Dumesic group and the catalysis community at the University of Wisconsin-Madison. I would especially like to thank Dr. Mark Tucker, Dr. Jean Marcel Gallo, and Dr. Mei Chia for their friendship, and advice in my projects and collaborations. I also would like to thank Yomaira, Sikander, Gretchen, Elif, Dong (Eric), Brandon, Jesse, Stephanie, David, Ronald, Tom, Max, Insoo, M, Zach, Janan, Ana, Duygu, Ali, Yifei, Maddie and Siddarth, - I appreciate your invaluable discussions, help, and friendship. I am grateful to have worked with this group of intelligent and dedicated individuals.

I also owe a debt of gratitude to collaborators and investigators from other institutions. I would like to acknowledge Dr. Susannah L. Scott at the University of California, Santa Barbara for a fruitful collaboration. In particular, I am honored to have worked with Dr. Anthony Crisci who has been more than just a collaborator, but a great teacher, mentor, and friend. I am thankful to have worked with Dr. Long Qi and appreciate his patience, dedication, and great discussions. I would also like to thank Dr. Bethany Wigington for her friendship and advice, as well as the Center for Enabling New Technologies (CENTC) and my collagenous there for their support.

I am in debt for Judy Lewison for taking care of administrative issues in the group, listening to the woes of a graduate student, and for allowing us to be her guinea pigs for her own sugar experiments. I would also like to thank my friends in the Chemical Engineering department and those I have made in Madison, especially Jaron Acker, David Coppini, and Ramona Lowery. The summer sails, bike rides through town, nights in the city, and constant encouragement are

memories I will forever cherish. My friends would really be surprised if I did not thank Beyoncé; her music has kept me moving through those longs days in the lab, as well as being a uniting force within my friends, and her amazing live shows that I shared with friend, all nights that I will treasure in my heart.

I am grateful for my family for their unconditional love, inspiring thoughts and immeasurable support. Their dedication and perseverance in life are a constant source of inspiration, hope, and thanksgiving. My father, who worked tirelessly in the construction industry to provide everything for us unselfishly, my mother who has a homemaker and entrepreneur who ensured we would be prepared for life, my brother and sisters who have worked hard for their own goals, and my two nephews who inspire me to be better and take nothing in life for granted. I would like to thank my grandparents who could not all be here to see this important step in my life, you are my heroes and in my heart forever. I would like to thank my extended family – my aunts, uncles, cousins, and a great network of family and friends who have kept me in their thoughts throughout the years.

To My Family

Para mi familia

Table of Contents

Abstract		i
Acknowledge	ements	iii
Dedication		v
Table of Con	tents	vi
List of Figure	es	xi
List of Tables	s	xviii
Chapter 1	Introduction	1
1.1	Fuels and Chemicals	1
	1.1.1 U.S. Energy Consumption and Chemical Consumption	1
	1.1.2 Outlook on Energy and Fossil Fuels	4
1.2	Biomass as a Renewable Source of Carbon	6
	1.2.1 Biomass as a Source of Fuels and Chemicals	6
1.3	Catalytic Strategies for the Production of Chemicals from Biomass	9
	1.3.1 5-Hydroxymethylfurfural as a Platform Chemical	10
	1.3.2 Production of 5-Hydroxymethylfurfural from Sugars	11
1.4	Solid Acid Catalysts for Biomass Conversion	16
	1.4.1 Synthesis of Novel Acid Catalysts	17
	1.4.2 Catalysts for the Continuous Production of HMF	18
1.5	Phase and Surface Modifiers	20
	1.5.1 Polyvinylpyrrolidone (PVP) as a Catalyst-Surface Modifier	21
	1.5.2 PVP Interactions with Silica Surfaces	22
	1.5.3 Crosslinking of PVP	23

		1.5.4 Current Surface Modifications for Catalytic Applications	24
1.6	Resea	arch Direction	25
1.7	Refer	rences	26
Chap	oter 2	Experimental	29
	2.1	Catalyst Synthesis and Preparation	29
	2.2	Catalyst Characterization	33
	2.3	Reaction Studies	36
		2.3.1 Batch Reaction Studies	36
		2.3.2 Flow Reaction Studies	38
	2.4	Sample Analysis	41
	2.5	Synthesis of DHMTHF for use as a solvent and standard	42
	2.5	References	43
Chap	oter 3	Selective hydrogenation of HMF	44
	3.1	Introduction	44
	3.2	Selective Hydrogenation of HMF to DHMTHF	45
		3.2.1 Support Effects with Ruthenium Catalysts	45
		3.2.2 Effect of Support and Solution Phase Acidity	49
		3.2.3 Solvent Effects on HMF Hydrogenation	53
		3.2.4 Effect of Metal Catalyst	55
	3.3	Conclusions	57
	3.4	References	58

vii

Chapter 4	Biomass-derived Solvent Systems for use in Fructose Dehydration	59
4.1	Introduction	59
4.2	Results and Discussion	61
	4.2.1 The use of DHMTHF as a Co-solvent for Monophasic Fructose	61
	Dehydration	
	4.2.2 Fructose Dehydration with other Co-solvents	66
	4.2.3 Solvent effects on D-Fructose Tautomer Distribution	69
4.3	Conclusions	72
4.6	References	73
Chapter 5	Inorganic-Organic Catalysts for Selective HMF Production	75
5.1	Introduction	75
	5.1.1 Organosilicas for Biomass Conversions	75
	5.1.2 Intercalation of Polyvinyl Pyrrolidone	76
5.2	The use of PVP as a Surface Modifier for Selective Production of HMF	77
	5.2.1 PVP Modified Silicycle	77
	5.2.2 PVP-Catalyst Characterization	78
	5.2.3 PVP-Catalyst Reactivity Studies	83
	5.2.4 Catalyst-Surface Localization and Functionality Effects	84
	5.2.5 Catalyst-Surface Effects on Fructose Tautomer Distributions	85
	5.2.6 Catalyst-Surface Effects on Catalyst Stability	86
5.3	Acid Functionilized Mesoporous Carbon for the Continuous Production	90
	of HMF	

		5.3.1	Introduction	90
		5.3.2	Catalyst Characterization Studies	91
		5.3.3	Catalyst Reaction Kinetic Studies	93
		5.3.4	Catalyst Deactivation Studies	95
	5.4	Rh-Re	e Bimetallics for Fructose Dehydration	97
		5.4.1	Introduction	97
		5.4.2	Catalyst Reactivity Studies for Fructose Dehydration	98
	5.5	Conclu	usions	102
	5.6	Refere	ences	103
Chap	ter 6		Design of Catalytic Systems for the Selective Isomerization acose to Fructose	105
	6.1	Introd	uction	105
	6.2		genous Base-catalyzed Glucose Isomerization	105
	6.2	Homo	genous Base-catalyzed Glucose Isomerization genous Lewis Acid-catalyzed Glucose Isomerization	105 109
		Homo	•	
		Homo	genous Lewis Acid-catalyzed Glucose Isomerization	109
		Homo, 6.3.1 6.3.2	genous Lewis Acid-catalyzed Glucose Isomerization Cellobiose Hydrolysis by a Brønsted Acid	109 110
	6.3	Homo, 6.3.1 6.3.2	genous Lewis Acid-catalyzed Glucose Isomerization Cellobiose Hydrolysis by a Brønsted Acid Solvent Studies using Homogenous Lewis Acids	109 110 111
	6.3	Homo, 6.3.1 6.3.2 Solid I	genous Lewis Acid-catalyzed Glucose Isomerization Cellobiose Hydrolysis by a Brønsted Acid Solvent Studies using Homogenous Lewis Acids Base-Catalyzed Reactions	109 110 111 113
	6.3	Homo, 6.3.1 6.3.2 Solid I	genous Lewis Acid-catalyzed Glucose Isomerization Cellobiose Hydrolysis by a Brønsted Acid Solvent Studies using Homogenous Lewis Acids Base-Catalyzed Reactions Adsorption on FAU Zeolites	109 110 111 113 114

Sn- substituted Periodic Ordered Mesoporous Materials for

6.5

ix

130

	Tandem Glucose Isomerization and Fructose Dehydration	
	6.5.1 Synthesis and structural characterization of	133
	Sn-containing Periodic Mesoporous Organosilicas (Sn-PMOs)	
	6.5.2 Reactivity Studies using Sn-PMO Materials	140
	6.53 Tandem Glucose Isomerization and Fructose Dehydration	146
6.6	Conclusions	148
6.7	References	149
Chapter 7	Summary of Conclusions and Future Directions	151
Chapter 7 7.1	Summary of Conclusions and Future Directions Conclusions	151 151
•	·	
7.1	Conclusions	151
7.1	Conclusions Future Directions	151 155
7.1	Conclusions Future Directions 7.2.1. Increasing Catalyst Stability 7.2.2 Optimizing Tandem Glucose Isomerization	151 155 155

List of Figures

Figure 1.1.	Global energy consumption by resource in 2010.	1
Figure 1.2.	US renewable energy consumption by type	2
Figure 1.3.	Primary Energy Consumption in the US by source and sector. Numbers are in units of quadrillion Btu	3
Figure 1.4.	Prduction of fuels and chemicals from crude oil.	4
Figure 1.5.	Projected Worl Energy Consumption in Tons of Oil equivalent	5
Figure 1.6.	Structural composition of the principal components in lignocellulosic biomass	7
Figure 1.7.	Lignocellulosic biomass conversion strategies	9
Figure 1.8.	HMF and its respective derivatives	10
Figure 1.9.	Fructose conversion, selectivity to HMF, and reaction time for various material in a batch reaction	15
Figure 1.10.	Active acid site for commercial catalysts	16
Figure 1.11.	Strategies for grafting organic groups R onto mesoporous silica using grafting (A) and co-condensation (B)	18
Figure 1.12.	Polyvinylpyrrolidone (PVP)	21
Figure 2.1.	Schematic for the incipient wetness impregnation of a metal salt aqueous solution on a support	29
Figure 2.2.	Preparation route for acid mesoporous carbons	31
Figure 2.3.	(A) Thick-walled glass reactor with triangular magnetic stir bar used in batch dehydration and isomerization experiments (B) Stirrer hotplate with silicon oil bath used for dehydration experiments.	38
Figure 2.4.	Detailed schematic of the up-flow reactor setup used for reaction kinetic experiments	40
Figure 2.7.	Detailed schematic of the up-flow reactor setup used for reaction kinetic experiments.	42

Figure 3.1.	Formation of DHMTHF (triangle), DHMF (square) and polyols (diamond) as a function of reaction time for the hydrogenation of HMF using 1 wt% Ru/CeOx	46
Figure 3.2.	Selectivity to DHMF(black), DHMTHF(white), polyols(grey) and unidentified products (striped) as a function of reaction time for the hydrogenation of HMF over Ru/CeO _x	46
Figure 3.3.	Hydrogenation of HMF to DHMTHF with DHMF as an intermediate and the proposed mechanism for the formation of 1,2,6-hexanetriol, 1,2,5,6-hexaneterrol, and 1,2,5-hexanetriol. Mechanism based on Horvat, et. al	47
Figure 3.4.	Selectivity to DHMTHF(white), polyols (grey), and unidentified products (striped) in the hydrogenation of HMF over Ru-black and 1 wt% Ru/Vulcan without and with feed pretreatment with Amberlite IRA-400(OH).	50
Figure 3.5.	HMF hydrogenation to DHMTHF (white), polyols (grey), and unidentified products (striped) using 50 mg of Ru-black as a catalyst and 500 mg of high-isoelectric point solids.	51
Figure 3.6.	Product selectivities for the hydrogenation of HMF to DHMTHF (white), polyols (grey) and unidentified (striped) over Ru-black (50 mg) in the presence of added acids. Feed was treated with 1.5g Amberlite IRA-400(OH) prior to acid addition.	52
Figure 3.7.	HMF hydrogenation in different solvents using 50 mg Ru-black as a catalyst. Products include DHMTHF(white), 1,2,6-HT (dark grey), 1,2,5-HT (light grey), 1,2,5,6-HT (black), and unidentified products (downward vertical stripes).	54
Figure 3.8.	HMF Hydrogenation over Vulcan supported Ru, Pd, or Pt at various time points. Feed was purified with 1.5 g Amberlite IRA-400(OH) before reaction. Products observed DHMF (black), DHMTHF(white), polyols (grey), and unidentified products (striped).	56
Figure 4.1.	HMF selectivity as a function of fructose conversion in mono-phasic dehydration experiments with Amberlyst® 70 as the catalyst in a mixed solvent consisting of DHMTHF:water in molar ratios of 0:1 (triangles), 1:1 (diamonds), 3:1 (squares), and 9:1 (circles).	62

Figure 4.2.	Solvent effects on the time-dependent yield of HMF by dehydration of fructose using an Amberlyst® 70 catalyst in DHMTHF:water ratios with molar ratios of: 0:1 (triangles), 1:1 (diamonds), 3:1 (squares), and 9:1 (circles).	64
Figure 4.3.	Structures of the various fructose tautomers in solution.	65
Figure 4.4.	Comparison of HMF selectivity as a function of fructose conversion for over an Amberlyst® 70 catalyst in mixed solvents consisting of 9:1 DMSO:water (triangles), 4:1 THF:water (diamonds), 9:1 ethanol:water (squares), and 9:1 THFA:water (circles).	67
Figure 4.5.	Comparison of HMF selectivity as a function of fructose conversion over an Amberlyst® 70 catalyst in 9:1 THFA:water for fructose feeds at 2 wt% (squares) and 10 wt% (diamonds).	68
Figure 4.6.	Tautomer distributions for D-fructose in various solvents at 303 K; and 333 K. Values for the α and β forms of the pyranose (blue) and furanose (red) tautomers have been combined. Keto is shown in black.	70
Figure 5.1.	Solid-state NMR spectra: (a) 13 C CP/MAS; and (b) 29 Si MAS NMR. for PVP-pSO ₃ H-SBA-15.	79
Figure 5.2.	SEM Images of the PVP-pSO ₃ H-SBA-15 catalyst, at two different magnifications.	81
Figure 5.3.	XRD reflection patterns for pSO $_3$ H-SBA-15 prior to (blue) and after (red) the intercalation of PVP.	81
Figure 5.4.	STEM images of (a) pSO ₃ H-SBA-15, (b) PVP-pSO ₃ H-SBA-15 at two different magnifications. Pore channels are visible for pSO ₃ H-SBA-15. However, the density increases and the contrast decreases when these channels are filled with polymer in PVP-pSO ₃ H-SBA-15. Consequently, the pore channels are no longer vis	82
Figure 5.5.	The effect of PVP intercalated (red) versus that in free solution (blue) for various ratios of PVP to catalyst ratios on the selectivity to HMF at 50% fructose conversion.	84

			xiv
Figure 5.6.	Thermogravimetric analysis of PVP-SBA-15 prior to (blue squares) and after (red diamonds) Soxhlet extraction of soluble PVP with ethanol. Post-extraction, PVP-SBA-15 was subjected to simulated reaction conditions by treatment in 4:1 THF-H ₂ O at 403 K for 30 min. The solid was recycled (recovered, washed with ethanol and dried) and again subjected to simulated reaction conditions. A portion of the solid from each cycle was examined by TGA: cycle 1 – orange triangles, and cycle 2 – green circles.	87	
Figure 5.7.	Effect of pSO ₃ H-SS (red) and PVP-pSO ₃ H-SS (blue) catalyst recycle on HMF production rate at 403 K in 4:1 THF:H ₂ O (w:w). After each reaction, the catalyst was recovered, washed, dried and reused.	87	
Figure 5.8.	Effect of catalyst recycle on fructose conversion and HMF selectivity at 403 K in 4:1 THF:H ₂ O (w:w). After each batch reaction, the catalysts were recovered, washed, dried and reused.	88	
Figure 5.9.	Determination of the first-order deactivation rate coefficient for the (a) PVP-pSO ₃ H-SBA-15 and (b) PVP-pSO ₃ H-SS catalysts.	89	
Figure 5.10.	Comparison of the first-order deactivation rate coefficient for the (a) PVP-pSO ₃ H-SBA-15 and (b) PVP-pSO ₃ H-SS catalysts.	90	
Figure 5.11.	X-ray diffractograms for (a) CMK-3-PSA, (B) CMK-3-NSA, (C) CMK-3-SA, (d) CMK-5-PSA. Arrows indicate peaks assigned to (110) and (200) planes.	92	
Figure 5.12.	Conversion (white bars) and selectivity (black bars) for the CMK-3 and CMK-5 based catalysts, pSO ₃ H-SBA-15, and SAC-13.	94	
Figure 5.13.	Natural logarithm of the HMF production TOF as a function of the time on stream. (open purple circles) CMK-3-PSA, (full red circles) CMK-3-NSA, (open green squares) CMK-3-SA, (full blue triangles) CMK-5-PSA, (full black squares) SBA-15-pSO ₃ H, and (full orange stars) Nafion SAC-13.	96	
Figure 5.14.	Conversion of fructose (×), selectivity to 5-hydroxymethylfurfural (•), and specific formation rate of HMF (■) as a function of time on stream over RhRe/C catalyst pretreated at 523 K. Reaction conditions: 300 psi He 403 K, 2 wt% fructose in THF/water (mass ratio of THF: water = 4:1) as feed, WHSV =0.1h ⁻¹ .	99 e,	

		X	V
Figure 5.15.	Fructose dehydration in a continuous flow reaction system over RhRe/C catalyst pretreated at different reduction temperatures of 523 K (■ and 723 K (×). Reaction conditions: 300 psi He, 403 K, 2 wt% fructose in THF/water (mass ratio of THF: water = 4:1) as feed, WHSV =0.1h ⁻¹ .	100	
Figure 5.16.	Conversion of fructose (×), selectivity to HMF (•), and specific formation rate of HMF (\blacksquare) as a function of time on stream over ZSM-5. Reaction conditions: 300 psi He, 403 K, 2 wt% fructose in THF/water (mass ratio of THF: water = 4:1) as feed, WHSV =1.4 h ⁻¹ .	101	
Figure 5.17.	Specific formation rates of HMF over RhRe/C pretreated at 523 K (×) and ZSM-5 (■). Reaction conditions: 300 psi He, 403 K, 2 wt% fructose in THF/water (mass ratio of THF: water = 4:1) as feed.	102	
Figure 6.1.	Glucose isomerization in water. Reactions were carried out at 403 K using 1.5 mL solutions of 2 wt% glucose and 5 mM NaOH.	107	
Figure 6.2.	Cellobiose hydrolysis at varied acid concentrations in water (circles) and 2:1 (w:w) THF:water (triangles). Reactions were carried out at 403 K using 1.5 mL solutions of 2 wt% glucose and varied HCl and AlCl ₃ concentrations.	111	
Figure 6.3.	Glucose isomerization at varied THF concentrations. Reactions were carried out at 403 K using 1.5 mL solutions of 2 wt% glucose and 2 mM AlCl ₃ . Initial glucose consumption TOF (circle) and initial fructose product TOF (triangle)	112	
Figure 6.4.	Initial rate of HMF formation for fructose dehydration reactions at varied THF concentrations using 2 mM AlCl3 (triangle) and 2 mM HCl (circle). Reactions were carried out at 403 K using 1.5 mL solutions of 2 wt% fructose and respective acid.	112	
Figure 6.5.	Change in liquid phase concentration of glucose (C), upon combining 1.0 mL of a 0.100 mol L ⁻¹ solution of glucose in a GVL/water mixture with various zeolites (200 mg), as measured by quantitative solution-state ¹ H NMR. Each result is the average of three independent experiments; error bars show the standard deviation.	115	
Figure 6.6.	Direct polarization solid-state MAS ¹³ C NMR spectra of NaX slurry with 0.10 mol/L 1- ¹³ C glucose in GVL:water (46:54 mol:mol), recorded <i>in situ</i> at 25 °C and 90 °C. A long relaxation delay (30 s) was used to ensure quantitative analyses in both cases.	117	

Figure 6.7.	Ratio of α-Glc <i>p</i> :β-Glc <i>p</i> adsorbed in zeolite and in the bulk solution at 25 °C and 130 °C. NaX zeolite with 1 mL 1- ¹³ C-glucose solution (0.1 mol L ⁻¹) in GVL:water mixture (46:54 by mole). (A) containing 6.1 wt% silica, and a more crystalline structure (B) containing 2.3 wt% silica.	118
Figure 6.8.	(A) Conversion of 1- ¹³ C-glucose catalyzed by NaX in GVL-H ₂ O (46:54 mol:mol) in a high T/P solid-state NMR rotor, recorded at 130 °C (total of 20 h) and spin rate 5 kHz. (B) Variable temperature kinetic profiles for glucose conversion to fructose. The inset shows an Arrhenius plot, from which the activation energy was estimated.	119
Figure 6.9.	Ratio of mobile and adsorbed β -Glc p during the conversion of 1- 13 C-glucose to 1- 13 C-fructose by NaX in a GVL-H ₂ O mixture (46:54 by mole) in a high T/P solid-state NMR rotor, recorded at 130 °C (total of 20 h) and spin rate 5 kHz.	120
Figure 6.10	Ratio of combined α -Glc p : β -Glc during the conversion of 1- 13 C-glucose to 1- 13 C-fructose by NaX in a GVL-H ₂ O mixture (46:54 by mole) in a high T/P solid-state NMR rotor, recorded at 130 °C (total of 20 h) and spin rate 5 kHz.	121
Figure 6.11	Conversion of 1^{-13} C-fructose by NaX in a GVL-H ₂ O mixture (46:54 by mole) in a high T/P solid-state NMR rotor, recorded at 130 °C (total of 20 h) and spin rate 5 kHz.	121
Figure 6.12	Fructose production TOF for glucose isomerization flow studies using NaX (A) and NaY (B) using H ₂ O (circle), 1:4.5 (v:v) GVL: H ₂ O (triangle), and 4.5:1 (v:v) GVL: H ₂ O. Reactions were carried out using 100 mg of NaX or NaY zeolite at 403 K using a feed of 2 wt% glucose flowed in at 0.04 mL min ⁻¹ .	124
Figure 6.13	Initial fructose production TOF for glucose isomerization flow studies using NaX using varying GVL: H_2O ratios. Reactions were carried out using 100 mg of NaX at 130 °C using a feed of 0.1 mol L^{-1} glucose flowed in at 0.04 mL min ⁻¹ .	125
Figure 6.14	Fructose Production Rate flowing in 0.04 mL/min 0.1 M glucose in 46 mol% GVL at 130°C in packed reactor with 100 mg of NaX. Triangles represent Run 1 and Circles Run 2 after regeneration step.	127
Figure 6.15	Fructose Production Rate flowing in 0.04 mL/min 0.1 M glucose in H ₂ O at 130°C in packed reactor with 100 mg of NaX. Triangles represent Run 1 and Circles Run 2 after regeneration step.	127

Figure 6.16	BET surface area and t-plot micropore volume as determined by nitrogen physisorption for varied NaX reaction conditions. Bars represent surface area and dots micropore volume.	xvii 128
Figure 6.17	Combined fructose and HMF specific production rate for tandem glucose isomerization and fructose dehydration flow studies using NaX (triangles) using H ₂ O (solid) and 46 mol% GVL: H ₂ O (hollow). Reactions were carried out using 100 mg of catalysts at 403 K using a feed of 2 wt% glucose flowed in at 0.04 mL min ⁻¹ .	129
Figure 6.18	Fructose production TOF for glucose isomerization flow studies using Sn-Beta zeolite using H ₂ O (circle), 1:4.5 (v:v) GVL: H ₂ O (triangle), and 4.5:1 (v:v) GVL: H ₂ O. Reactions were carried out using 10 mg of Sn-Beta zeolite at 368 K using a feed of 2 wt% glucose flowed in at 0.04 mL min ⁻¹ .	130
Figure 6.19	Powder X-ray diffraction patterns for PMO (containing no Sn) and various Sn-PMOs, in two different regions of 2θ ; (*) indicates major reflections for SnO ₂ nanoparticles.	134
Figure 6.20	TEM (left) and STEM (right) images of Sn-PMO-1	135
Figure 6.21	N ₂ sorption isotherms typical of PMOs with low and high loading Sn-loading.	135
Figure 6.22	Solid-state NMR spectra of Sn-PMO-1: (a) ¹³ C CP/MAS spectrum; and (b) ²⁹ Si CP/MAS spectrum; (*) indicates a spinning sideband.	136
Figure 6.23	Thermogravimetric analyses of various PMOs, recorded in flowing O ₂ .	137
Figure 6.24	Comparison of the Sn K-edge EXAFS, as k^3 -weighted FT magnitudes (not phase-corrected), for Sn-Beta and two Sn-PMOs.	138
Figure 6.25	Sn K -edge EXAFS (points) for Sn-PMO-3, shown k^3 -weighted in R -space (not phase-corrected) as FT magnitude and its imaginary component. The curve-fit (lines) corresponds to the parameters in Table 6.4	139 4.
Figure 6.26	Effect of Sn loading on batch glucose isomerization/dehydration in 4:1 THF:H ₂ O. Reaction conditions: 2 h at 413 K with 2 wt% glucose in 4:1 (w:w) THF:water with a Sn: glucose molar ratio of 1:100.	141

		xviii
Figure 6.27	Comparison of batch glucose isomerization over various Sn-containing catalysts: (a) Sn-Beta; (b) Sn-PMO-1; (c) Sn-PMO-4; and (d) bifunctional pSO ₃ H-Sn-PMO. Reaction conditions: 1.5 g feed, comprised of 2 wt% glucose in 4:1 (w:w) THF:water at 413 K. For (a) – (c), the Sn:glucose molar ratio was 1:100. For (d), the Sn:glucose:H ⁺ loading of (d) was 1:100:1.4.	143
Figure 6.28	Comparison of catalyst performance in batch fructose dehydration to HMF. Reaction conditions: 2 h at 413 K with 1.5 g of 2 wt% fructose in 4:1 THF:water, at a molar ratio Sn:fructose of 1:100.	147
Figure 7.1	Monomers of interest for copolymerization including the acid site (red) and pyrrolidone functionality (blue)	157
Figure 7.2.	Synthesis approach for solid acid functionalized PVP PMOs for biomass conversion	158
List of Tab	les	
Table 3.1.	Product distribution for HMF hydrogenation at full conversion for various supports and reaction times. All reaction were run with 200 mg of catalyst in 2:1 bi-phasic 1-butanol:water batch reactor at 403 K and 400 psi $\rm H_2$.	49
Table 3.2.	Chemisorption and reaction information for individual metals for comparison.	57
Table 4.1.	Initial Rates of HMF Production in DHMTHF:H ₂ O	64
Table 4.2.	Tautomer distributions in various solvents, based on ¹³ C NMR spectroscopy of 2- ¹³ C-labeled D-fructose	71
Table 5.1.	Batch reactions for fructose dehydration using Silicycle (SC) and SC/PVP modified catalysts.	78
Table 5.2.	Physicochemical properties of catalysts	80
Table 5.3.	Batch fructose dehydration catalyzed by unmodified and PVP-modified silica-based materials	83
Table 5.4.	The effect of changing the polymer type on HMF selectivity.	85
Table 5.5	Fructose tautomer composition determined by ¹³ C NMR	86

		Х	xix
Table 5.6.	Acids site loading, surface area, and pore sizes for CMK-3 and CMK-5 catalysts.	93	
Table 5.7.	Initial HMF production TOF and first order deactivation rate coefficient for CMK-3 and CMK-5 based catalysts, pSO ₃ H-SBA-15, and SAC-13.	95	
Table 6.1.	Glucose isomerization in different solvents mixtures of THF and water, and varied NaOH concentrations. Reactions were carried out at varied temperatures using 1.5 mL solutions of 2 wt% glucose. Reported values are average of points after reaching a steady-state value.	108	
Table 6.2.	Initial Turnover Frequency (TOF) for glucose isomerization in different solvents mixtures of THF and water. Reactions were carried out at 323 K using 1.5 mL solutions of 2 wt% glucose and 25 mM NaOH.	109	
Table 6.3.	Physico-chemical characteristics of PMO catalysts	133	
Table 6.4.	EXAFS curvefit parameters from a first-shell analysis, for various Sn catalysts	139	
Table 6.5	Solvent effects on glucose isomerization/dehydration	145	

Chapter 1: Introduction

1.1 Fuels and Chemicals

1.1.1 U.S. Energy Consumption and Chemical Consumption

Fossil fuels are currently our primary source for energy, materials, and chemicals. The US alone approximately consumed 20% of the total energy consumed worldwide in 2010, about 100 EJ (exa-joule; 1x10²⁹ J). From this 20% of total energy consumed by the US: 83% was derived from fossil fuel resources, 37% petroleum, 27% coal, and 23% natural gas (Figure 1.1). Renewable resources constituted only 4% in the US and 7% worldwide in the total energy demand. The primary sources of renewable energy in the US divide into 34% hydroelectric, 26% traditional biomass, 20% biofuels, 8% wind, 5% geothermal, 6% waste and 1% solar energy (Figure 1.2). These renewable technologies mainly supplement coal to fulfill the demands of the power sector. However, only biomass can help supplement fossil fuels to fulfill transportation energy demands (bio-ethanol/diesel) and industrial sectors (biomass combustion) with the current energy infrastracture.²

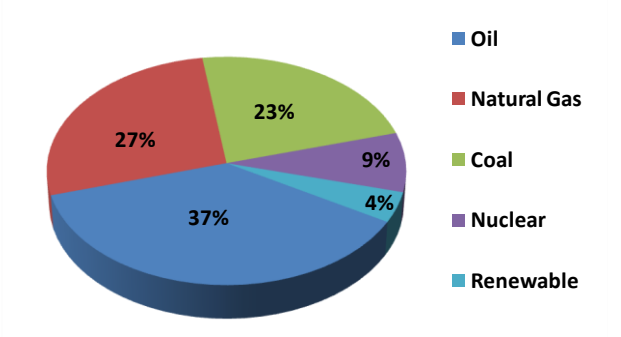


Figure 1.1. US energy consumption by resource in 2010.¹

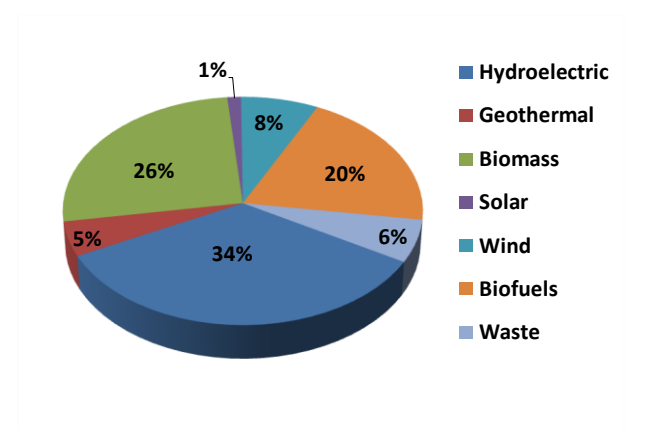


Figure 1.2. US renewable energy consumption by type.¹

The consumption of energy based on the demanding sectors and the supplying sources in the US is show in Figure 1.3. The consumption of energy is mainly dominated by the transportation sector (28%), followed by the industrial (21%), residential and commercial (11%), and the electrical power sectors (40%). Coal and natural gas are the main source for the generation of electricity and heat, for the industrial, residential and electrical sectors, and petroleum provides the majority (95%) of the energy consumed by the transportation sector.

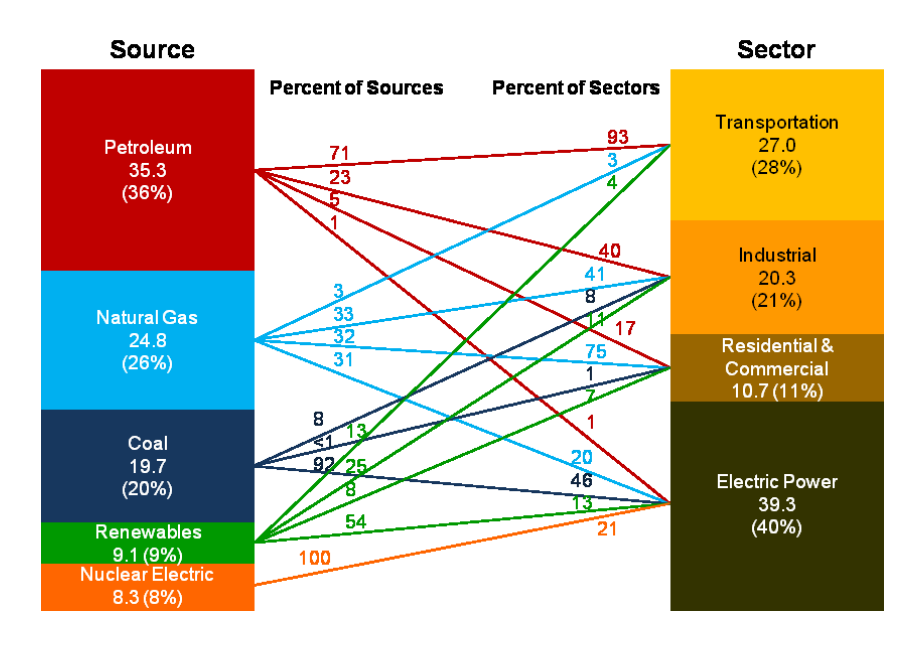


Figure 1.3. Primary Energy Consumption in the US by source and sector. Numbers are in units of quadrillion Btu. Adapted from ³.

The chemical industry heavily relies on fossil fuels for feedstocks in addition to energy. Approximately 95% of organic chemicals are manufactured from fossil fuels, mainly petroleum.^{3, 4} Only 10% of the crude petroleum consumed is used for the production of chemicals. Fossil fuel-derived chemicals are more valuable than the fuels themselves with profits from petro-derived products (minus pharmaceuticals) almost equivalent to that in the transportation sector, Figure 1.4.^{4, 5}

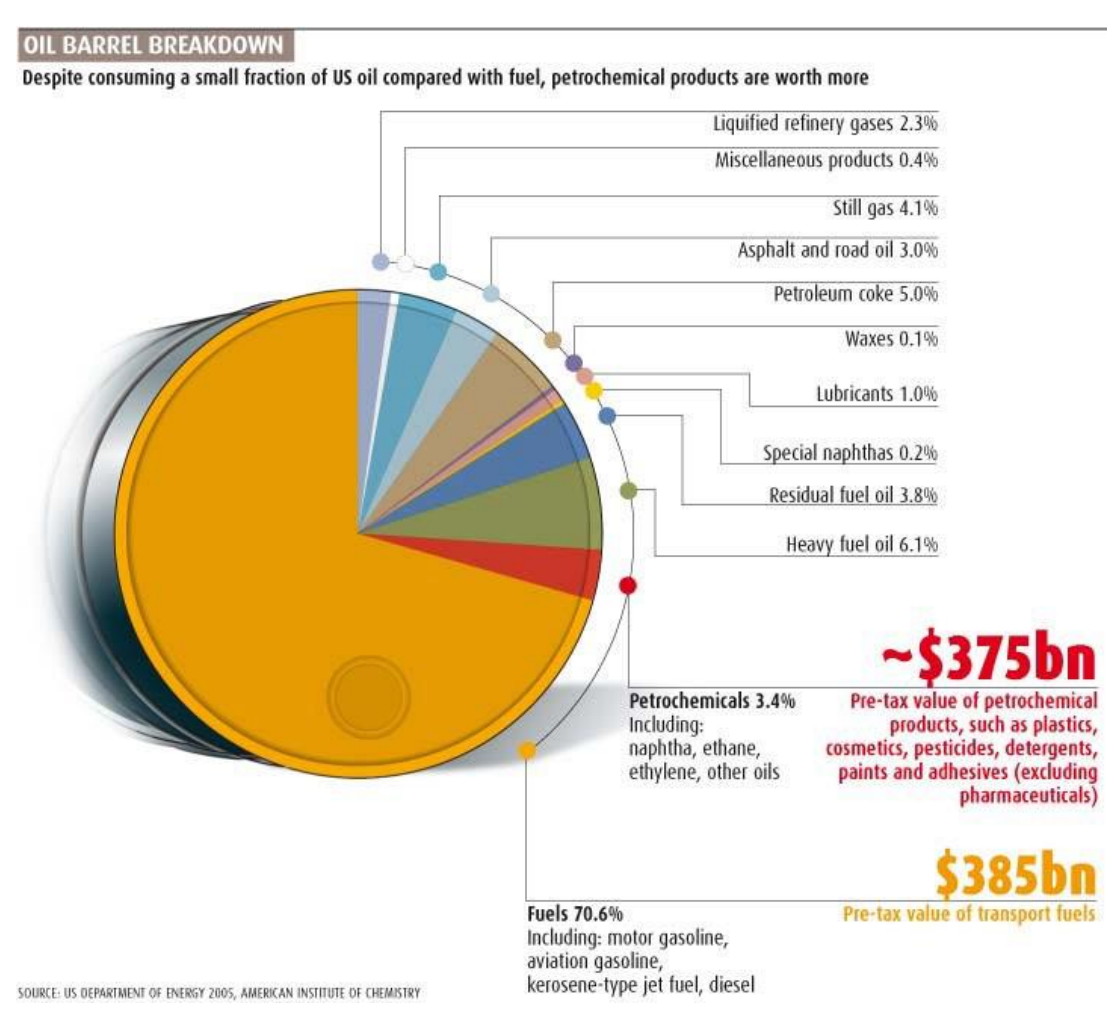


Figure 1.4. Production of fuels and chemicals from crude oil. Adapted from ⁵.

1.1.2 Outlook on Energy and Fossil Fuels

Society's current and projected demand of fossil fuel resources surpasses the supplies available for the next upcoming years. Nearly half of the energy consumed worldwide was by a fifth of the world's total population. The energy consumption is primarily by developed membernations of the OECD (Organization for Economic Cooperation and Development). The disparity in energy consumption between developed (OECD) and underdeveloped (non-OECD) countries is significant, with developed countries and underdeveloped consuming 2.0 GJ and 0.4 GJ per capita, on average. As a country becomes developed, the energy demand increases significantly

with both population and economic growth.^{6, 7} Between 2000 and 2009, OECD countries experienced a population and annual energy consumption of 6.2 % and 2.4 %, respectively. Non-OECD countries saw an increase in population and annual energy consumption of 12.4% and 63%, respectively. This significant growth in non-OECD countries in population and energy demand in the last decade suggests significant increases for worldwide energy consumption in the future, Figure 1.5. By 2035, the projected total energy demand world will approach 800 EJ with non-OECD countries alone consuming 500 EJ.⁷

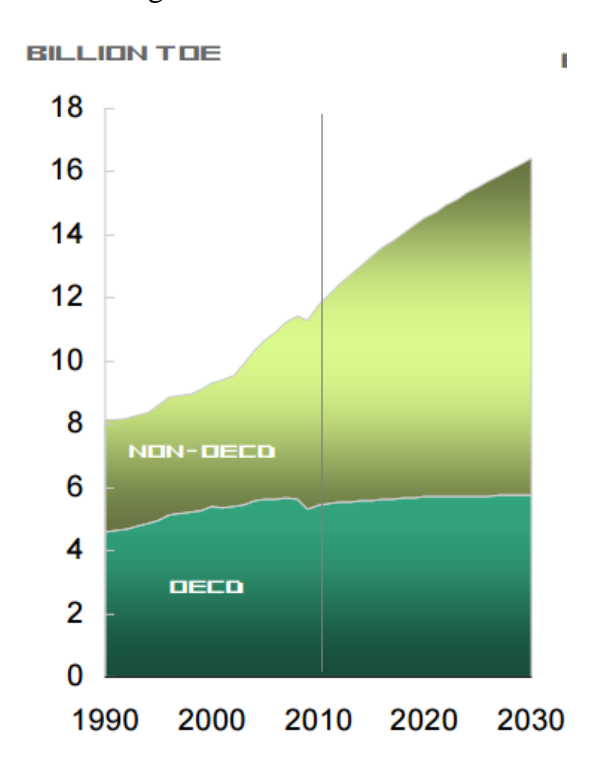


Figure 1.5. Projected World Energy Consumption in Tons of Oil Equivalent.⁷

1.2 Biomass as a Renewable Source of Carbon

Heightened demand for both diminishing, environmentally detrimental petroleum resources has increased the importance for developing clean and renewable alternatives. The U.S. produces 1.3 billion dry tons of cellulosic biomass annually. This biomass could potentially replace half of the transportation fuels consumed.^{2, 8} Carbohydrates are a key component of biomass and can serve as a reliable carbon source for the production of fuels and chemicals. The investigation of carbohydrate chemistry are essential for the efficient utilization of biomass.

Annually, only 10% of extracted crude oil is used as feedstock to produce industrial chemicals;^{9,10} biomass may replace or supplement petroleum feedstock. Biomass derived chemical commodities have significantly higher market prices than that biomass or petroleum derived fuels. Also, current petroleum derived industrial chemicals involve processes that produce large amounts of waste¹¹ and have high CO₂ emissions.¹² Potential biomass utilization presents an excellent opportunity to retool existing technologies with new production routes and catalytic strategies to minimize environmental costs.

1.2.1 Biomass as a Source of Fuels and Chemicals

Lignocellulosic biomass refers to fibrous, woody, and the inedible portions (for humans) of plants. Non-lignocellulosic consists of starches, oils, and proteins found in specific portions of the plant and competes with its use as a food source and has limited availability. However, lignocellulosic biomass is an abundant and underutilized resource that does not compete with the production of food. Thus, this basic building block of plants has the potential as a source for the synthesis of renewable chemicals.

Lignocellulosic biomass is abundant in all plant matter and again does not compete for the world's food resources. It is composed of cellulose (40-50 %), hemi-cellulose (25-35 %), and

lignin (15-20 %), Figure 1.6.¹³ Cellulose is a linear glucose polymer linked by β -glycosidic bonds that are difficult to hydrolyze (relative to the α -glyosidic bonds). It serves as a support scaffold within the plant cell walls.¹⁴ Hemicellulose is an amorphous polymer containing both five- and six-carbon sugars (xylose, a five-carbon sugar) being the most abundant.¹⁵ Lignin is an amorphous polymer composed of hydroxylated and methoxyated phenylpropane structures.² Lignocellulosic biomass can be collected from a variety of sources including: agricultural, industrial, and municipal waste or grown as energy crops.^{2, 16, 17} The U.S. produces 1.3 billion dry tons of cellulosic biomass annually that can potentially replace half of the transportation fuels consumed.^{2, 8} However to be viable industrially, biomass-derived fuels must be domestic and economical. Fuel production costs can be reduced by the co-production of low-volume, high value chemicals.

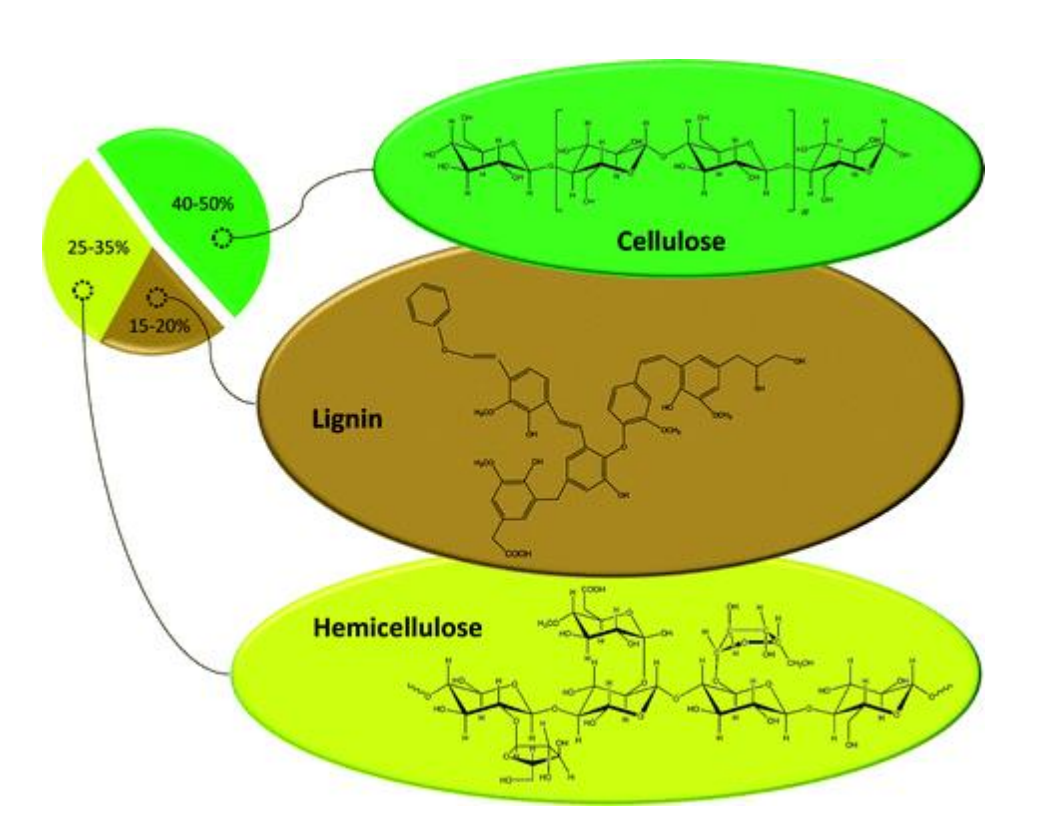


Figure 1.6. Structural composition of the principal components of lignocellulosic biomass. 13

The production of monosaccharides from lignocellulosic biomass starts with a variety of physical and chemical pretreatment processes aiming to separate lignin from cellulose and to de-crystallize the cellulose. Hydrolysis of the β -glycoside ether linkages is applied to break bonds and yield simple carbohydrates. Enzymatic and dilute acid hydrolysis treatments at temperatures of 273 K and 373-423 K respectively can produce monosaccharides in ~ 90% yields. Recent advances from the Dumesic group used non-enzymatic acid hydrolysis in combination with biomass-derived γ -valerolactone as a co-solvent to achieve similar sugar yield as previous systems developed. The resulting mixture consists of C_5 and C_6 sugars representing a water-soluble source of carbon that can be further processed by hydrolysis, dehydration, isomerization, aldol-condensation, hydrogenation, selective oxidation and hydrogenolysis for the selective removal of oxygen functionalities for the production of fuels and chemicals (Figure 1.7).^{2, 15, 16, 19}

Because of the high extent of functionality and low extent of volatility, unlike petroleum, these processes are mainly conducted in liquid-phase conditions and at mild temperatures. Heterogeneous catalyst used for these reactions can be acids, bases, supported metals and metal oxides.²⁰ These chemical processes can occur simultaneous or sequentially allowing for the opportunity of the use of multifunctional catalysts in the system.

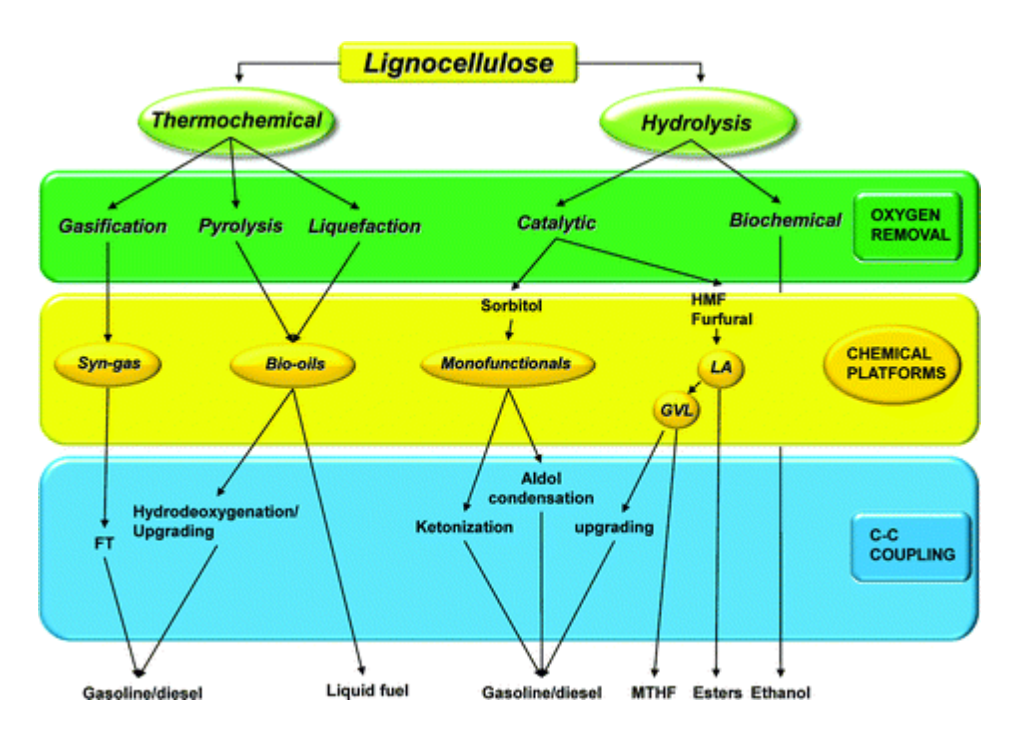


Figure 1.7 Lignocellulosic biomass conversion strategies. ¹⁶

1.3 Catalytic Strategies for the Production of Chemicals from Biomass

The renewable chemicals industry can be established by two approaches. The first approach is to produce biomass-derived chemicals identical to current petrochemicals, while the second seeks to manufacture novel molecules that could be substitutes for current petrochemicals. HMF has been identified as a key precursor for the production of biofuels and high value chemicals that can potentially replace petrochemicals. HMF is produced by the acid-catalyzed dehydration of monosaccharides, such as glucose and fructose. There has been a vast quantity of recent literature and patents on strategies to produce HMF and its chemical derivatives in high yields, though they have associated major drawbacks for industrial scale-up such as corrosion, sensitivity to water, and/or high separation and operating costs.

1.3.1 5-Hydroxymethylfurfural as a Platform Chemical

Biomass-derived HMF has been converted to a variety of specialty chemicals for various applications. The main reaction pathways for the production of chemicals from HMF are oxidation and hydrogenation, as shown in Figure 1.8. The oxidation of HMF leads to 2,5-diformylfuran (DFF) or 2,5-furandicarboxylic acid (FDCA).^{25, 26} DFF can be used as a monomer and starting material for pharmaceuticals.²⁷ FDCA can be used to replace teraphthalic acid (TA) for the production of polyesters²⁸ or be converted to TA via a Diels-Alder reaction with ethylene, followed by a dehydration step to remove the bridge-headed oxygen.²⁹ HMF can also undergo other chemistry to synthesize 2,5-furfuryldiamine (FDA) or a 2,5-furfuryldiiscocynate (FDI) for production of polyamides or polyurethanes²⁸ or esterification to 5,5'(oxy-bis(methylene))bis-2-furfural (OBMF) for use as a hepatitis antiviral precursor³⁰. HMF can also be converted to high-octane gasoline additive via hydrogenation and hydrogenolysis reactions.²² Biomass derived HMF is a versatile platform chemical for a variety of high value products.

Figure 1.8. HMF and its respective derivatives

The hydrogenation of the aldehyde group in HMF forms 2,5-dihydroxymethylfuran (DHMF) while complete hydrogenation of the ring leads to 2,5-dihydroxymethyltetrahydrofuran (DHMTHF). DHMF and DHMTHF can be used as a useful chemical with applications as a

solvent³¹, a monomer²⁸, or precursor to the production of other high-value chemicals.^{32, 33} For example, DHMTHF can be converted to 1,6-hexanediol, a valuable chemical for use in polymers and specialty chemicals, through the use of hydrogenolysis and dehydration reactions.³³⁻³⁸ Recent work in the group has shown that DHMTHF can be used as an effective solvent for the dehydration of fructose to HMF, and a dual reactor design was proposed for the formation of DHMTHF from fructose (Figure 1.8, Chapter 4).³⁹ This reactor design presents a unique strategy to increase the overall efficiency of fructose conversion to high-valued HMF derivative products while minimizing separation costs.

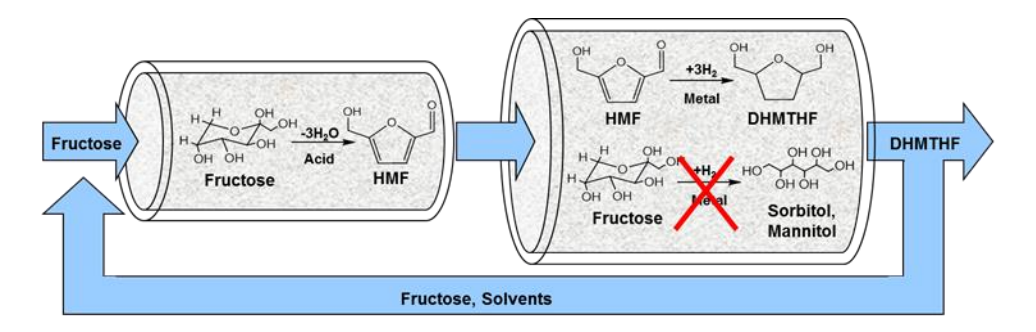


Figure 1.8 Proposed coupled fructose dehydration and HMF hydrogenation reactor system³⁹

1.3.2 Production of 5-Hydroxymethylfurfural from Sugars

Extensive effort has been devoted on the efficient and cost-effective production of HMF. However, HMF is accompanied by numerous side reactions taking place between reactant, products, and intermediates. Side reactions catalyzed during the dehydration of hexoses are the rehydration of HMF to from levulinic acid and formic acid, condensation of HMF with hexoses, condensation of hexoses to from oligosaccharides, and condensation of HMF with itself to form polymeric species, known as humins, Scheme 1.1.⁴⁰

Scheme 1.1. Reaction pathways for the formation of side products from hexose dehydration.⁴⁰

1.3.2.1 Current Strategies for Fructose Dehydration to 5-Hydroxymethylfurfural

Mineral Acids HMF is produced by the acid-catalyzed dehydration of monosaccharides (commonly glucose and fructose). HMF has been produced in high yields (> 90%) with polaraprotic solvents such as dimethylsulfoxide (DMSO). DMSO has been shown to increase the rate of HMF production, decrease the formation of organic acids (by decreasing the water concentration), and decrease the formation of humins.^{21, 23, 24, 41, 42} An obstacle to using DMSO is its high boiling point which makes for an energy intensive separation due to the reactive nature of HMF at high temperatures.^{21, 22, 40, 43}

Because of HMF's reactive nature, bi-phasic systems were thoroughly investigated in our group using a water-immiscible extracting organic phase to protect HMF from further degradation reactions.²³ This resulted in being able to achieve high HMF yields (>80%) at high fructose concentrations (10-50 wt %). The system used mineral acids, such as HCl, with phase modifiers

such as DMSO and/or poly(1-vinyl-2-pyrrolidine) (PVP) in a separation-friendly organic phase (2-butanol and methyl-isobutyl ketone (MIBK)). The phase modifiers were in low concentration at about 15 wt % of the total system. For glucose, this system achieved selectivities to HMF of about 53%. It was demonstrated that under optimized conditions for the monosaccharides, the corresponding polysaccharide, such as sucrose, inulin, starch, and cellobiose, could be converted with comparably good selectivities at high conversions. Using DMSO in this system, the extraction ratio (concentration of HMF in the organic phase divided by the concentration of HMF in the aqueous phase) also increased from about 0.9 to 1.7, however DMSO partitions into the organic phase ⁴⁰ leading again to increased separations costs. Bi-phasic systems also used salts to increase the partition ratio by a salting-out effect and achieved high selectivities to HMF (89%) without the use of high boiling solvents. ²² However, a major challenge is the corrosive nature of salts combined with mineral acids at high temperatures.

Ionic Liquids Most recently, a large amount of work has been devoted to the use of ionic liquids for the production of HMF from mono- and polysaccharides. Moreau et. al.⁴⁴ found HMF yields of up to 92% from fructose in 1-H-3-methyl imidazolium chloride which was both the solvent and catalyst. HMF was extracted using diethyl ether and it was found that the ionic liquid deactivated unless water was continuously removed. Zhao et. al.⁴⁵ used a system of 1-ethyl-3-methyl imidazolium chloride and CrCl₂ to convert glucose to HMF in 70% yield. The major limitations of ionic liquids for industrial use includes their sensitivity to water (leading to energy intensive biomass pretreatments), they are expensive, often require purification after recycling, and lead to complex separations after reaction.^{19, 45, 46} They will play no role in the scope of this thesis.

Solid Acid Catalysts Heterogeneous catalysts dominate industrial catalysts with an estimated 80% of catalytic processes using solid catalysts.⁴⁷ Solid catalysts are advantageous to homogenous catalysts as their ease in separations, which usually accounts for over half the initial equipment costs for fuel and chemical industries.⁵ They are also non-corrosive, which can minimize the capital and operating costs, compared to mineral acids.

A variety of solid acid catalysts for fructose dehydration to HMF have been investigated including zeolites, ion-exchange resins, metal oxides and phosphates, and sulfonic acid based materials. ^{19, 21, 48, 49} Most studies are conducted in batch reactions using DMSO as an aqueous phase modifier, however for comparative purposes, a solvent system which does not have major promotional effects should be used differentiate the effects of solid acid catalysts. This led to a benchmark study of commercial and literature based catalysts where an aqueous feed of 30 wt% fructose and a 7:3 (wt:wt) extracting layer of MIBK:2-butanol were used. ⁵⁰ DMSO was not used to reduce downstream energy intensive separation processes. ⁴⁰ Salts, which have been shown to increase the extraction of HMF into the organic phase, were also not used as the salt cation and the solid Brønstead acid proton can exchange and form a homogenous catalysts *in-situ*.

From the benchmark study conducted in our lab⁵⁰, the most selective zeolite catalyst was Mordenite, which required a three hour reaction time, at 54% at 88% conversion (Figure 1.9). Selectivities were lower than that of literature most likely because of the use of higher fructose concentration and lower amount of extracting solvent. The metal oxides and phosphates explored in this benchmark study included cubic zirconium phosphate, amorphous zirconium phosphate, niobic acid, and H₃PO₄ treated niobic acid, and titanium dioxide. This subgroup of catalysts achieved high fructose conversion at lower reaction times than the zeolite based catalysts. The most selective catalysts were the zirconium phosphate based materials achieving around 65%

selectivity, with the amorphous material being more active achieving higher conversions at lower reaction times. This can most likely be due to the fact the cubic material loses surface area (with a corresponding loss in active sites) during transformation from amorphous to cubic materials. The final class of materials investigated were sulfonic acid based materials including a polymeric based ion-exchange resin, Amberlyst 70 (A70), and sulfonic acid functionalized silica, Phophonics Si-SPhSA (Fig 1.10). A70 is a halogenated polystyrene-co-divinylbenzene sulfonic acid resin (Rohm and Haas) that is resistant to degradation at higher temperatures above 130°C.⁵¹ Phosphonics Si-SPhSA is an aryl-sulfonic acid functionalized unordered silica. A70 had a higher acid site density (2.55 mmol/g compared to 0.75 mmol/g) than Phosphonics Si-SPhSA which in terms gave a higher conversion at lower reaction time. Both catalysts had selectivity above 65% with high activity attributed to the strong sulfonic acid sites. Novel solid acid catalysts will thus be synthesized using sulfonic acid groups as the active sit as an approach to achieve high activity and selectivity to HMF.

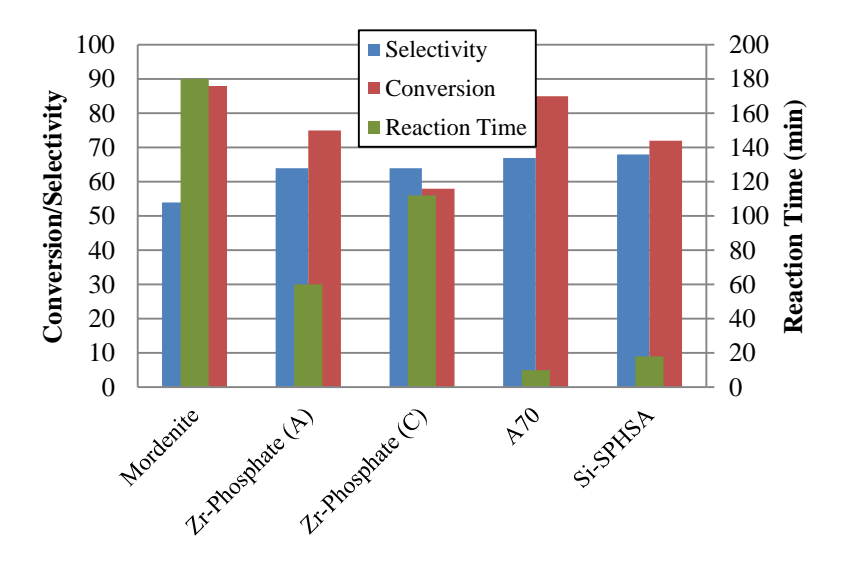


Figure 1.9. Fructose conversion, selectivity to HMF, and reaction time for various material in a batch reaction. Adapted from ⁵⁰.

Figure 1.10 Active acid site for commercial catalysts

1.4 Solid Acid Catalysts for Biomass Conversion

The development of efficient catalytic processes for the selective removal of oxygen from lignocellulosic biomass is not the only challenge encountered when producing platform molecules. Another major challenge is the synthesis of hydrothermally stable solid acid catalysts. The high oxygen to carbon stoichiometry of 1:1 in carbohydrates inherently makes biomass derived molecules very soluble in water, inevitably making water the most attractive reaction solvent. Even if water is not used as a solvent, carbohydrates and biomass process have water inherently or produces water in some reactions. Hydrothermally stability issues arise for the solid acid catalyst possible by: loss of catalyst surface area, structure collapse of the support, and sintering or leaching of the active site.

There have been few reports on the production of HMF using heterogeneous catalysts such as titania, zirconia, H-mordenite, and niobia. 52-57 In collaboration with the Scott group at UCSB, we have synthesized and investigated bifunctional silica containing alkylsulfonic acid as the active sites and a thioether group as a promoter as potential solid materials for fructose dehydration to HMF. 58, 59 Major advantages of using solid acid catalysts include *reduced separations costs* compared to the homogenous counterparts. Because no mineral acids will be used, the process will

be *less corrosive* lowering both capital and operating costs. Finally, solid catalysts can be implemented in a continuous process and be used in *tandem catalysis*. For example we can couple fructose dehydration either with an upstream and/or downstream catalyst for glucose isomerization to fructose and HMF hydrogenation to DHMTHF, respectively. This would be advantageous as glucose is the more abundant carbohydrate and DHMTHF is a more stable product than HMF. However, there are major challenges for a technologically competitive solid acid catalyst which includes achieving high selectivities to HMF and increased catalyst stability.

1.4.1 Synthesis of Novel Acid Catalysts

Hoffman et. al.⁶⁰ has reviewed current synthesis strategies for novel mesoporous organic-inorganic hybrid materials. These new class of materials are characterized by large specific surface areas and tunable pore sizes between 2 and 15 nm. Novel catalysts have been made by coupling inorganic and organic components by template synthesis with the incorporation of functionalities achieved in three ways: 1) the modification of the pore surface of a purely inorganic silica material ("grafting") (Fig 1.11.A), 2) the simultaneous reaction of condensable inorganic silica species and silyated organic compounds (co-condensation, one pot synthesis) (Fig 1.11.B), and 3) the use of bissilyated organic precursors that lead to periodic mesoporous organosilicas (PMOs). Work presented in this thesis will incorporate all strategic methods for the synthesis of new solid acid catalysts for various sugar chemistries. We used PMOs were used in our group to increase hydrothermal stability and minimize deactivation of catalytically active materials relative to non-PMO silica based catalysts.⁶¹

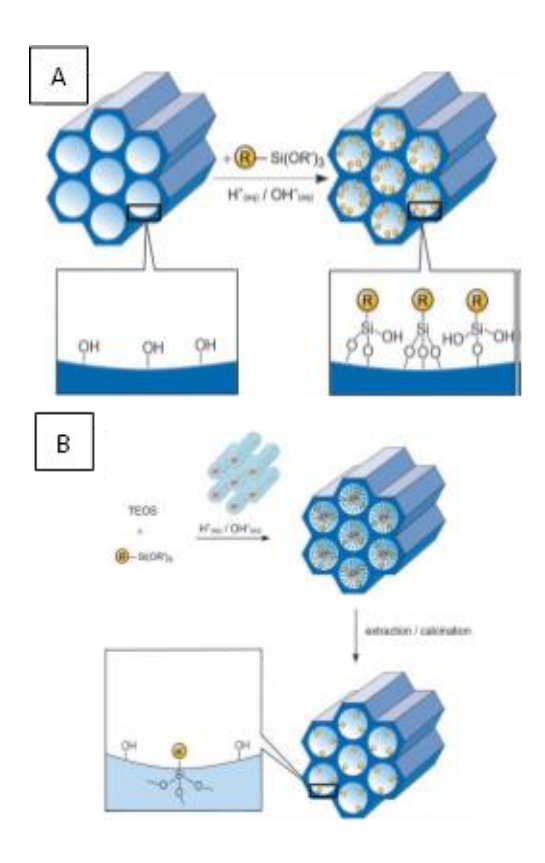


Figure 1.11. Strategies for grafting organic groups R onto mesoporous silica using grafting (A) and co-condensation (B).⁶⁰

1.4.2 Catalysts for the Continuous Production of HMF

The continuous production of HMF would be ideal to be economically competitive with petrochemical production. There have been few reports on the continuous production of HMF using solid catalysts. ⁵²⁻⁵⁷ H-mordenite has been reported as a highly active solid acid catalyst and used in the construction of a continuous pilot plant reactor; however, the catalyst stability was not reported. ^{53, 54} There has been work in the formation of HMF from glucose and fructose in subcritical and supercritical water (>350°C and >40 MPa), however yields of less than 10% to HMF were accomplished. ⁶² Niobia and silica-niobia based catalysts were used in a fixed bed reactor for the dehydration of fructose in water ^{56, 57} that were shown to be stable, despite the

formation of coke and humins. However, the selectivity to HMF from fructose was low (<15% selectivity at 15-35% fructose conversion).

A continuous flow reactor using an ion-exchange resin in dimethyl sulfoxide (DMSO) solvent was also used for fructose dehydration; however, the reaction was run at high conversions of fructose where catalyst stability cannot be accurately measured. As previously noted, DMSO should be avoided in comparative studies as it increases the selectivity to HMF so it is difficult to determine the effect of the acid catalyst and for industrial use would result in high separation costs. Due to a minimal comparable literature on continuous production of HMF over solid acid catalysts, a detailed study of promising solid acid catalysts in a packed bed reactor was performed by our group to determine catalyst stability and probe the mechanism of catalyst deactivation. ⁵⁰

The catalysts that were surveyed can be grouped into 1) commercial sulfonic acid catalysts, 2) silica supported catalysts (prepared by grafting and co-condensation), 3) and propylsulfonic acid modified silica (PMOs). The commercial catalyst each had a distinct functional group, but the most active and stable after over 100 hours on stream was Amberlyst 70. It lost over 62% of its activity from 20 to 110 hours on stream, but the selectivity remained high (60-75%). The catalyst was first attempted to be regenerated and then to remove any possible site blocking polymeric degradation products, but both proved unsuccessful. A70 was difficult to characterize due to its ability to swell in polar solvents, so the exact deactivation mechanism was not determined. Next, the propylsulfonic acid functionalized SBA-15 (pSO₃H-SBA-15) showed the highest activity of the synthesized silica supported catalysts in a packed bed reactor yet deactivated when on stream. The pSO₃H acid was chosen as the active site to be incorporated into ethane-bridged PMOs in hopes to address long term catalyst stability.

To increase catalyst stability, three PMOs were synthesized by the condensation of 10% (3-Mercapto)-trimethoxysilane, 90,45, or 0% bis(trimethoxysilyl)ethane (BTME), and the remaining amount with a tetraalkoxysilane (TMOS or TEOS) and compared to commercial propylsulfonic Silicycle (SC) (both unendcapped and endcapped). The PMOs had a deactivation rate 3-4 lower than that of SC and maintained selectivity to HMF of over 60% after 60 hours on stream. It was determined the primary deactivation mechanism for these catalyst was the cleavage of the propylsulfonic acid group, which was improved to some degree with the use of silica gel downstream. It should be noted that Nafion SAC-13, a nano-composite of silica and the Nafion resin, expected to be a more hydrophobic material than the synthesized PMOs had a deactivation rate four times lower than that of the most stable PMO. The only shortfall of Nafion SAC-13 is its low acid site density, thus having low rates on a per mass basis. However, this gives tremendous insight on the effect of the local structure environment on catalyst activity and stability.

1.5 Phase and Surface Modifiers

Catalyst-surface modifications provide a unique opportunity to enhance the stability and/or activity of a catalyst. PVP was used as a phase modifier in biphasic reaction that promoted the efficient production of HMF.²³ It is proposed that PVP, analogous to the phase modifier dimethylsulfoxide (DMSO), can efficiently produce HMF by decreasing the formation of organic acids and the formation of humins.²³ PVP can also favor the production of HMF by favoring the alpha-furanose form at the expense of the beta-pyranose tautomer of fructose,⁴¹ facilitating the subsequent dehydration steps. By anchoring PVP on the catalyst surface, the local environment on the surface is modified and used to promote the production of HMF without the need to recycle or separate PVP from the products. Understanding the localized environment of catalyst-surface modifiers presents new approaches to synthesizing solid catalysis with increased performance.

1.5.1 Polyvinylpyrrolidone (PVP) as a Catalyst-Surface Modifier

Previously, PVP was used as a phase modifier in a biphasic reactor for fructose dehydration showing increased selectivity for the production of HMF.²³ This was attributed to similar effects to that of DMSO by increasing the rate of HMF production and minimizing undesirable parallel reactions of HMF, inhibiting possible rehydration products²¹ and acyclic reaction sequences.⁶⁴ PVP (Figure 6) is an amphiphilic polymer that has a monomer unit consisting of a highly polar amide group having hydrophilic and polar-attracting properties. The backbone consists of apolar CH₂, CH group, and the ring giving the compound its hydrophobic nature. This polymer has been studied as a material to be incorporated with metal oxides to synthesize nano-composite or hybrid materials.^{65, 66} PVP has applications in the medical and pharmaceutical fields due to its nontoxicity⁶⁷, for development of membranes for separation purposes⁶⁸, and most recently as a potential tool to stabilize metal nanoparticles.^{69, 70} In this work we incorporate PVP on the surface of a mesoporous support, such as silica, to modify the local environment around the active acid site to increase the selectivity to HMF (Chapter 5.2).⁷¹

Figure 1.12. Polyvinylpyrrolidone (PVP)

1.5.2 PVP Interactions with Silica Surfaces

There are few studies that deal with the interaction or incorporation of functionalized polymeric materials and oxide materials that are relevant for surface modification techniques. However, it has been suggested that in the formation of nano-composite or hybrid materials, that the PVP material smothers the oxide material leading to a dense hybrid structure with hydrogen-bonding between the amide carbonyl group of PVP and the surface hydroxyl groups of the oxide material. This has been suggested for a variety of oxide materials including silica. However, the materials are usually composed of 2:1 (wt:wt) PVP:SiO₂ ratios during a sol-gel procedure where the both the specific area and pore volume decreases by three orders of magnitude. It would be ideal to maintain the high surface area per gram of silica to have a high acid site density for practical applications. PVP is also soluble in water and alcoholic solvents; however, this may be overcome by multilayer deposition that can be accomplished via a UV-curing step.

Gun'ko, et. al.⁷² had a detailed study on the interaction of PVP with fumed silica in dry and wet powders and aqueous suspensions. Mechanical mixing was inefficient for the distribution of PVP on the silica surface, however the diffusion of PVP at a wet silica surface is promoted by water or ethanol adsorbed from saturated vapor. The amount of PVP strongly bounded to silica was measured by temperature programmed desorption (TPD) over air and its interaction with silica was surveyed using ¹H NMR, infrared spectroscopy, electrophoresis, and rheology methods. It was shown that that PVP irreversibly adsorbed on silica surfaces at concentrations less than 10% of the amount of silica. This would be the expected amount of PVP on the silica surface of the novel catalyst.

1.5.3 Crosslinking of PVP

As an attempt to minimize the solubility of PVP in reaction solvents, the PVP can be crosslinked. This is where one polymer chain is bonded to another polymer chain through either covalent or ionic bonds. PVP is a photo-sensitive polymer that can be UV-cured using short wavelength irradiation with persulfate⁶⁷ and 4,4'-diazostillbene-2,2'-disulfonic acid disodium salt (DAS)⁷³ as crosslinking agents. The crosslinking mechanism of DAS has been previously reported^{74,75} and is usually accomplished by decomposing the crosslinking agent to liberate a reactive intermediate (i.e dinitrene for DAS) that reacts with the polymer molecules to form a water-insoluble three dimensional network. In the case DAS and PVP, the dinitrene intermediate is inserted into to C—H bonds to give an interchain crosslink with the substituted amine groups. The DAS concentration was varied and at high concentrations DAS dimerized and lowered the overall efficacy of the crosslinking. Therefore the DAS concentration should be optimized and can high DAS concentrations are easily observed by a bronze color formation of the dimerization.

A study on the photochemical immobilization of poly(1-vinylphenol) (PVPol) on silica wafers with a native oxide layer elucidated the PVPol anchoring mechanism. There was a variety of possible UV-induced reactions of PVPol, such as crosslinking (various combinations dependent on the radicals formed), rearrangement, oxidation, and chain scission. IR, UV-Vis, and XPS were used to qualitatively and quantitatively provide details on the photochemical reaction products and probe the chemical composition of the surface. Both the presence of oxygen and UV exposure doses were the main factors in the degree of desired crosslinking between phenoxy and benzyl radicals versus oxidation reactions that breaks apart the PVPol chain. This system can potentially describe a PVP and a UV-sensitive crosslinking agent. There is an open area of research to investigate the adsorption of polymers onto mesoporous silica.

1.5.4 Current Surface Modifications for Catalytic Applications

Active site and surface cooperatively has been proposed to enhance heterogeneous organic and organometallic catalysis. This is based from biological catalysts, which show remarkably high activity and selectivity, usually by precise organization of chemical functionality near the active site. For most heterogeneous catalyst, the support is usually viewed as an inert spectator; however, contrast to homogeneous and enzymes, it contains two advantageous features: 1) the surface provides a continuum for acid-base bifunctional catalysts and 2) an increased ease of forming supramolecular assemblies on the surfaces.⁷⁷ An example of the latter includes molecular imprinting aimed at creating materials with chemical functionalities that are spatially organized by covalent or non-covalent interactions with template molecules during the synthesis process.^{78, 79} The objective of some of these works has been to anchor metal complexes to surfaces and use as a heterogeneous catalyst. Cellulose, a polymer, has also been grafted on the surface of silica that demonstrated the effect of the local environment on increasing the reactivity for hydrolysis of glycosidic bonds under mild conditions.⁸⁰

Catalyst-surface modification techniques can be used to increase the catalyst stability. This is in important in biomass processing as water (as a solvent or product) in high temperatures and pressures results in a loss of surface area (and active sites) for mesoporous silica supports. Efforts at UW-Madison have used atomic layer deposition (ALD) to coat titania, niobia, and zirconia onto SBA-15 and propyl-sulfonic-acid modified SBA-15 where titania/silica ALD coating resulted in a threefold lower deactivation rate for fructose dehydration to HMF. TGA indicated that fewer sulfonic acid groups are cleaved under reaction conditions with the ALD coating present.⁸¹ As previously mentioned PMOs were also shown to increase catalyst stability in flow reactor.⁶³

Surface modifications provide opportunities to synthesize novel catalyst for improved performance. Incorporation of PVP can change the local environment and increase the selectivity to HMF. Further incorporation with hydrophobic surface modifiers can help minimize hydrolysis of the silica framework and/or acid leaching. The investigation of catalyst-surface modifiers presents a unique opportunity in understanding fundamental nature of the local environment on the reaction system.

1.6 Research Direction

The selective and efficient catalytic conversion of biomass to fuels and chemicals remains an important challenge for the renewable production to liquid fuels and chemicals. The conversion to HMF as a platform chemical could be an important starting point for the synthesis of biomass derived compounds for the use as specialty chemicals, pharmaceuticals, and fuels. Current production methods currently employ difficult to separate solvents and/or corrosive homogenous acid catalysts.

This thesis explores the production of furan derivatives (HMF and DHMTHF) using separation friendly co-solvents as well as investigating heterogeneous catalysts for continuous flow systems starting from both glucose and fructose. In Chapter 3, the hydrogenation of HMF to DHMTHF upon supported metal catalysts are studied with a focus on elucidating the selectivity to desired products. In Chapter 4, we use the hydrogenation product of HMF as a biomass-derived monophasic co-solvent with water to study fructose dehydration. These monophasic co-solvents are further investigated in Chapter 5 when using novel catalysts which included PVP-over coated acid-functionalized organosilicas, acid-functionalized ordered mesoporous carbons, and supported bimetallic catalysts. Chapter 6 explores the design of catalytic systems for the selective isomerization of glucose to fructose using homogenous base, homogeneous Lewis acids, faujasite

zeolites, and Sn-incorporated PMOs and elucidating solvent effects. Additionally, the feasibility of tandem glucose isomerization and fructose dehydration to HMF in a single system are explored as well. The experimental methods used in this thesis are presented in Chapter 2 and a summary of conclusions and recommendations for future work are presented in Chapter 7.

1.7 References

- [1] A.E. Outlook, Department of Energy, (2010).
- [2] G. Huber, B. Dale, in: Scientific America, 2009.
- [3] C.H. Christensen, J. Rass-Hansen, C.C. Marsden, E. Taarning, K. Egeblad, ChemSusChem, 1 (2008) 283-289.
- [4] K. Weissermel, H.-J. Arpe, Industrial organic chemistry, John Wiley & Sons, 2008.
- [5] R. Rinaldi, F. Schüth, Energy & Environmental Science, 2 (2009) 610-626.
- [6] B. Petroleum, in, 2011.
- [7] B.E. Outlook, Retrieved on 8th May, (2014).
- [8] R.D. Perlack, L.L. Wright, A.F. Turhollow, R.L. Graham, B.J. Stokes, D.C. Erbach, in, Oak Ridge National Laboratory, 2005.
- [9] L. Qi, I.n.T. Horváth, Acs Catalysis, 2 (2012) 2247-2249.
- [10] D.R. Dodds, R.A. Gross, Science, 318 (2007) 1250-1251.
- [11] R.A. Sheldon, Green Chemistry, 9 (2007) 1273-1283.
- [12] C.H. Christensen, J. Rass-Hansen, C.C. Marsden, E. Taarning, K. Egeblad, ChemSusChem, 1 (2008) 283-289.
- [13] N. Mosier, C. Wyman, B. Dale, R. Elander, Y. Lee, M. Holtzapple, M. Ladisch, Bioresource technology, 96 (2005) 673-686.
- [14] R.F. Boyer, Concepts in biochemistry, Wiley, 2006.
- [15] B.C. Saha, Journal of Industrial Microbiology and Biotechnology, 30 (2003) 279-291.
- [16] D.M. Alonso, J.Q. Bond, J.A. Dumesic, Green Chemistry, 12 (2010) 1493-1513.
- [17] J.P. Lange, Biofuels, bioproducts and biorefining, 1 (2007) 39-48.
- [18] J.S. Luterbacher, J.M. Rand, D.M. Alonso, J. Han, J.T. Youngquist, C.T. Maravelias, B.F. Pfleger, J.A. Dumesic, Science, 343 (2014) 277-280.
- [19] M.J. Climent, A. Corma, S. Iborra, Green Chemistry, 13 (2011) 520-540.
- [20] G.W. Huber, S. Iborra, A. Corma, Chemical Reviews, 106 (2006) 4044-4098.
- [21] B.F.M. Kuster, in: Starch, 1990, pp. 314-321.
- [22] Y. Roman-Leshkov, C.J. Barrett, Z.Y. Liu, J.A. Dumesic, Nature, 447 (2007) 982-985.
- [23] Y. Roman-Leshkov, J.N. Cheda, J.A. Dumesic, Science, 312 (2006) 1933-1937.
- [24] H.E. van Dam, A.P.G. Kieboom, H. van Bekkum, Starch Stärke, 38 (1986) 95-101.
- [25] S.E. Davis, L.R. Houk, E.C. Tamargo, A.K. Datye, R.J. Davis, Catalysis Today, 160 (2011) 55-60.
- [26] A. Gandini, M.N. Belgacem, Chapter 6 Furan Derivatives and Furan Chemistry at the Service of Macromolecular Materials, in: B. Mohamed Naceur, G. Alessandro (Eds.) Monomers, Polymers and Composites from Renewable Resources, Elsevier, Amsterdam, 2008, pp. 115-152.
- [27] X. Tong, Y. Ma, Y. Li, Applied Catalysis A: General, 385 (2010) 1-13.

- [28] C. Moreau, M.N. Belgacem, A. Gandini, Topics in catalysis, 27 (2004) 11-30.
- [29] W.H. Gong, in, BP Corporation North America Inc., U.S., 2009.
- [30] O. Casanova, S. Iborra, A. Corma, Journal of Catalysis, 275 (2010) 236-242.
- [31] A.J. Sanborn, P.D. Bloom, in, US, 2008.
- [32] T.J. Connolly, J.L. Considine, Z. Ding, B. Forsatz, M.N. Jennings, M.F. MacEwan, K.M. McCoy, D.W. Place, A. Sharma, K. Sutherland, Organic Process Research & Development, 14 (2010) 459-465.
- [33] T. Buntara, S. Noel, P.H. Phua, I. Melián-Cabrera, J.G. de Vries, H.J. Heeres, Angewandte Chemie International Edition, 50 (2011) 7083-7087.
- [34] M. Chia, Y.J. Pagan-Torres, D. Hibbitts, Q. Tan, H.N. Pham, A.K. Datye, M. Neurock, R.J. Davis, J.A. Dumesic, Journal of the American Chemical Society, (2011).
- [35] M. Faber, in, US, 1983.
- [36] S. Koso, N. Ueda, Y. Shinmi, K. Okumura, T. Kizuka, K. Tomishige, Journal of Catalysis, 267 (2009) 89-92.
- [37] Y. Nakagawa, K. Tomishige, Catalysis Communications, 12 (2010) 154-156.
- [38] J.D. Garber, in, US, 1962.
- [39] M.H. Tucker, R. Alamillo, A.J. Crisci, G.M. Gonzalez, S.L. Scott, J.A. Dumesic, ACS Sustainable Chemistry & Engineering, 1 (2013) 554-560.
- [40] J.N. Chheda, Y. Roman-Leshkov, J.A. Dumesic, Green Chemistry, 9 (2007) 342-350.
- [41] A.S. Amarasekara, L.D. Williams, C.C. Ebede, Carbohydrate Research, 343 (2008) 3021-3024.
- [42] K.-i. Shimizu, R. Uozumi, A. Satsuma, Catalysis Communications, 10 (2009) 1849-1853.
- [43] D.W. Brown, A.J. Floyd, R.G. Kinsman, Roshanhyphen, Y. Ali, Journal of Chemical Technology and Biotechnology, 32 (1982) 920-924.
- [44] C. Moreau, A. Finiels, L. Vanoye, Journal of Molecular Catalysis A: Chemical, 253 (2006) 165-169.
- [45] H. Zhao, J.E. Holladay, H. Brown, Z.C. Zhang, Science, 316 (2007) 1597-1600.
- [46] M.E. Zakrzewska, E. Bogel-Łukasik, R. Bogel-Łukasik, Chemical Reviews, 111 (2010) 397-417.
- [47] K.P. de Jong, General Aspects, in: Synthesis of Solid Catalysts, Wiley-VCH Verlag GmbH & Co. KGaA, 2009, pp. 1-11.
- [48] J. Lewkowski, ARKIVOC, 2001 (2005) 17-25.
- [49] A.A. Rosatella, S.P. Simeonov, R.F.M. Frade, C.A.M. Afonso, Green Chemistry, 13 (2011) 754-793.
- [50] M. Tucker, in: Chemical and Biological Engineering, The University of Wisconsin-Madison, 2011, pp. 184.
- [51] P.F. Siril, H.E. Cross, D.R. Brown, Journal of Molecular Catalysis A: Chemical, 279 (2008) 63-68.
- [52] C.V. McNeff, D.T. Nowlan, L.C. McNeff, B. Yan, R.L. Fedie, Applied Catalysis A: General, 384 (2010) 65-69.
- [53] C. Moreau, R. Durand, S. Razigade, J. Duhamet, P. Faugeras, P. Rivalier, P. Ros, G. Avignon, Applied Catalysis A: General, 145 (1996) 211-224.
- [54] P. Rivalier, J. Duhamet, C. Moreau, R. Durand, Catalysis Today, 24 (1995) 165-171.
- [55] P. Carniti, A. Gervasini, M. Marzo, Catalysis Today, 152 (2010) 42-47.
- [56] P. Carniti, A. Gervasini, S. Biella, A. Auroux, Catalysis Today, 118 (2006) 373-378.

- [57] Y. Nakamura, S. Morikawa, Bulletin of the Chemical Society of Japan, 53 (1980) 3705-3706.
- [58] A. Crisci, M. Tucker, J. Dumesic, S. Scott, Topics in Catalysis, 53 (2010) 1185-1192.
- [59] A. Crisci, M. Tucker, M. Lee, S. Jang, J. Dumesic, S. Scott, Acs Catalysis, 1 (2011) 719-728.
- [60] F. Hoffmann, M. Cornelius, J. Morell, M. Fröba, Angewandte Chemie International Edition, 45 (2006) 3216-3251.
- [61] M.H. Tucker, A.J. Crisci, B.N. Wigington, N. Phadke, R. Alamillo, J. Zhang, S.L. Scott, J.A. Dumesic, Acs Catalysis, 2 (2012) 1865-1876.
- [62] T.M. Aida, Y. Sato, M. Watanabe, K. Tajima, T. Nonaka, H. Hattori, K. Arai, The Journal of Supercritical Fluids, 40 (2007) 381-388.
- [63] M.C. Tucker, AJ; Wigington, B; Phadke, N; Alamillo, R.; Zhang, J; Scott, SL; Dumesic, JA, in, University of Wisconsin-Madison; University of California, Santa Barbara, 2012.
- [64] M.J. Antal Jr, W.S.L. Mok, G.N. Richards, Carbohydrate Research, 199 (1990) 91-109.
- [65] C. Sanchez, B. Julian, P. Belleville, M. Popall, Journal of Materials Chemistry, 15 (2005) 3559-3592.
- [66] T. Saegusa, Macromolecular Symposia, 98 (1995) 719-729.
- [67] C.C. Anderson, F. Rodriguez, D.A. Thurston, Journal of Applied Polymer Science, 23 (1979) 2453-2462.
- [68] R.S. Parnas, M. Chaimberg, V. Taepaisitphongse, Y. Cohen, Journal of Colloid and Interface Science, 129 (1989) 441-450.
- [69] X. Zhou, T. Wu, B. Hu, T. Jiang, B. Han, Journal of Molecular Catalysis A: Chemical, 306 (2009) 143-148.
- [70] B. Tamami, H. Allahyari, S. Ghasemi, F. Farjadian, Journal of Organometallic Chemistry, 696 (2011) 594-599.
- [71] R. Alamillo, A.J. Crisci, J.M.R. Gallo, S.L. Scott, J.A. Dumesic, Angewandte Chemie International Edition, 52 (2013) 10349-10351.
- [72] V.M. Gun'ko, E.F. Voronin, V.I. Zarko, E.V. Goncharuk, V.V. Turov, S.V. Pakhovchishin, E.M. Pakhlov, N.V. Guzenko, R. Leboda, J. Skubiszewska-Zięba, W. Janusz, S. Chibowski, E. Chibowski, A.A. Chuiko, Colloids and Surfaces A: Physicochemical and Engineering Aspects, 233 (2004) 63-78.
- [73] J. Lu, Q. Nguyen, J. Zhou, Z.-H. Ping, Journal of Applied Polymer Science, 89 (2003) 2808-2814.
- [74] L. Liu, in, Fudan University, China, 1992.
- [75] M. Akagi, S. Nonogaki, T. Kohashi, Y. Oba, M. Oikawa, Y. Tomita, Polymer Engineering & Science, 17 (1977) 353-355.
- [76] S. Uppalapati, S. Chada, M.H. Engelhard, M. Yan, Macromolecular Chemistry and Physics, 211 (2010) 461-470.
- [77] J.M. Notestein, A. Katz, Chemistry A European Journal, 12 (2006) 3954-3965.
- [78] M.E. Davis, A. Katz, W.R. Ahmad, Chemistry of Materials, 8 (1996) 1820-1839.
- [79] A. Katz, M.E. Davis, Nature, 403 (2000) 286-289.
- [80] O.M. Gazit, A. Charmot, A. Katz, Chemical Communications, 47 (2011) 376-378.
- [81] M.K.P.-T. Wiedmann, Y.J.; Tucker, M.H.; Dumesic, J.A.; Kuech, T. F., in: MRS Spring Meeting, 2011.

Chapter 2: Experimental

2.1 Catalyst Synthesis and Preparation

Hydrogenation Catalysts. Catalysts were prepared by incipient wetness impregnation of supports with aqueous solutions of Ru(NO)(NO₃)₃ (Strem Chemical), H₂PtCl₆·6H₂O (Strem Chemical), or Pd(NO₃)₂ (Aldrich) (Figure 2.1). The supports used were Vulcan XC-72 (Cabot Corp.), γ-Al₂O₃ (Strem), CeO_x (prepared as in ¹), magnesia-zirconia (as prepared in ²) and fumed SiO₂ (Cab-O-Sil EH-5, Cabot Corp.). After impregnation, the catalysts were dried at 393 K overnight, reduced under flowing H₂ using a 3 hour ramp and a 5 hour hold at 573 K, and passivated with 2% O₂ in helium at 298 K. Ru-black was purchased from Sigma Aldrich and used after reduction at 573 K for 5 hours followed by passivation using 2% O₂ in He at 298 K.

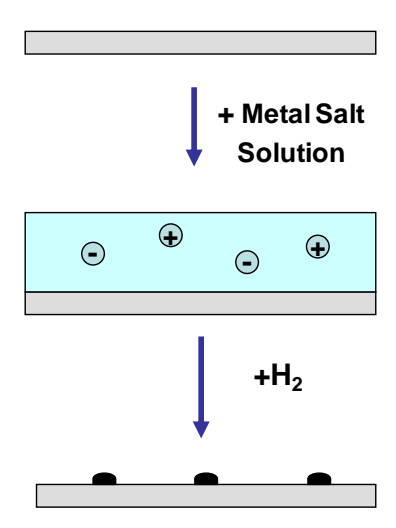


Figure 2.1. Schematic for the incipient wetness impregnation of a metal salt aqueous solution on a support.

Commercial Brønsted Acid Catalysts. Propylsulfonic acid functionalized silica spheres were purchased and used as is from Silicycle and used in Chapter 5.

Propylsulfonic Acid functionalized SBA-15 (pSO₃H-SBA-15). Sulfonic acid modified catalysts were prepared in the Scott Lab (University of California, Santa Barbara) and were

stored in an argon-filled glovebox to prevent readsorption of atmospheric moisture. The synthesis methods of sulfonic acid functionalized silica or SBA-15 was done by grafting or co-condensation. No catalysts acid functionalities were prepared via post-synthetic modification.

Nanocomposite synthesis. Each silica-based catalyst was modified using an incipient wetness (IW) method. The IW solution contained PVP (Sigma, MW ca. 29,000) dissolved in a warm (313 K) solvent mixture. The IW solution was optimized by varying PVP loading for each silica support. After cooling to RT, benzyl peroxide (BP) was added to the solution in the dark. For SBA-15 and pSO₃H-SBA-15, the solutions contained 0.1 g PVP and 0.1 g BP in 4 g 1:1 THF:H₂O. For pSO₃H-MCM-41, the solution contained 1 g PVP and 0.5 g BP in 4 g 1:1 THF:H₂O. For pSO₃H-SS, the solution contained 2 g PVP and 0.5 BP in 4 g H₂O. The mixture was added to the silica until it reached its IW point. The solids were dried under vacuum at 313 K for 2 h, crushed, and cross-linked under UV radiation (240 nm) for 10 min. Soluble polymer was removed using a Soxhlet extractor and DI water for 15 h. The resulting solids were dried overnight in a vacuum oven at 313 K. Polyvinyl alcohol (Sigma, MW. Ca 50,000) was used a control for polymer functionaility test runs.

Acid functionilized Mesoporous Carbons. The synthetic approaches for acid-functionalized mesoporous carbons are shown in Figure 2.2. CMK-3 and CMK-5 were synthesized based on previous reports ^{3, 4}, however, pyrolysis was carried out at 1273 K under helium flow. The carbon functionalization reaction was based on the method reported by Wang et al. ⁵. First, a solution of 0.075 mol of p-sulfanilic acid or 4-Amino-1-naphthalenesulfonic acid in 750 mL of 1 mol L⁻¹ aqueous HCl was prepared. The solution was cooled to 276-278 K followed by the dropwise addition of 82.5 mL of 1 mol L⁻¹ aqueous NaNO₂. Then, 1.2 g of the carbon support was added and the dispersion was stirred for 5 h at 3-5 °C. Finally, the material

was filtered and washed thoroughly with water. The functionalization reaction mechanism involves the *in situ* formation of a diazonium compound that binds to the carbon support through a C-C bond. Throughout this synthesis method, CMK-3 was functionalized with phenylsulfonic acid (PSA) or naphthalenesulfonic acid (NSA) and CMK-5 was functionalized with PSA. CMK-3 was also functionalized with sulfonic acid groups by treatment with sulfuric acid ⁶.

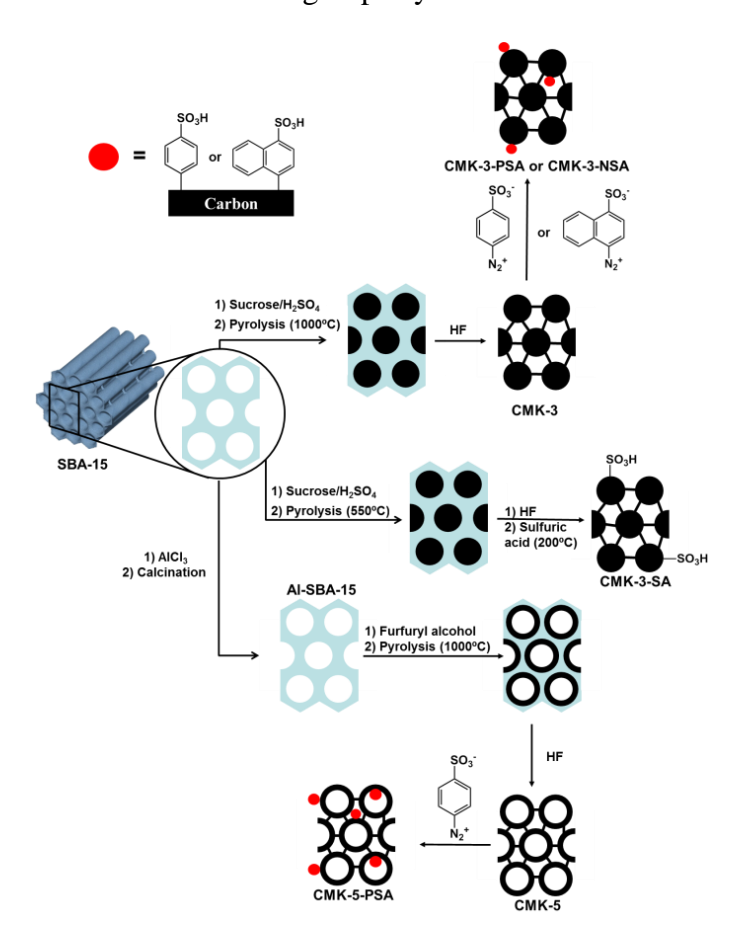


Figure 2.2. Preparation route for the acid mesoporous carbons.

RhRe Bimetallic Catalysts. Metal catalysts were prepared by incipient wetness impregnation of Vulcan XC-72 with aqueous solutions of RhCl₃ and NH₄ReO₄. The RhRe/C catalyst was obtained by successive impregnation of dried, unreduced Rh/C with NH₄ReO₄. This RhRe/C catalyst consisted of 4 wt% Rh and an atomic ratio of Rh:Re = 1:0.5. Prior to use in

experiments, catalysts were dried in air (393 K), reduced in flowing H_2 (723 K), and passivated with flowing 1% O_2 in He (298 K). ZSM-5 (Engelhard, Si/Al = 30) was calcined *in situ* at 723 K for 4 h in flowing air prior to introduction of liquid feed in continuous flow studies

Synthesis of benzene-bridged periodic mesoporous organosilica (PMO). The PMO was synthesized utilizing a modified literature protocol. Pluronic P123 (1.00 g) was dissolved with stirring in 0.2 M aqueous HCl (108 mL) at 298 K in a 500 mL HDPE bottle (Nalgene). BTEB (1.00 g, 2.48 mmol) was added dropwise. After 1 h, the sol-gel reaction mixture was heated to 313 K and stirred for 23 h. The resulting suspension was transferred into two Parr bombs, and heated at 373 K for 24 h. The solid was isolated by vacuum filtration and washed with 500 mL ethanol. The air-dried solid was re-suspended in ethanol and refluxed for 15 h. The solid was re-collected and dried overnight at room temperature. The templating surfactant was removed by calcination in a tube furnace at 373 K for 2 h (5 K min⁻¹) then at 573 K for 4 h (2.5 K min⁻¹) under flowing air.

General synthetic procedure for Sn-containing PMOs (Sn-PMO). The procedure described above for PMO synthesis was followed, with one modification. At 15 min following the addition of BTEB, the appropriate amount of solid SnCl₄·5H₂O (either 0.026, 0.052, 0.134, or 0.268 mmol) was added to the reaction mixture.

Post-synthetic Sn addition to PMO. SnCl₄·5H₂O (24 mg, 0.068 mmol) was dissolved in 4 mL methanol. This solution was added dropwise to a 20 mL vial containing 750 mg PMO, and stirred for 24 h. Triethylamine (38 μL, 0.274 mmol) was then added to catalyze the hydrolysis of remaining SnCl₄ and neutralize the HCl generated. After both additions, the suspension was stirred for an additional 2 h. The solid was isolated by filtration, washed with ca. 500 mL methanol, and then calcined according to the method described above.

Synthesis of propylsulfonic acid-functionalized Sn-PMO (pSO₃H-Sn-PMO). Pluronic P123 (3.00 g) was dissolved with stirring in 0.2 M aqueous HCl (108 mL) at 298 K in a 500 mL HDPE bottle (Nalgene). BTEB (2.88 g, 7.15 mmol) was added dropwise. After 15 min, SnCl₄·5H₂O (28 mg, 0.080 mmol) and MPTMS (150 μL, 0.81 mmol) were added sequentially to the solution. After 1 h, H₂O₂ (1 mL, 30 wt. %) was added and the sol-gel reaction mixture was heated to 313 K with stirring for 23 h. The suspension was transferred into two Parr bombs that were heated at 373 K for 24 h. The solid was isolated by vacuum filtration and washed with 500 mL ethanol. To extract the templating surfactant, the air-dried solid was suspended and refluxed three times in ethanol for 15 h. After the third extraction, the solid was re-collected and air-dried overnight at room temperature. The powder was further dried in a tube furnace at 373 K (5 K min⁻¹) for 4 h under flowing N₂.

Faujasites. NaX (SiO₂/Al₂O₃ = 2.8:1) and NaY (SiO₂/Al₂O₃ = 5.1:1) zeolites were purchased through Strem. The catalyst were calcined in static air at 573 K before reactivity studies. FAU zeolites are typical large-pore microporous solids, with supercages 11.24 Å in diameter and 12 atom-ring apertures of 7.35 Å.

Sn-Beta Zeolite. Dealuminated Sn-beta zeolite (Si/Sn = 200) was synthesized at the Technical University of Denmark (DTU) based on a zeotype synthesis procedure reported by Corma et al.⁸

2.2 Catalyst Characterization

Nitrogen Physisorption. Nitrogen adsorption-desorption isotherms were measured at 77 K using a Micromeritics ASAP 2020 system or a Quantachrome Autosorb-1 analyzer. The samples were pretreated under vacuum at 393 K for 12 h. Surface areas were determined using the BET method.

Chemisorption Studies. Measurements of CO chemisorption on 1 wt% Ru, Pt, and Pd supported catalysts were carried out using a Micromeritics ASAP 2020 system. Prior to measurements, catalysts were reduced in flowing H₂ for 3 h at 538 K (1.5 K min⁻¹) and purged for 1 h with ultra-high purity He (200 cm³(STP) min⁻¹) at 538 K. Catalysts were cooled to 300 K, followed by subsequent dosing of CO. The gas phase was then evacuated for 1 h and a second isotherm was collected, and the irreversible CO uptake was determined by subtracting the two isotherms. Pd dispersions were calculated based on a Pd:CO stoichiometry of 2:1.

Scanning and Transmission Electron Microscopy. SEM and TEM images were acquired using a Hitachi S-4800 microscope and a FEI G2 T20 microscope, respectively.

ICP Analysis. Any metal leaching was studied and analyzed using a Perkin-Elmer Plasma 400 ICP emission spectrometer.

Elemental Analysis. For CHNSO elemental analysis, samples will be sent to and performed by Columbia Analytics (Tucson, AZ). The results are quantitative amounts of total acid sites (S) and the total amount of PVP (N) on the catalyst.

Thermogravimetric Analysis. TGA was collected on a TA Instruments Q500 Thermogravimetric Analyzer using a platinum sample pan, a ramp rate of 10 K/min to 1073 K and a N_2 purge.

Powder X-Ray Diffraction. Data was collected from 0.6 to 5.0° [2 θ] using a Siemens STOE diffractometer with Cu K α radiation.

NH₃ Temperature Program Desorption. Temperature programmed desorption of NH₃ was used to measure the total numbers of acid sites. The reactor consisted of a tube furnace connected to a variable power-supply and PID temperature controller (Love Controls) with a K-type thermocouple (Omega). The effluent was monitored by a mass spectrometer system

comprising a quadruple residual gas analyzer (Stanford Instruments RGA 200) inside a vacuum chamber. Vacuum was provided by a diffusion pump backed by a rotary pump. The effluent was introduced into the vacuum chamber via a constricted quartz capillary tube, creating a pressure of 5x10⁻⁵ Torr inside the chamber. Dried catalysts (~100 mg) were loaded into a 12.6 mm outer diameter glass flow through cell, fritted quartz tube. The samples were degassed with flowing helium for 1 hr at the reduction temperature (200 cm³ (STP) min⁻¹), and then cooled to 423 K. Samples were dried under flowing He at 423 K prior to NH₃ adsorption. NH₃ was adsorbed on the samples by exposure to a flowing gas mixture of 1 mol% NH₃ in He (100 cm³(STP) min⁻¹) at 423 K for 45 min. Residual ammonia was desorbed at 423 K with a He purge (150 cm³(STP) min⁻¹). Temperature programmed desorption was performed using a temperature ramp of 10 K min⁻¹ from room temperature to 1073 K under flowing He (50 cm³(STP) min⁻¹), and NH₃ desorption was quantified by an on-line mass spectrometer.

Solution and Solid State NMR. Polymer-over coated samples were studied using a Solid-state NMR spectra (²⁹Si MAS and ¹³C CP/MAS) were recorded (25,000 scans) on a Bruker IPSO500 WB spectrometer operating at 12.0 T, with a 4 mm probe at a spin rate of 10,000 Hz. Chemical shifts were referenced using tetrakis(trimethylsilyl)silane.

Fructose tautomer compositions in NMP and PVP solutions were analyzed according to our method described previously.^[1] To determine the effects of PVP-SBA-15 and SBA-15 on fructose tautomerization, slurries of each material were prepared with 0.10 M ¹³C-labeled D-fructose (2-¹³C, Cambridge Isotopes Laboratories) and ¹³C-labeled dimethylformamide (Cambridge Isotopes, analytical standard, 0.10 M) in THF-*d*₈:D₂O (4:1). The wet solids were packed into 4 mm rotors. ¹³C HR-MAS spectra (pulse sequence: zgig30, relaxation delay: 10 s,

25,000 scans, without spin) were collected on a Bruker DMX500 SB spectrometer operating at 12.0 T.

2.3 Reaction Studies

2.3.1 Batch Reaction Studies

2.3.1.1 HMF Hydrogenation Studies

Batch HMF hydrogenation experiments used to study selectivity (Chapter 3) were carried out using a 50 mL pressure vessel (Hastelloy C-276, Parr Instrument). In a typical experiment 8 g of aqueous layer, 16 g organic layer and a specified amount of catalyst were added to the pressure vessel. The aqueous layer consists of 5 wt% 5-hydroxymethylfurfural, HMF (99%, Aldrich) in water pre-saturated with 1-butanol. The aqueous layer was filtered before reaction (to remove insoluble impurities from the commercial HMF), and in noted reactions, the feed was contacted with 1.5 g of Amberlite IRA-400(OH) (Aldrich) before filtering. In noted experiments, levulinic acid or sulfuric acid was added to the aqueous layer after the HMF solution was contacted with Amberlite IRA-400(OH) and filtered. The organic layer consisted of 1-butanol saturated with water. Alternatively, in several single phase experiments, 24 g of the single phase solvent with 1.67 wt% HMF was added to the reaction vessel after filtering. The reactor was sealed, purged with He and then H2 and then pressurized to 400 psi H2. The reactor was heated using a 30 minute ramp to 130 °C and held for a specified amount of time before the reaction was quenched in an ice bath. The reaction was stirred with a magnetic stirrer bar and a magnetic stirrer plate.

After reaction the contents were filtered, separated and analyzed using HPLC.

The conversion and selectivity were calculated using the equations below, where substrate is

HMF. 1,2,5-Hexanetriol and 1,2,5,6-hexaneterrol were purified from the reaction mixture by HPLC, dried using a rotary evaporator, and analyzed in D2O using solution state NMR. The HPLC sensitivity for 1,2,5-hexanetriol and 1,2,5,6-hexaneterrol were assumed to be equal to the measure sensitivity of 1,2,6-hexanetriol.

Conversion, selectivity, and yield are defined as:

$$Conversion = \frac{moles\ substrate\ reacted}{moles\ of\ \ initial\ substrate}$$

$$Selectivity = \frac{moles\ of\ product}{moles\ of\ substrate\ reacted}$$

$$Yield = \frac{moles\ of\ product}{moles\ of\ initial\ substrate}$$

2.3.1.2 Fructose Dehydration and Glucose Isomerization Studies

Batch dehydration and isomerization reaction studies with varied solvent systems in Chapters 4-5, were carried out in 10 mL thick-walled glass reactors (Alltech) with a triangular magnetic stir bar and a cap liner (Figure 2.3). In a typical experiment, 1.5 mL of the aqueous layer were added to the reactor. Reactors were tightly sealed and placed in an oil bath heated at 403 K or the specified temperature and stirred at 700 rpm by an Isotemp digital stirring hotplate (Fisher Scientific). Reactors were removed at specific reaction times and cooled in an ice water bath. After reaction the reactors were centrifuged for 4 min at 3000 rpm for complete separation of the solid catalysts and aqueous phases for subsequent catalyst recovery. The aqueous phases were collected with pipettes and the density of each phase was recorded. Systems mixed with an organic solvent were diluted with Milli-Q water by a factor of 5 before HPLC injection.





Figure 2.3. (A) Thick-walled glass reactor with triangular magnetic stir bar used in batch dehydration and isomerization experiments (B) Stirrer hotplate with silicon oil bath used for dehydration experiments.

2.3.2 Flow Reaction Studies

Flow reaction studies were carried out in an up-flow tubular reactor, Figure 2.4. The reactor consisted of a 1/4 inch-outer diameter stainless steel tube. In a typical run, approximately 0.05-0.5 g of catalyst was mixed with silica chips and loaded in the tube. The catalyst bed was held in place by quartz wool at each end (Alltech). The tubular reactor was connected to inlet and outlet gas and liquid flow lines and placed in the heating zone of the furnace lined with aluminum blocks. A thermocouple (K-type) was placed between the aluminum blocks and the

reactor tube to monitor the reactor temperature controlled by a series 16A temperature controller (Dwyer or Love Controls). Liquid feeds were introduced by an HPLC pump (Lab Alliance Series 1). Gas flow rates for catalyst pre-treatment or as a sweep gas flow to the reactor were controlled by a mass flow controller Brooks Model 5850. A gas-liquid separator connected at the outlet of the reactor was used to collect the reaction mixture.

At higher flow rates, the HPLC pump was turned off during sampling of the reactor. To maintain constant pressure in the reactor, a valve just after the reactor was closed during sampling, and pressurized with He before resuming the HPLC pump. When the flow rates would be low, the HPLC pump was maintained on, and the valves were closed at the top of the reactor, liquid effluent samples collected, and reopened to assume operation. Pressure lost was minimal and the system was pressurized with the sweeping He gas in the system. Gas effluents from the reaction were analyzed by on-line GC equipment. Liquid effluents were collected in a liquid-gas separator at room temperature and compositions were quantified by HPLC or GC. WHSV was calculated based on the reactant mass (on a dilute free basis). Detailed experimental procedures for the flow reaction studies are discussed in Chapter 5 and 6, including catalyst pretreatment conditions prior to reaction kinetic measurements and feed compositions.

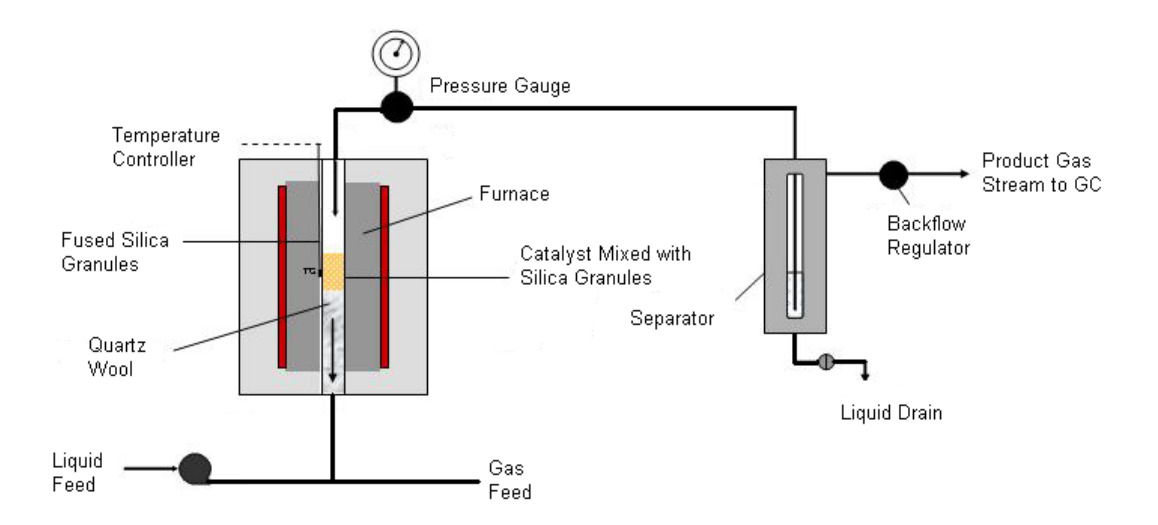


Figure 2.4. Detailed schematic of the up-flow reactor setup used for reaction kinetic experiments. Adapted from ⁹.

Catalyst deactivation studies in Chapter 5 were down in a down-flow reactor and consisted of a ½" diameter stainless steel tubing. The bottom of the catalyst bed was held in position by a ½" diameter by 1/16" thickness stainless steel porous disk (2 micron, McMaster-Carr) which was places between the end of the reactor tubing and a Swagelok fitting. The catalyst was packed tighyly with quartz wool (Grace) and remaining space in the ½" tubing was filled with fused silica granules (4-16 mesh, Sigma) to minimize dead volume. The reactor was well insulated and heated using a single piece of electric heating tape (Cole-Parmer) which was wrapped around the reactor bed and around the preceding section of the reactor to preheat the liquid stream and minimize temperature fluctuations and maintain a constant temperature. The feed flow rate was kept constant over the course of reaction. This reactor was set-up to decrease catalyst bed length to eliminate channeling effects and to quantify deactivation rate coefficients. Instrumentation before and after the reactor bed are analogous to those mentioned in the previous paragraph for the ¼" reactor set-up.

The first data point collected in all samples was considered transient and only points after were collected and used to quantify reaction rates. Glucose, fructose, and HMF were quantified using an HPLC (Section 2.4). Conversion was calculated by the moles of substrate (feed) reacted divided by the moles of substrate fed into the reactor as shown Equation 1. Substrates in these cases were either fructose or glucose. Selectivity to a product (i) is given in equation 2. $R_{i,in}$ and $R_{i,out}$ are the molar flow rates of species in and out of the reactor system, respectively. The weight-hour space velocity (WHSV) was calculated as the mass of substrate (on a diluent free method) divided by the mass of catalyst in the reactor. Initial rates of reactions were extrapolated back to time zero when the reactor was started. The first order deactivation rate coefficient was calculated by the slope of the log of product formation rate with time (multiplied by -1).

$$Conversion_{substrate} = \left(\frac{R_{substrate,in} - R_{substrate,out}}{R_{substate,in}}\right) x \ 100\% \tag{1}$$

$$Selectivity_{Product,i} = \frac{R_{product,i}}{R_{substrate,in} - R_{substrate,out}} \times 100\%$$
 (2)

2.4 Sample Analysis

HPLC Analysis. A Waters e2695 HPLC system equipped with a 2998 PDA UV detector and a 2414 refractive index detector was used for quantification of reactants and products. The system was equipped with an Aminex HPX-87H column (Biorad) at 353 K, using 0.005 M H₂SO₄ solution as the mobile phase at a flow rate of 0.6 mL min⁻¹ or with an Aminex HPX-87P (Bio-Rad) column at a temperature of 358 K using Mili-Q (pH 7) water as the mobile phase at a flow rate of 0.6 mL min⁻¹. Both columns were typically used for analysis of species found in the aqueous layer. Details on the HPLC column and method used for each species are discussed in detail in each chapter.

GC Analysis. The gas effluent stream from the flow reactor was analyzed by an on-line GC system. Two different GC instruments in series were used; a Carle GC (Series 400 AGC) using a TCD detector and a Porapak Q packed column (Alltech) for CO, CO₂ analysis and a Varian GC (Saturn 3) equipped with an FID detector and a GS-Q column (J&W Scientific) for gaseous hydrocarbons, alcohols, and evaporated solvent. GC analysis of liquid collected from the gas-liquid separators of the flow reactor was analyzed in a Shimadzu GC-2010 equipped with an FID detector and SHRX5 column.

2.5 Synthesis of DHMTHF for use as a solvent and standard

In a typical synthesis, 28.45 g of DI water (saturated with 1-butanol), 60 g of 1-butanol (saturated with water), 1.55 g HMF (99%, Sigma-Aldrich), and 0.87 g of 10 wt % Pd/C (Sigma-Aldrich) were added to a 300 mL stainless steel Parr reactor. The reactor was purged three times with He, and four times with H₂, and charged to 400 psig H₂ at room temperature. The reactor was heated to 403 K at a 10 K/min and held for at least 8 hours. The selectivity to DHMTHF from HMF as above 90% after complete HMF conversion, as determined by HPLC. After cooling to room temperature, the contents were filtered and concentrated in a rotary evaporator to remove water and butanol.

2.6 References

- [1] E.I. Gürbüz, E.L. Kunkes, J.A. Dumesic, Applied Catalysis B: Environmental, 94 (2010) 134-141.
- [2] M.a.A. Aramendía, V. Boráu, C. Jiménez, A. Marinas, J.M. Marinas, J.A. Navío, J.R. Ruiz, F.J. Urbano, Colloids and Surfaces A: Physicochemical and Engineering Aspects, 234 (2004) 17-25
- [3] M. Kruk, M. Jaroniec, T.W. Kim, R. Ryoo, Chem. Mater., 15 (2003) 2815-2823.
- [4] S. Jun, S.H. Joo, R. Ryoo, M. Kruk, M. Jaroniec, Z. Liu, T. Ohsuna, O. Terasaki, J. Am. Chem. Soc., 122 (2000) 10712-10713.
- [5] X.Q. Wang, R. Liu, M.M. Waje, Z.W. Chen, Y.S. Yan, K.N. Bozhilov, P.Y. Feng, Chem. Mater., 19 (2007) 2395-2397.
- [6] R. Xing, Y.M. Liu, Y. Wang, L. Chen, H.H. Wu, Y.W. Jiang, M.Y. He, P. Wu, Microporous Mesoporous Mater., 105 (2007) 41-48.
- [7] Y. Goto, S. Inagaki, Chem. Commun., (2002) 2410-2411.
- [8] M. Renz, T. Blasco, A. Corma, V. Fornés, R. Jensen, L. Nemeth, Chemistry-A European Journal, 8 (2002) 4708-4717.
- [9] Y. Roman-Leshkov, C.J. Barrett, Z.Y. Liu, J.A. Dumesic, Nature, 447 (2007) 982-985.

Chapter 3: The Selective Hydrogenation of Biomass-derived 5-Hydroxymethylfurfural using Heterogeneous Catalysts¹

3.1 Introduction

The hydrogenation of the aldehyde group in platform chemical, 5-hydroxymethylfurfural (HMF) forms 2,5-dihydroxymethylfuran (DHMF) while complete hydrogenation of the ring leads to 2,5-dihydroxymethyltetrahydrofuran (DHMTHF). DHMF and DHMTHF can be used as a useful chemical with applications as a solvent²,a monomer³, or precursor to the production of other high-value chemicals.^{4, 5} For example, DHMTHF can be converted to 1,6-hexanediol, a valuable chemical for use in polymers and specialty chemicals, through the use of hydrogenolysis and dehydration reactions.⁵⁻¹⁰

The conversion of HMF to 2,5-dihydroxymethylfuran (DHMF) or DHMTHF has been studied previously in the literature by several authors^{9,11}. Schiavo, et al. achieved high selectivities (80-100%) to either DHMF or DHMTHF using heterogeneous catalysts based on Ni, Cu, Pt, Pd, or Ru in neutral solution¹¹. In an acidic solution using Ru or Pt as a catalyst, the major products were 1-hydroxyhexane-2,5-dione and 1,2,5-hexanetriol. Nakagawa and Tomishige studied the hydrogenation of HMF using Ni-Pd bimetallic catalysts and found that a Ni/Pd ratio of 7 led to high DHMTHF selectivities (96%).⁹ Nakagawa and Tomishige reported that the hydrogenation of HMF can proceed to DHMTHF either by saturating the aldehyde first (forming DHMF), or by saturating the ring first (forming 5-hydroxymethyl-2,3,4,5-tetrahydro-2-furaldehyde (HMTF)).

The use of DHMTHF as a solvent has been shown to be effective for the dehydration of fructose to HMF (Chapter 4), and a dual reactor design was proposed for the formation of DHMTHF from fructose (Section 4.1). In this chapter, we have studied the hydrogenation of HMF to assess the feasibility of a dual-reactor system employing fructose dehydration combined with

HMF hydrogenation for production of DHMTHF. The influence of catalyst support, solution acidity, solvent, and catalyst metal type on the selectivity to DHMTHF were studied, and we have probed the primary mechanism to side products.

3.2 Selective Hydrogenation of HMF to DHMTHF

3.2.1 Support Effects with Ruthenium Catalysts

The hydrogenation of HMF was carried out using catalysts consisting of ruthenium supported on carbon and various oxides. In this study, a biphasic system composed of water and 1-butanol was chosen as the reaction solvent because it has previously been used in the production of HMF from fructose, and because this solvent is inert under hydrogenation conditions. A reaction temperature of 403 K was used because fructose dehydration to HMF readily occurs at this temperature, and this hydrogenation temperature would thus be suitable for coupling of fructose dehydration to HMF with the subsequent hydrogenation of HMF to DHMTHF.

A typical reaction profile for the hydrogenation of HMF over Ru/CeO_x is shown in Figure 3.1. The selectivity to each product as a function of time is shown in Figure 3.2. At a reaction time of 2 hours, complete conversion of HMF was achieved, and the primary products formed were DHMF and DHMTHF at selectivities of 81% and 4%, respectively. Upon increasing the reaction time to 6 hours, the DHMF was converted to DHMTHF, leading to overall selectivities of 32% and 48% to DHMF and DHMTHF, respectively. The other major products observed were the following polyols: 1,2,6-hexanetriol (1,2,6-HT), 1,2,5-hexanetriol (1,2,5-HT), and 1,2,5,6-hexanetetrol (1,2,5,6-HT) at 2%, 2%, and 11% selectivity, respectively. After increasing the reaction time to 12 hours, the HMF and DHMF were both fully converted, and the main products were DHMTHF (91% selectivity), 1,2,6-HT (3% selectivity), 1,2,5-HT (1% selectivity), and 1,2,5,6-HT (6% selectivity). After complete hydrogenation was achieved, a longer reaction time

(i.e., 20 hours) did not significantly change the product distribution, indicating that the triols and tetrol were formed by reactions in parallel to the formation of DHMTHF rather than in series (Figure 3.1), as will be further discussed later (Section 3.2.3).

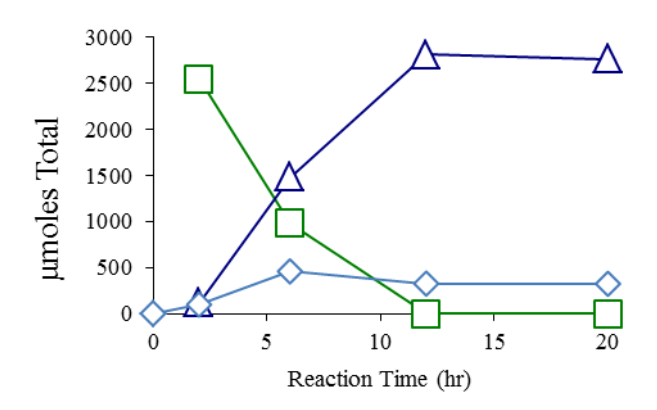


Figure 3.1. Formation of DHMTHF (triangle), DHMF (square) and polyols (diamond) as a function of reaction time for the hydrogenation of HMF using 1 wt% Ru/CeOx.

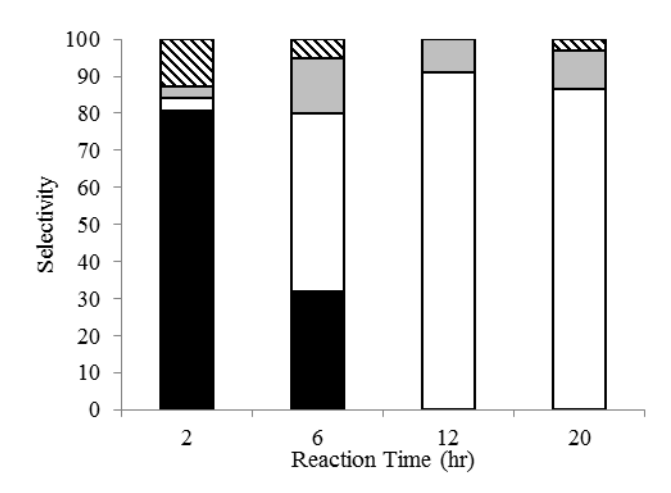


Figure 3.2. Selectivity to DHMF(black), DHMTHF(white), polyols(grey) and unidentified products (striped) as a function of reaction time for the hydrogenation of HMF over Ru/CeO_x

Figure 3.3. Hydrogenation of HMF to DHMTHF with DHMF as an intermediate and the proposed mechanism for the formation of 1,2,6-hexanetriol, 1,2,5,6-hexaneteriol, and 1,2,5-hexanetriol. Mechanism based on Horvat, et. al.¹²

Table 3.1 gives results for the hydrogenation of HMF using unsupported ruthenium (Rublack) and ruthenium supported on Vulcan carbon and oxides including fumed silica (SiO₂), magnesia-zirconia (Mg-Zr), and γ -Al₂O₃. The reaction network shown in Figure 3.3 adequately describes the results obtained for all of the catalysts, including (1) the presence of DHMF at low reaction times, (2) the appearance of the following polyols 1,2,5- HT, 1,2,6-HT, and 1,2,5,6-HT as byproducts, and (3) the stability of the completely hydrogenated products at long reaction times (for example when using Ru-black or Ru/Vulcan at long reaction times). The selectivity to DHMTHF varied considerably for the different catalysts. Of the oxide based supports, materials with high isoelectric points (Mg-Zr, CeO_x and Al₂O₃) produced DHMTHF at high selectivities of around 90%, while SiO₂ having a low isoelectric point produced DHMTHF with a lower selectivity. Unsupported Ru (Ru-black) and ruthenium supported on Vulcan carbon also exhibited

low selectivities to DHMTHF (about 50%). Interestingly, the selectivity to DHMTHF changed substantially with the amount of Ru/Vulcan used, while keeping all other conditions constant (Table 3.1). For example, DHMTHF was the major product observed using 200 mg of catalyst (with a selectivity of about 50%), followed by 1,2,5,6-HT (30%), and 125 HT and 126 HT (9% and 2%). Decreasing the catalyst mass to 50 mg decreased the amount of DHMTHF produced to a selectivity of 15% (when all of the HMF and DHMF were converted). The selectivity to 1,2,5-HT increased to 29%, the amount of 1,2,5,6-HT decreased, and the amount of 1,2,6-HT remained low. Furthermore, the selectivity to observed products decreased from about 90% to 56%. These changes in selectivity with catalyst loading indicate the contributions of reactions occurring in the liquid solvent that are not catalyzed by metal. Due to the higher selectivities achieved using supports with higher isoelectric points, it is suggested that these undesirable reactions in solution are acid-catalyzed degradation reactions.

Table 3.1. Product distribution for HMF hydrogenation at full conversion for various supports and reaction times. All reaction were run with 200 mg of catalyst in 2:1 bi-phasic 1-butanol:water batch reactor at 403 K and 400 psi H₂.

		Reaction Time (hr)	HMF Conversion (%)	Selectivity (%)					
	Support			DHMF	DHMTHF	1,2,6- HT	1,2,5- HT	1,2,5,6- HT	Total
Oxide Support, Isoelectr ic Point > 7	CeOx	2	100	81	4	0	1	2	87
		6	100	32	48	2	2	11	95
		12	100	0	91	3	1	5	100
		20	100	0	87	3	1	6	97
	Mg-Zr	2	99	94	2	0	0	2	99
		20	100	0	88	2	0	1	92
	γ-	2	92	81	5	0	0	2	88
	Alumina	12	100	0	89	2	3	5	100
Non- oxide Support	Vulcan Carbon	1 ^a	95	29	3	0	2	2	36
		10 ^a	100	0	15	1	29	12	56
		1	100	0	51	2	9	28	90
		2	100	0	50	2	9	28	89
		10	100	0	56	2	9	27	94
	Ru-Black	1 ^a	100	0	53	13	13	15	94
		2 a	100	0	46	13	13	11	84
		18 ^a	100	0	48	9	13	13	83
Isoelectr		1 ^a	80	64	0	0	0	1	65
ic Point									
< 7		2	100	0	53	3	13	20	89

^a 50 mg of catalyst was used in this run

3.2.2 Effect of support and solution phase acidity

Based on the hypothesis that acid-catalyzed degradation reactions take place in solution during the hydrogenation of HMF, we have explored whether acidic impurities could be present in the HMF feed. If this is the case, the beneficial effect of using supports with high isoelectric points may be due to the adsorption of acidic species in solution. In this respect, HMF is commonly produced by the dehydration of monosaccharides in acidic solutions, with levulinic acid and formic acid being generated as byproducts from HMF rehydration.

Either the acid catalyst or these acidic byproducts could be present in the HMF feed. To study if acidic impurities are the cause of low selectivities for hydrogenation of HMF, the feed was treated with a basic ion-exchange resin before reaction, i.e., using Amberlite IRA-400(OH). After treatment, the resin was removed by filtration, and the hydrogenation of HMF was carried out using either Ru/Vulcan or Ru-black as a catalyst. Treatment of the HMF feed with resin led to an increase of over 20% in the selectivity to DHMTHF using both Ru catalysts, as seen in Figure 3.4. Furthermore, treatment of the feed with the resin resulted in an increase in pH from slightly acidic (pH 5) to neutral (pH 6-7). This increase in pH suggests that minor impurities of acid mixed with HMF decrease the selectivity to DHMTHF.

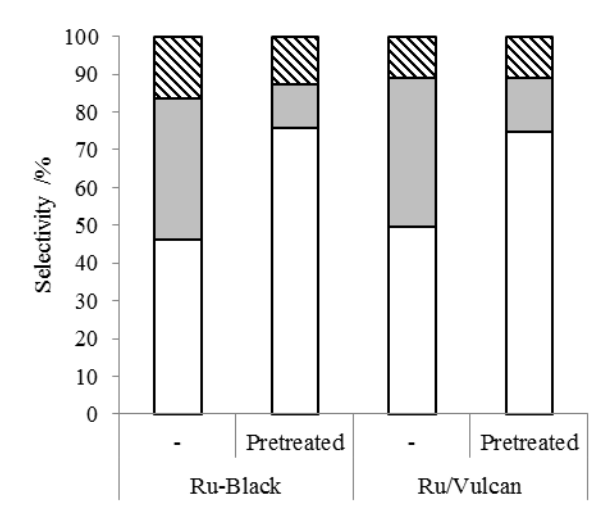


Figure 3.4. Selectivity to DHMTHF(white), polyols (grey), and unidentified products (striped) in the hydrogenation of HMF over Ru-black and 1 wt% Ru/Vulcan without and with feed pretreatment with Amberlite IRA-400(OH).

The selectivity to DHMTHF was also increased by adding solid materials with high isoelectric points to the Ru-black catalyst. When γ -Al₂O₃, with an isoelectric point of approximately 7-8, was added to the reaction mixture, the selectivity to DHMTHF increased from 46 to 85% at the expense of the polyols, as shown in Figure 3.5. This effect was more pronounced

when using magnesium oxide, which has an isoelectric point of 10-12, leading to a DHMTHF selectivity of 89%. The increase in DHMTHF selectivity in the presence of solid oxide materials with high isoelectric points demonstrates that the basicity of the catalyst support strongly affects the final product distribution in the hydrogenation of HMF.

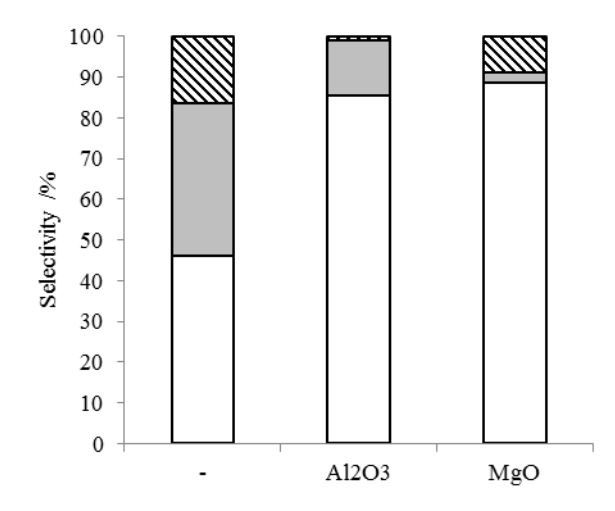


Figure 3.5. HMF hydrogenation to DHMTHF (white), polyols (grey), and unidentified products (striped) using 50 mg of Ru-black as a catalyst and 500 mg of high-isoelectric point solids.

As shown in Table 3.1, DHMTHF was formed with low selectivity (53%) when ruthenium supported on silica was used as a catalyst. In addition to the acidic impurities in solution, the low isoelectric point of silica could lead to a decrease in the selectivity to DHMTHF. Thus, the hydrogenation of HMF was studied using a feed that had been contacted with Amberlite IRA-400(OH), and using Ru-black as a catalyst with the addition of 500 mg of silica. As seen in Figure 6, the addition of silica decreased the selectivity to DHMTHF from 76% to 64% and increased the formation of polyols, indicating the important effect of the weak acidity of silica.

To elucidate the effects on the hydrogenation of HMF of specific types of acids, levulinic acid and H_2SO_4 were added to the reaction mixture that had been contacted with Amberlite IRA-400(OH), to isolate the effects of each acid. Levulinic acid is an example of an acidic degradation

product of HMF, whereas H₂SO₄ was studied as an example of a homogeneous catalyst that can be used for the production of HMF. As shown in Figure 3.6, addition of levulinic acid to the reaction mixture (1:4 wt:wt ratio of levulinic acid to HMF) resulted in a decrease in DHMTHF yield and an increase in the selectivity to the triols and tetrol, whereas the overall selectivity to known products remained constant. Addition of H₂SO₄ had a more significant effect on the selectivity to DHMTHF, which decreased from 76% to 9% with the addition of H₂SO₄ (0.084 M with respect to the aqueous layer, 3 times lower than the amount used in literature for the dehydration of fructose¹³). This decrease in DHMTHF selectivity was accompanied by an increase in the polyols selectivity, and the selectivity to observable products decreased. This decrease in selectivity to observable products may be due to formation of insoluble polymer of the reactive DHMF intermediate.

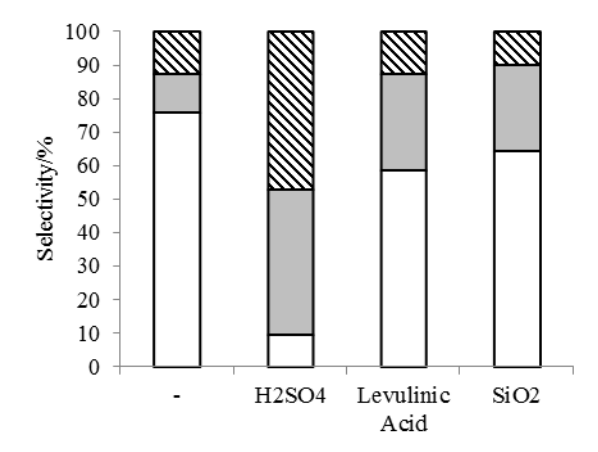


Figure 3.6. Product selectivities for the hydrogenation of HMF to DHMTHF (white), polyols (grey) and unidentified (striped) over Ru-black (50 mg) in the presence of added acids. Feed was treated with 1.5g Amberlite IRA-400(OH) prior to acid addition.

Because polyols are formed in parallel to the production of DHMTHF, it is possible that either the HMF or DHMF undergo acid-catalyzed degradation reactions. Accordingly, the hydrogenations of HMF and DHMF were each studied in a 1-butanol/water biphasic system with

0.011 M H₂SO₄ (with respect to the aqueous phase). Under these conditions, HMF did not undergo reaction after 10 minutes at 403 K. On the other hand, DHMF reacted rapidly, with 59% and 98% conversion after 4 and 10 minutes at 403 K. With these results, it appears that the production of 1,2,6-HT, 1,2,5-HT, and 1,2,5,6-HT originates from DHMF by acid catalyzed reactions, followed by hydrogenation of acid-catalyzed ring-opening and hydration/dehydration reactions.

Proposed mechanisms for the production of 1,2,6-HT, 1,2,5-HT, and 1,2,5,6-HT are shown in Figure 3.3. The mechanisms for the formation of 1,2,5-HT, and 1,2,5,6-HT are based on the mechanism for conversion of HMF to levulinic acid proposed by Horvat, et al.¹² The mechanism for the formation of 1,2,6-HT is based on ring opening of DHMF to form a conjugated ketone-diene, followed by hydrogenation. The mechanisms for the formation 1,2,5-HT and 1,2,5,6-HT require the presence of water. Therefore, the selectivity to DHMTHF should be affected by the solvent system, as studied below.

3.2.3 Solvent Effects on HMF Hydrogenation

Figure 3.7 presents results for the hydrogenation of HMF using the water/1-butanol biphasic system, and single phase systems composed of water, a mixture of tetrahydrofuran (THF) with water, and tetrahydrofurfuryl alcohol (THF-alcohol). The overall weight percent of HMF in the reactor (1.7 wt%), the loading of the Ru-black catalyst (50 mg), and the reaction time (2 hours) were held constant. Both HMF and DHMF were completely converted in each of the reactions. It can be seen that the selectivity to DHMTHF decreased from 43% to 18% and the selectivity to 1,2,5-HT increased from 13% to 32%, when the solvent was changed from the water/1-butanol biphasic mixture to pure water.

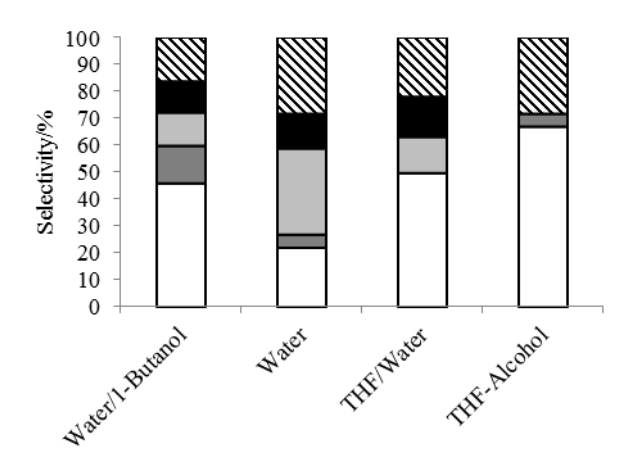


Figure 3.7. HMF hydrogenation in different solvents using 50 mg Ru-black as a catalyst. Products include DHMTHF(white), 1,2,6-HT (dark grey), 1,2,5-HT (light grey), 1,2,5,6-HT (black), and unidentified products (downward vertical stripes).

These changes give support to the proposed reaction mechanism for the formation of 1,2,5-HT, which includes a hydration step. Surprisingly, the formation of 1,2,5,6-HT, which requires the net addition of water regardless of mechanism, remained nearly constant when changing from the water/1-butanol system to the pure water system. The overall selectivity to known products decreased when changing from water/1-butanol to water as the solvent, indicating the presence of additional degradation pathways in the presence of water.

The hydrogenation of HMF was studied in a solvent consisting of a THF/water mixture (4:1 THF:water), because this solvent system is selective for the production of HMF from fructose. The product distribution for THF/water was nearly the same as that of the water/1-butanol biphasic system. This result indicates that degradation reactions involving water are important in monophasic systems containing water, as well as in biphasic systems where one of the phases is water. This behavior is caused by the low partition coefficient of HMF in the 1- butanol/water system, (where the partition coefficient is equal to the concentration of HMF in the organic phase divided by the concentration in the aqueous phase).

Studies of HMF hydrogenation were also carried out using THF-alcohol as a solvent, because THF-alcohol is similar to the reaction product DHMTHF. Accordingly, the selectivity achieved using THF-alcohol as a solvent can give an indication of the selectivity that should be achieved when using DHMTHF as a solvent. As shown in Figure 3.7, the use of THF-alcohol as a solvent gave rise to an increase in the selectivity of DHMTHF, likely as a result of the absence of water. In agreement with the mechanism of Figure 3.3, 1,2,5-HT and 1,2,5,6-HT were not formed in the THF-alcohol solvent.

3.2.4 Effect of Metal Catalyst

Studies were conducted to probe how the selectivity for hydrogenation of HMF is affected by changing the nature of the metal component of the hydrogenation catalyst. All catalysts were studied using a biphasic system of water and 1-butanol, and the feed was contacted with Amberlite IRA-400(OH) before reaction to eliminate the effect of impurities in solution. The results are shown in Figure 3.8. Using either palladium or platinum as the catalyst, the majority of the HMF was converted to unidentified products except when using higher loading of Pd. The HPLC spectra of the product mixture did not reveal any significant peaks, which may indicate that the undetected carbon is in the form of insoluble polymers. These polymers may be formed through the loss of formaldehyde from DHMF, followed by furfuryl alcohol polymerization, which is well known in the literature. As evidence for this chemistry, we have detected the formation of formaldehyde dibutyl acetal (which was identified by GC/MS) when reacting DHMF in butanol under acidic conditions.

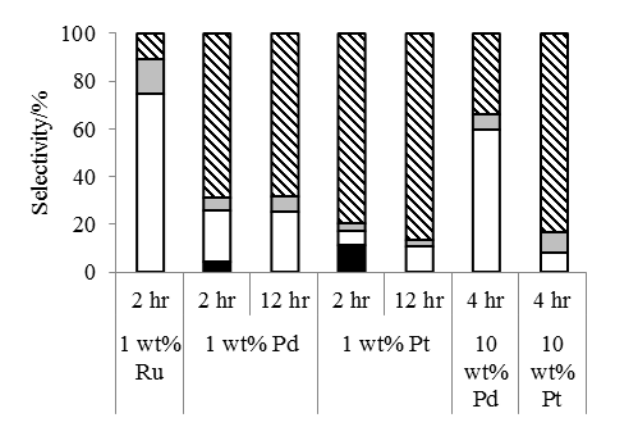


Figure 3.8. HMF Hydrogenation over Vulcan supported Ru, Pd, or Pt at various time points. Feed was purified with 1.5 g Amberlite IRA-400(OH) before reaction. Products observed DHMF (black), DHMTHF(white), polyols (grey), and unidentified products (striped).

After a reaction time of 2 hours, DHMF was observed from the hydrogenation of HMF when using palladium and platinum as catalysts, whereas DHMF had been fully consumed when using ruthenium, indicating that the same weight loading palladium and platinum catalysts were less active compared to the ruthenium catalyst (at least in terms of DHMF hydrogenation). As was seen in Table 3.1 when using a lower loading of Ru/Vulcan, a decrease in rate of hydrogenation is accompanied by a decrease in selectivity due to an increased relative rate of degradation reactions in solution. This behavior is consistent with an increased yield of unidentified products when using both a lower amount and/or weight loading of Ru/Vulcan or when using Pd/Vulcan or Pt/Vulcan.

The irreversible uptake of CO was measured for each catalyst (Table 3.2) to calculate metal dispersion and particle size. Pt is known to catalyze both hydrogenation and C—C scission reactions during aqueous phase reforming, which can account for the lower selectivity to DHMTHF using Pt.^{16, 17} To probe the difference between Ru and Pd, HMF hydrogenation was studied using low catalyst amounts (50 mg) and low reaction times to calculate specific rates of HMF hydrogenation (Table 3.2). Pd showed the highest rate of HMF hydrogenation relative to Pt

and Ru. This behavior can be detrimental to the overall production of DHMTHF if the rate of DHMF hydrogenation is slow and permits time for this reactive intermediate to undergo degradation reactions. The relative rates of DHMF hydrogenation were estimated using furfuryl alcohol (FA) hydrogenation as a model reaction. Indeed, Ru showed a faster rate than Pd for FA hydrogenation. Accordingly, the overall selectivity to DHMTHF is dependent on both the rates of hydrogenation as well as solution acidity.

Table 3.2. Chemisorption and reaction information for individual metals for comparison.

Metal Catalyst	Irreversible CO	Conversion of HMF /	Specific Rate ^b	TOF ^c	FAL
on Vulcan	uptake (µmol/g)a	Selectivity to DHMF	(µmol g ⁻¹ min ⁻¹)	(min ⁻¹)	Conversion ^d
		(%/%)			(%)
1 wt% Ru	71.4	29/>99	265	3.7	100
1 wt% Pt	42.2	16/>99	141	3.3	67
1 wt% Pd	7.9	98/96	844	107	-

a. Data from Micromeritics ASAP 2020C

3.3 Conclusions

The selectivity for hydrogenation of HMF to DHMTHF is affected by the acidity of the aqueous solution containing HMF. In particular, the selectivity to DHMTHF decreases when acidic impurities (for example levulinic acid, an HMF degradation product) are present in the reaction mixture, or when metal oxides with low-isoelectric point are used as supports for Ru hydrogenation catalysts. The primary by-products observed are 1,2,5-HT, 1,2,5,6-HT, and 1,2,6-HT. These molecules appear to be formed by the hydrogenation of acid-catalyzed

b. Specific rate defined as moles of HMF converted per gram of catalyst per minute

c. TOF defined as the specific rate divided by the irreversible CO uptake

d. Furfuryl alcohol was hydrogenated to tetrahydrofuran alcohol using the same conditions in a biphasic reaction for 1 hour at 403 K and 400 psi H₂. This reaction was studied to model DHMF hydrogenation.

degradation products of dihydroxymethylfuran (DHMF). Importantly, high selectivities to DHMTHF can be achieved when the hydrogenation catalyst is comprised of ruthenium deposited on a support with a high isoelectric point oxide (e.g., ceria).

3.4 References

- [1] R. Alamillo, M. Tucker, M. Chia, Y. Pagan-Torres, J. Dumesic, Green Chemistry, 14 (2012) 1413-1419.
- [2] A.J. Sanborn, P.D. Bloom, in, US, 2008.
- [3] C. Moreau, M.N. Belgacem, A. Gandini, Topics in catalysis, 27 (2004) 11-30.
- [4] T.J. Connolly, J.L. Considine, Z. Ding, B. Forsatz, M.N. Jennings, M.F. MacEwan, K.M. McCoy, D.W. Place, A. Sharma, K. Sutherland, Organic Process Research & Development, 14 (2010) 459-465.
- [5] T. Buntara, S. Noel, P.H. Phua, I. Melián-Cabrera, J.G. de Vries, H.J. Heeres, Angewandte Chemie International Edition, 50 (2011) 7083-7087.
- [6] M. Chia, Y.J. Pagan-Torres, D. Hibbitts, Q. Tan, H.N. Pham, A.K. Datye, M. Neurock, R.J. Davis, J.A. Dumesic, Journal of the American Chemical Society, (2011).
- [7] M. Faber, in, US, 1983.
- [8] S. Koso, N. Ueda, Y. Shinmi, K. Okumura, T. Kizuka, K. Tomishige, Journal of Catalysis, 267 (2009) 89-92.
- [9] Y. Nakagawa, K. Tomishige, Catalysis Communications, 12 (2010) 154-156.
- [10] J.D. Garber, in, US, 1962.
- [11] V. Schiavo, G. Descotes, J. Mentech, Bull. Soc. Chim. Fr, 128 (1991) 704–711.
- [12] J. Horvat, B. Klaic, B. Metelko, V. Sunjic, Tetrahedron letters, 26 (1985) 2111-2114.
- [13] J.N. Chheda, Y. Roman-Leshkov, J.A. Dumesic, Green Chemistry, 9 (2007) 342-350.
- [14] R. González, R. Martínez, P. Ortíz, Die Makromolekulare Chemie, Rapid Communications, 13 (1992) 517-523.
- [15] M. Choura, N.M. Belgacem, A. Gandini, Macromolecules, 29 (1996) 3839-3850.
- [16] R.R. Davda, J.W. Shabaker, G.W. Huber, R.D. Cortright, J.A. Dumesic, Applied Catalysis B: Environmental, 43 (2003) 13-26.
- [17] R.D. Cortright, R.R. Davda, J.A. Dumesic, Nature, 418 (2002) 964-967.

Chapter 4: Biomass-derived Solvent Systems for use in Fructose Dehydration¹

4.1 Introduction

The development of a sustainable, large-scale chemical processing of biomass is critical to its efficient utilization. In addition to the feedstock, the other components (e.g., reaction solvent) within the system must be renewable and energy efficient (e.g., low boiling point) for an economical and environmentally sustainable process.

5-Hydroxymethylfurfural (HMF) is a platform chemical that can be derived from carbohydrates for the production of petrochemical alternatives such as biofuels and high value chemicals.²⁻⁵ Biomass-derived HMF is most commonly obtained by the dehydration of fructose. The overall efficiency of HMF production is hindered by multiple side-reactions, including rehydration of HMF to levulinic and formic acid, and condensation of HMF and fructose to form polymeric humins.^{2, 5, 6} Some solvents are effective in suppressing these undesired reactions. For example, polar aprotic solvents such as DMSO cause both an increase in the rate of HMF production and the selectivity to HMF. However, separating HMF from DMSO is energyintensive due to its high-boiling point, and consequentially, the overall efficiency and economics of the process decreases.^{2, 3, 7, 8} The use of a Brønsted acid catalyst with DMSO as the solvent results in high selectivities and yields of HMF from fructose, making the intrinsic comparison of different acid catalysts in DMSO difficult as most catalysts demonstrate high yields at similar conditions. High yields of HMF from biomass have also been reported using ionic liquids as solvents, 9, 10 although the subsequent separation is also complex. Thus there is a need for sustainable solvent systems that enable a high HMF selectivity at high conversion required for its large-scale production, while facilitating product separation to minimize energy use.

In this chapter we explore various single-phase solvent systems, including 2,5-(dihydroxymethyl)tetrahydrofuran, (DHMTHF, the product of complete HMF hydrogenation), for their use in acid-catalyzed fructose dehydration to HMF. Scheme 4.1 shows a sustainable continuous process for the conversion of fructose to DHMTHF, using DHMTHF as a co-solvent with water to increase the overall efficiency of carbohydrate conversion to high value products. In the first step, fructose is dehydrated to HMF in the presence of DHMTHF, using a solid acid catalyst. In the second step, HMF is hydrogenated to DHMTHF over a metal catalyst. Both reactions have been investigated using heterogeneous catalysts in single-phase solvent systems under similar conditions. In this respect, we reported previously an acid-functionalized SBA-15type periodic mesoporous organosilicas that can be used in conjunction with a single-phase solvent system in the production of HMF from fructose. 11 In Chapter 3 it was reported high yields (above 90%) in the production of DHMTHF from HMF using 1 wt% Ru dispersed on a support with a high isoelectric point (e.g., ceria or magnesia-zirconia) under conditions similar to those used in the dehydration reaction. 12 Scheme 4.1 shows that a fraction of the reactor effluent can be recycled as solvent to convert unreacted fructose and to take advantage of the promoting effect of DHMTHF on fructose dehydration. This tandem reaction system shows how linking two reactions can result in a more efficient and sustainable process.

Scheme 4.1. Proposed tandem catalytic sequence in which fructose is first dehydrated to HMF, then HMF is hydrogenated to DHMTHF. A certain amount of DHMTHF is recovered as product, while the remainder is recycled to serve as the co-solvent in the dehydration reaction.

In the present chapter, we have also studied tetrahydrofurfuryl alcohol (THFA), ethanol, tetrahydrofuran (THF), and DMSO as phase modifiers in the exploration of sustainable single solvent systems for fructose dehydration. These co-solvents were chosen as examples of alcoholic or aprotic solvents, to explore the nature and importance of side-reactions between fructose and the solvent. In addition, THF may be of practical importance due to its low boiling point, allowing for efficient separation from HMF and/or DHMTHF. Fructose tautomer distributions were evaluated in each solvent system using ¹³C NMR, to shed light on the observed trends in HMF selectivity.

4.2 Results and Discussion

4.2.1 The use of DHMTHF as a Co-solvent for Monophasic Fructose Dehydration

The selectivity for the conversion of fructose to HMF in water as a solvent decreases monotonically with increasing conversion (Figure 4.1). This behavior indicates that HMF degradation reactions, for example, to form humins and formic acid, take place in series with fructose dehydration. Addition of DHMTHF as a co-solvent in an equal weight amount with water resulted in the same trend. Importantly, however, the HMF selectivity increased by 20-30% at all conversions. In contrast, a 3:1 (by weight) mixture of DHMTHF:water showed a maximum in selectivity at intermediate conversion. The maximum was displaced to higher conversion when the DHMTHF:water ratio was increased further, to 9:1.

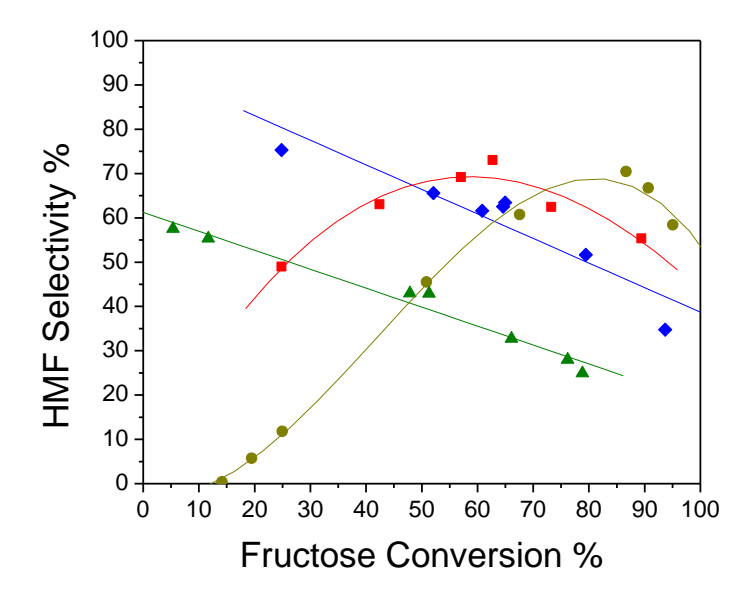


Figure 4.1. HMF selectivity as a function of fructose conversion in mono-phasic dehydration experiments with Amberlyst® 70 as the catalyst in a mixed solvent consisting of DHMTHF:water in molar ratios of 0:1 (triangles), 1:1 (diamonds), 3:1 (squares), and 9:1 (circles).

At the highest DHMTHF content, we observed formation of DHMTHF-fructosides (Scheme 2, where R = DHMTHF) via LC/MS. Fructosides are ethers formed by condensation at the anomeric carbon, and they form reversibly from fructose in alcohol solvents. At short reaction times, some fructose is converted rapidly to fructosides, leading to the low observed HMF selectivity at low fructose conversions. However, these fructosides hydrolyze back to fructose as the reaction proceeds, accounting for the increased selectivity with conversion. At high conversion in 9:1 DHMTHF:water, the selectivity begins to decrease, due to formation of the HMF-DHMTHF ether (Scheme 4.2), which was also observed by LC/MS. When 0.1 M HCl was used as a homogeneous acid catalyst instead of Amberlyst A70, a high HMF selectivity (64%) was also observed at high fructose conversion (99%) in 9:1 DHMTHF:water. For comparison, the HMF selectivity in water was only 36% at 86% fructose conversion.

Scheme 4.2. Reaction pathways observed for the dehydration of fructose in alcohol and non-alcohol solvents

In addition to enhancing the selectivity to HMF, using DHMTHF as a co-solvent enhances the initial rate of HMF formation (Figure 4.2 and Table 4.1). Higher rates at lower water concentrations have been previously reported and a variety of explanations have been proposed. For example, higher HMF production rates in DMSO compared to water have been attributed to: (i) the effect of water on the position of the equilibrium for reversible removal of the first water molecule (assumed to be the rate-determining step), and/or (ii) formation of a fructosyl cation intermediate that reverts back to fructose by reaction with water. ¹³ The lower rate in water was also suggested to be caused by solvation of the proton catalyst. ^{2,14} Another possibility for the effect of water involves the fructose tautomer equilibrium, Figure 4.3, which shifts toward the furanose forms in non-aqueous solvents. ^{15,16} It has been suggested that this shift is responsible for higher rates of HMF formation in DMSO compared to water, because the fructo-furanose tautomers are proposed to be intermediates in the reaction pathway to HMF from fructose. ⁸ Finally, a quantum mechanics/molecular mechanics study of a closed-ring mechanism for the acid-catalyzed dehydration of fructose predicted an increase in rate with decreasing water concentration. In

particular, the authors showed that one of the proton transfer steps in the overall mechanism was inhibited by high concentrations of water.¹⁷ Accordingly, the single-phase co-solvents used in the present study could displace excessive water, and thus lead to increased rates of HMF formation.

Table 4.1. Initial Rates of HMF Production in DHMTHF:H₂O

Solvent ratio	Initial TOF h ⁻¹
9:1	1.5
3:1	0.67
1:1	0.42
0:1	0.22

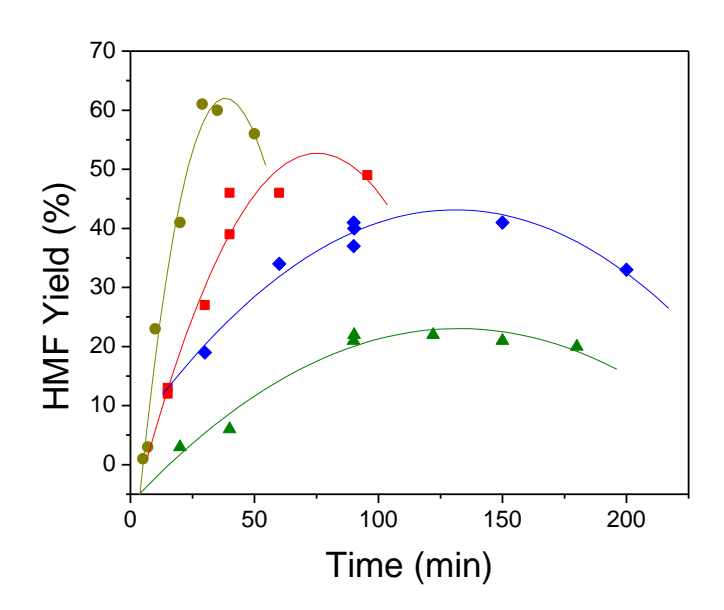


Figure 4.2. Solvent effects on the time-dependent yield of HMF by dehydration of fructose using an Amberlyst® 70 catalyst in DHMTHF:water ratios with molar ratios of: 0:1 (triangles), 1:1 (diamonds), 3:1 (squares), and 9:1 (circles).

$$\alpha$$
-D-Fructopyranose β -D-Fructopyranose β -D-Fructose β -D-Fructose β -D-Fructofuranose β -D-Fructofuranose β -D-Fructofuranose

Figure 4.3. Structures of the various fructose tautomers in solution.

Fructose dehydration is first-order with respect to fructose concentration.⁵ The rate of fructose tautomerization in 9:1 ethanol:water was estimated to be 250 times faster than the rate of fructose dehydration in 9:1 DHMTHF:water, and it is estimated that the various fructose tautomers are quasi-equilibrated at 403 K.¹⁸ A first-order rate constant can be estimated for a particular solvent system using the measured rate constant in water if the tautomer distribution in the solvent system of interest is known, by assuming that the dehydration rate is proportional to the fructo-furanose fraction. The fraction of fructose present in the furanose form in water at 333 K is 40% (Table 4.2). However, this underestimates the value at the reaction temperature of 403 K, since the fraction of fructose in the furanose form increases with temperature.¹⁹ The first-order rate constant for dehydration of the furanose tautomer in water is therefore ca. 0.45 h⁻¹ based on the TOF for fructose dehydration in water (Table 4.1) and an estimated furanose fraction of 50%. Next, the initial concentrations of fructo-furanose in the 1:1, 3:1, and 9:1 DHMTHF:water solvent systems

were estimated to be 0.094, 0.15, and 0.34 mol L⁻¹, respectively, based on their observed first order rate constants (0.45 h⁻¹) and their respective TOF (Table 4.1). The acid loading of the catalyst in these systems was 2.55 mmol H+/g. However, the latter two concentration values estimated exceed by far the total concentration of fructose in these solvent mixtures (0.125 and 0.130 mol L⁻¹, respectively). Therefore, the increased rate with decreasing water concentration is not caused solely by shifts in tautomer equilibria, although this effect is a contributing factor, as discussed below.

2.2.1 Fructose Dehydration with other Co-solvents

To further explore the effect of solvent on the fructose dehydration rate, ethanol and tetrahydrofurfuryl alcohol (THFA) were also studied as co-solvents with water. Using A70 as the catalyst, trends similar to those observed for DHMTHF:H₂O were found for both of these alcohol co-solvents: selectivity initially increased, then decreased with conversion, although the trends were less pronounced with ethanol and THFA, Figure 4.4. As with DHMTHF, the corresponding fructosides and HMF-solvent ethers were observed by LC/MS. In addition, difructose anhydrides (DFAs) were observed. The same reactivity trends were observed when A70 was replaced by a homogeneous catalyst, 0.1 M HCl.

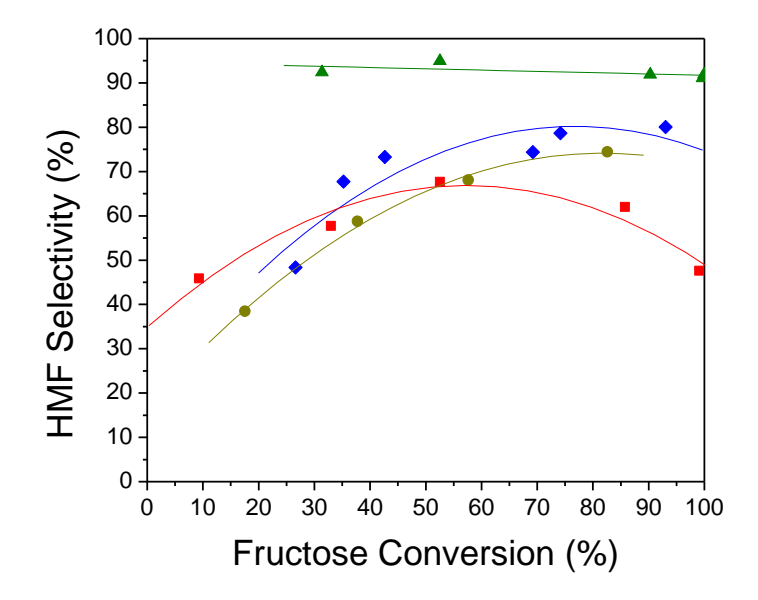


Figure 4.4. Comparison of HMF selectivity as a function of fructose conversion for over an Amberlyst® 70 catalyst in mixed solvents consisting of 9:1 DMSO:water (triangles), 4:1 THF:water (diamonds), 9:1 ethanol:water (squares), and 9:1 THFA:water (circles).

In 9:1 THFA:water, high selectivity (78%) to HMF was achieved at high fructose conversion (95%) when the feed concentration was 2 wt%. The trend of increasing selectivity with conversion was also observed with a 10 wt% fructose feed, Figure 4.5. However, at the higher fructose concentration, HMF selectivity was consistently lower, and rehydration of HMF to levulinic acid and formic acid was observed, as well as formation of humins. Previous reports have suggested that these humins are derived mainly from HMF, rather than from either levulinic or formic acid. This expectation is consistent with the large decrease in HMF selectivity at the higher fructose concentration. It has also been suggested that 2,5-dioxo-6-hydroxyhexanal, a proposed intermediate in the mechanism of HMF formation, plays an important role in humin formation via aldol addition/condensation with HMF.²⁰

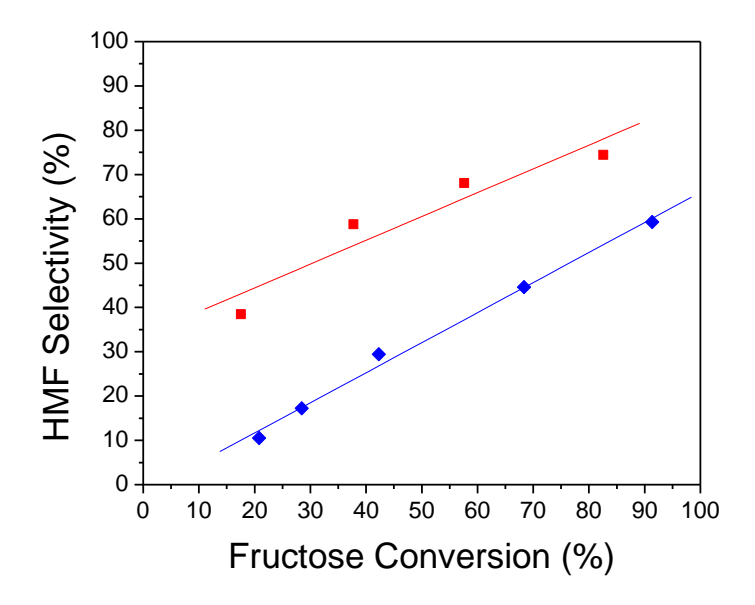


Figure 4.5. Comparison of HMF selectivity as a function of fructose conversion over an Amberlyst® 70 catalyst in 9:1 THFA:water for fructose feeds at 2 wt% (squares) and 10 wt% (diamonds).

Difructose anhydrides (DFAs, an example of which is shown in Scheme 4.2) are formed by loss of two water molecules in a reaction analogous to the formation of fructosides (in which a fructose molecule forms a glycosidic bond by reacting with a hydroxyl group of another fructose molecule). A variety of DFAs can be formed, because of the many tautomers of fructose and the variety of hydroxyl groups that can react.^{2, 21} To establish the importance of these side-reactions, fructose dehydration was studied in two polar aprotic co-solvents: DMSO and THF. Their lack of hydroxyl groups limits the number of possible side-reactions, resulting in higher selectivity for HMF (as reported previously for DMSO).²² This behavior is confirmed by the results in Figure 4.4. The HMF selectivity does not change significantly with conversion in 9:1 DMSO:water. The stability of HMF in this solvent mixture is confirmed by the high selectivity even when fructose had been completely converted. For THF:water, a 4:1 ratio was used because 9:1 THF:water

undergoes phase separation in the presence of 2 wt% fructose. In 4:1 THF:water, high selectivity to HMF was also observed, and a slight increase in selectivity with increasing conversion was observed. This trend for THF can be explained by the formation of DFAs, which were observed in the reaction mixture by LC/MS.

To explore whether DFA formation is reversible, a 2 wt% solution of DFA III was heated at 403 K in 4:1 THF:water using the same catalysts in previous reactions. After 35 min, all of the DFA had been converted. The major products were HMF (78%) and fructose (7%). The presence of fructose indicates that its dimerization to DFA III is reversible. The high HMF yield suggests that the DFA has a positive effect on selectivity. This phenomenon has been observed previously, and it was proposed that DFA formation protects the reactive anomeric hydroxyl groups from polymerization.²

4.2.3 Solvent effects on D-Fructose Tautomer Distribution

In solution, fructose adopts five structural conformations: α -pyranose, β -pyranose, α -furanose, β -furanose and a keto form, as shown in Figure 4.3 and Table 4.2. The relative amounts of each tautomer depend on both solvent and temperature. In fructose dehydration, the tautomer distribution can have a significant effect on product selectivity. Since HMF is derived from the α -furanose and β -furanose tautomers, increasing their concentrations through solvent-effects_leads to higher HMF yields by minimizing side reactions with water. In water at 303 K, ca. 30% of fructose exists in these furanose forms, while in DMSO, the corresponding fraction is increased to 53%. At 333 K, the furanose fractions increase to ca. 40 and 70% in water and DMSO, respectively.

At 80% fructose conversion in water, we observed an HMF selectivity of ca. 30%. However, in neat DMSO, near-quantitative yields (> 90%) have been reported.^{2, 4, 24, 25} Although

the lower HMF selectivity in water relative to DMSO is not solely due to the lower concentration of the furanose tautomers, it is a factor. The effect of various co-solvents on the fructose tautomer distributions was assessed by analyzing the 13 C NMR spectra of isotopically-labeled fructose (13 C₂). 26

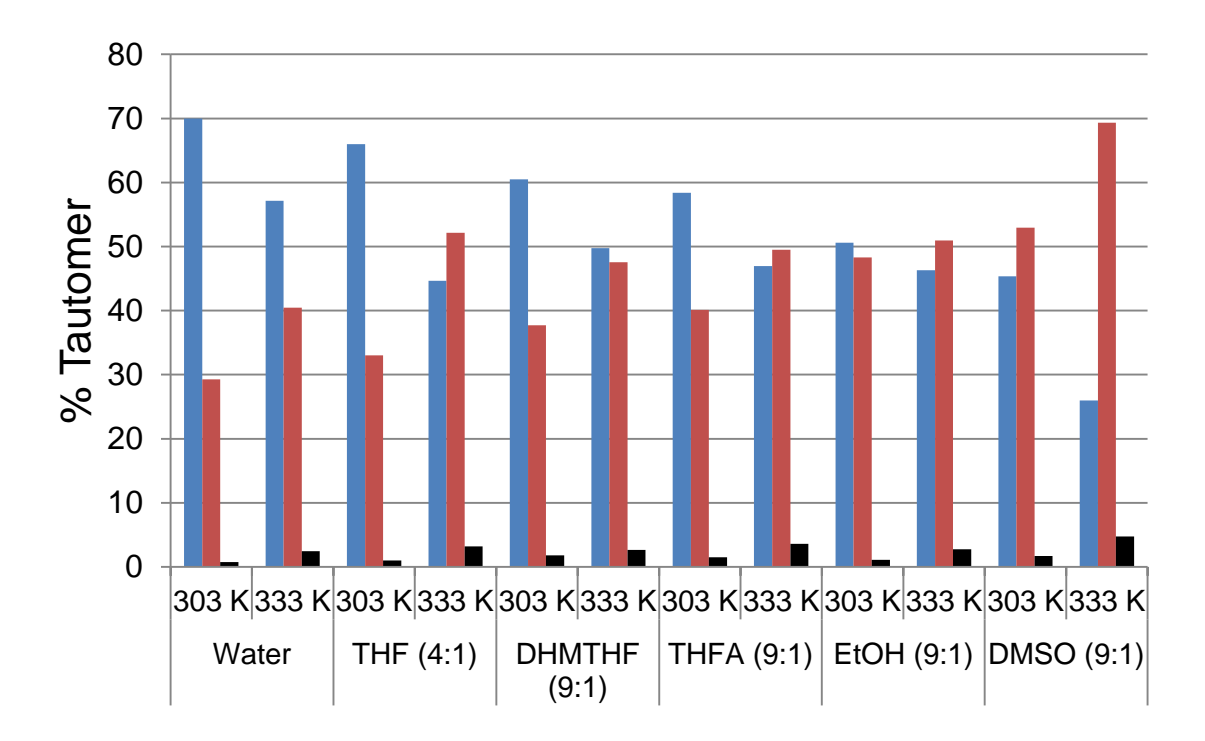


Figure 4.6. Tautomer distributions for D-fructose in various solvents at 303 K; and 333 K. Values for the α and β forms of the pyranose (blue) and furanose (red) tautomers have been combined. Keto is shown in black.

Table 4.2. Tautomer distributions in various solvents, based on ¹³C NMR spectroscopy of 2-¹³C-labeled D-fructose

Solvent	Tautome	Tautomer Distribution (%)				
	T (K)	α-Pyr	β-Pyr	α-Fur	β-Fur	Keto
D ₂ O	303	2.48	67.49	6.09	23.20	0.74
	333	3.15	53.97	9.68	30.76	2.44
DHMTHF:D ₂ O	303	3.84	56.63	10.01	27.70	1.82
(9:1)	333	3.98	45.78	13.57	33.99	2.67
THFA:D ₂ O	303	2.37	56.00	11.14	28.98	1.51
(9:1)	333	2.77	44.17	33.51	15.96	3.59
THF:D ₂ O	303	2.30	63.71	8.88	24.13	0.99
(4:1)	333	4.13	40.53	15.16	36.99	3.18
EtOH:D ₂ O	303	5.10	45.50	13.71	34.59	1.10
(9:1)	333	4.73	41.57	16.34	34.62	2.74
DMSO:D ₂ O	303	3.26	42.09	15.42	37.54	1.69
(9:1)	333	4.14	21.81	21.46	47.85	4.75

Like DMSO, DHMTHF alters the relative amounts of the various fructose tautomers in favor of the furanose forms. At 303 K in 9:1 DHMTHF:D₂O, 38% of the fructose exists in the furanose form. At 333 K, the furanose concentration increases further, to 48%. At both temperatures, these values represent a 10% increase in the α , β -furanose fraction for the mixed solvent, relative to water alone. The higher concentrations of the α , β -furanoses contribute to the observed higher HMF selectivities in fructose dehydration.

The effects of THFA, THF, EtOH, and DMSO as co-solvents (mixed either 5:1 or 4:1 with D₂O) on fructose tautomer distributions are similar to those found for neat DMSO and DHMTHF.

Interestingly, the tautomer distributions in 9:1 DMSO:D₂O rapidly attained the values reported for fructose at equilibrium in pure DMSO, despite published reports that several weeks are required.²⁷ At 303 K, the furanose tautomers represent 52, 51, 40, 38, 33, and 29% of the total fructose concentrations in DMSO, THFA, DHMTHF, THF, and water, respectively, see Figure 4.6 and Table 4.2. Upon increasing the temperature to 333 K, the fractions increased further in favor of the furanose tautomers, Figure 4.6. We observed a nearly 20% increase in the furanose concentrations in both aprotic solvents (THF and DMSO) at 333 K, while the protic solvents (with the exception of 9:1 EtOH:D₂O) showed an increase of ca. 10%. Similar to a previous report,²⁸ we observed that the tautomer distribution in EtOH remains roughly constant despite the increase in temperature. For a variety of EtOD:D₂O ratios and temperatures, the pyranose and furanose concentrations remain approximately constant.

4.3 Conclusions

The use of DHMTHF as a co-solvent has a beneficial effect on both the rate of fructose dehydration and on the selectivity to HMF over a heterogeneous catalyst (Amberlyst® 70), compared to water alone. Fructose tautomerization favors the furanose form in the mixed solvent, relative to water alone, explaining at least part of the rate enhancement. The HMF selectivity depends on both the fructose conversion and the amount of DHMTHF present. With high levels of the co-solvent in water (e.g., ratios of 3:1 and 9:1), the HMF selectivity increases with fructose conversion. Thus a tandem approach may be feasible in the production of DHMTHF, based on the use of an inexpensive, easily-separable, non-corrosive solvent system. Other alcoholic co-solvents, including ethanol and THFA, showed similar, but less pronounced, selectivity enhancements.

The use of polar, aprotic THF as the co-solvent also leads to the selective production of HMF. Due to its high volatility, this solvent facilitates isolation of HMF by simple evaporation, which is an advantage relative to high-boiling DMSO. Side-reactions involving the anomeric hydroxyl groups of fructose give rise to fructosides and difructose anhydrides in alcoholic and aprotic solvents, respectively. However, their formation is reversible, and high yields of HMF can be obtained at high fructose conversions.

2.4 References

- [1] M.H. Tucker, R. Alamillo, A.J. Crisci, G.M. Gonzalez, S.L. Scott, J.A. Dumesic, ACS Sustainable Chemistry & Engineering, 1 (2013) 554-560.
- [2] B.F.M. Kuster, Starch Stärke, 42 (1990) 314-321.
- [3] Y. Roman-Leshkov, C.J. Barrett, Z.Y. Liu, J.A. Dumesic, Nature, 447 (2007) 982-985.
- [4] Y. Roman-Leshkov, J.N. Cheda, J.A. Dumesic, Science, 312 (2006) 1933-1937.
- [5] H.E. van Dam, A.P.G. Kieboom, H. van Bekkum, Starch Stärke, 38 (1986) 95-101.
- [6] Y. Roman-Leshkov, J.N. Chheda, J.A. Dumesic, Science, 312 (2006) 1933-1937.
- [7] D.W. Brown, A.J. Floyd, R.G. Kinsman, Y. Roshanali, J. Chem. Techn. Biotechn., 32 (1982) 920-924.
- [8] J.N. Chheda, Y. Roman-Leshkov, J.A. Dumesic, Green Chem., 9 (2007) 342-350.
- [9] C. Moreau, A. Finiels, L. Vanoye, Journal of Molecular Catalysis A: Chemical, 253 (2006) 165-169.
- [10] H.B. Zhao, J.E. Holladay, H. Brown, Z.C. Zhang, Science, 316 (2007) 1597-1600.
- [11] M.H. Tucker, A.J. Crisci, B.N. Wigington, N. Phadke, R. Alamillo, J. Zhang, S.L. Scott, J.A. Dumesic, ACS Catal., 2 (2012) 1865-1876.
- [12] R. Alamillo, M. Tucker, M. Chia, Y. Pagan-Torres, J. Dumesic, Green Chem., 14 (2012) 1413-1419.
- [13] M.J. Antal, Jr., W.S. Mok, G.N. Richards, Carbohydr Res, 199 (1990) 91-109.
- [14] B.F.M. Kuster, Carbohydr. Res., 54 (1977) 177-183.
- [15] P. Dais, A.S. Perlin, Carbohydr. Res., 169 (1987) 159-169.
- [16] M. Bicker, D. Kaiser, L. Ott, H. Vogel, J. Supercrit. Fluids, 36 (2005) 118-126.
- [17] S. Caratzoulas, D.G. Vlachos, Carbohydr. Res., 346 (2011) 664-672.
- [18] A.E. Flood, M.R. Johns, E.T. White, Carbohydr. Res., 288 (1996) 45-56.
- [19] L. Hyvonen, P. Varo, P. Koivistoinen, J. Food Sci., 42 (1977) 657-659.
- [20] S.K.R. Patil, C.R.F. Lund, Energy Fuels, 25 (2011) 4745-4755.
- [21] G. Gattuso, S.A. Nepogodiev, J.F. Stoddart, Chem. Rev., 98 (1998) 1919-1958.
- [22] Y.J. Pagán-Torres, T. Wang, J.M.R. Gallo, B.H. Shanks, J.A. Dumesic, ACS Catal, 2 (2012) 930-934.

- [23] T. Barclay, M. Ginic-Markovic, M.R. Johnston, P. Cooper, N. Petrovsky, Carbohydr. Res., 347 (2012) 136-141.
- [24] A.S. Amarasekara, L.D. Williams, C.C. Ebede, Carbohydr. Res., 343 (2008) 3021-3024.
- [25] K.-i. Shimizu, R. Uozumi, A. Satsuma, Catalysis Communications, 10 (2009) 1849-1853.
- [26] W. Funcke, C. von Sonntag, C. Triantaphylides, Carbohydr. Res., 75 (1979) 305-309.
- [27] B. Schneider, F.W. Lichtenthaler, G. Steinle, H. Schiweck, Liebigs Ann. Chem., 1985 (1985) 2443-2453.
- [28] A.E. Flood, M.R. Johns, E.T. White, Carbohydr. Res., 288 (1996) 45-56.

Chapter 5: Catalysts for Selective HMF Production from Fructose¹

5.1 Introduction

The efficient and selective conversion of biomass-derived renewable feedstocks to chemicals and fuels remains a major techno-economic challenge.^{2, 3} Fructose, a simple carbohydrate that can be obtained from cellulose, can be dehydrated to a potential platform chemical, 5-hydroxymethylfurfural (HMF).⁴ The selectivity to HMF is a function of the fructose tautomer distribution, which varies with solvent polarity and temperature.⁵ Near-quantitative conversion of fructose to HMF has only been obtained in non-aqueous, polar aprotic solvents (e.g., DMSO, NMP), or in ionic liquids.^{6, 7} However, HMF separation from such high-boiling and/or costly solvents is energy-intensive and lowers the yield, even when combined with immiscible, low-boiling solvents.⁸ In this chapter, an organic-inorganic nanocomposite catalyst converts fructose selectively (>80 %) to HMF in a flow reactor, while eliminating separation issues and the need for environmentally-unfriendly solvents. We obtain the highest reported HMF yields to-date in a mono-phasic, readily separable solvent, avoiding the undesirable use of salt. Other Brønsted acid catalysts, particularly acid functionalized ordered carbon mesoporous materials and a bimetallic Rh-Re on carbon catalyst are also investigated.

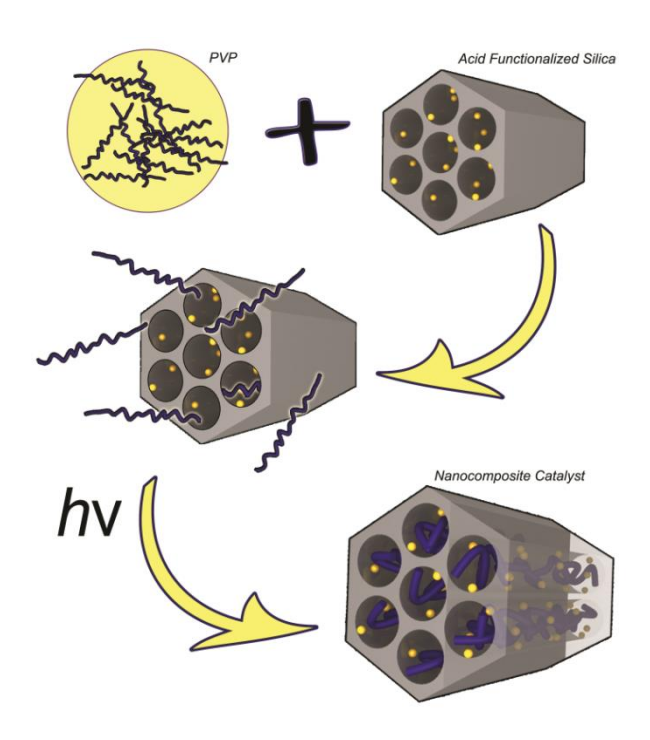
5.1.1 Organosilicas for Biomass Conversions

Previous studies of fructose dehydration to HMF employed silicas and organosilicas with pore-directed alkylsulfonic acid groups as heterogeneous catalysts. ^{9, 10} Ordered mesoporous silicabased catalysts were found to be more selective and robust than catalysts with similar chemical compositions but non-ordered pores. Upon incorporating bifunctional organosilanes containing both alkylsulfonic acid groups and thioether/sulfone groups to promote fructose tautomerization

to the desired furanose tautomers, it was observed further, modest selectivity improvements relative to propylsulfonic acid-functionalized silicas. It was hypothesized that in order to achieve HMF selectivities comparable to those reported with homogeneous systems the microenvironment throughout the pore channels (rather than just localized near the active sites) should promote fructose tautomerization. Soluble organic polymers have been reported to act as pseudo-solvents, encapsulating reactants in a local microenvironment that can be favorably tailored for catalysis. ¹¹ Furthermore, the pores of acid-functionalized ordered mesoporous materials (both silicas and organosilicas) are large enough to accommodate such macromolecules. ^{12, 13}

5.1.2 Intercalation of Polyvinyl Pyrrolidone

Poly(vinylpyrrolidone) (PVP), a polar, aprotic polymer, was intercalated via incipient wetness impregnation into the pores of unmodified SBA-15 silica (Scheme 1), as well as into three propylsulfonic acid-functionalized silica catalysts (pSO₃H-SBA-15, pSO₃H-MCM-41, and a nonordered mesoporous silica, pSO₃H-SS). Polymer intercalation is promoted by the dissolution and disentanglement of the PVP globules in water, and results in an extended hydrogen-bonded network between the pyrrolidone carbonyl groups and the surface silanols of the silica. ¹⁴ To suppress leaching, the intercalated PVP was then cross-linked ^{15, 16} using benzoyl peroxide and UV irradiation. Residual soluble polymer was removed from the support by Soxhlet extraction with water.



Scheme 5.1. Intercalation of PVP into the ordered mesopores of acid-functionalized silica by incipient wetness impregnation.¹

5.2 The use of PVP as a Surface Modifier for Selective Production of HMF5.2.1 PVP Modified Silicycle

A proof of concept for the solid acid catalyst modified with PVP was accomplished by use of commercial propylsulfonic modified silica, Silicycle (SC) with end-capping (EC). The composite material SC/PVP was modified using incipient wetness and achieved a PVP loading of about 8 wt% as determined by TGA. The composite SC/PVP material showed 30% higher selectivity to HMF than the bare SC catalyst (Table 5.1). To ensure this selectivity was due to the localized functionality of PVP near the acid site, the 8 mg of PVP, the estimated amount of PVP on the material, was added in solution and the reaction was run to the same conversion. The selectivity for the composite SC/PVP material was 20% higher that of SC with added PVP at about the same conversion. One major difference though is the composite material requires a longer

reaction time. Future work focused on investigating this, but it may be due to less accessible acid sites relative to bare SC. The composite SC/PVP catalyst was recycled and showed about 10% decrease in selectivity, which is most likely cause by PVP leaching, since the overall conversion and reaction was nearly constant. A solvent with γ-valerolactone showed no improvement with the SC/PVP material, indicating the solvent may also play an important role. A composite SC with polyvinylalcohol (PVA) did not result in a significant increase in selectivity to HMF, indicating the functionality of PVP group may be responsible for the increased selectivity to HMF.

Table 5.1. Batch reactions for fructose dehydration using Silicycle (SC) and SC/PVP modified catalysts.

Catalyst	Time (min)	Conversion %	Selectivity %
Silicycle (SC)	10	48	42
SC + 8mg PVP	10	43	50
Composite SC/PVP	40	46	73
Composite SC/PVP Recycle	40	51	60
Composite SC/PVP in GVL/Water	12	43	43
Composite SC/PVA	17	52	48

5.2.2 PVP-Catalyst Characterization

The polymer content of PVP-SBA-15 was 16 wt%, as determined by TGA. Signals characteristic of the polymer¹⁷ (Figure 5.1A) and the anchored propylsulfonic acid sites⁹ (Figure 5.1B) were observed in the ¹³C CP/MAS spectrum. This indicated that the intercalation of the polymer with the catalyst surface was successful and that the modified incipient wetness impregnation method did not destroy leach any of the propylsulfonic acid groups of the SBA-15 material.

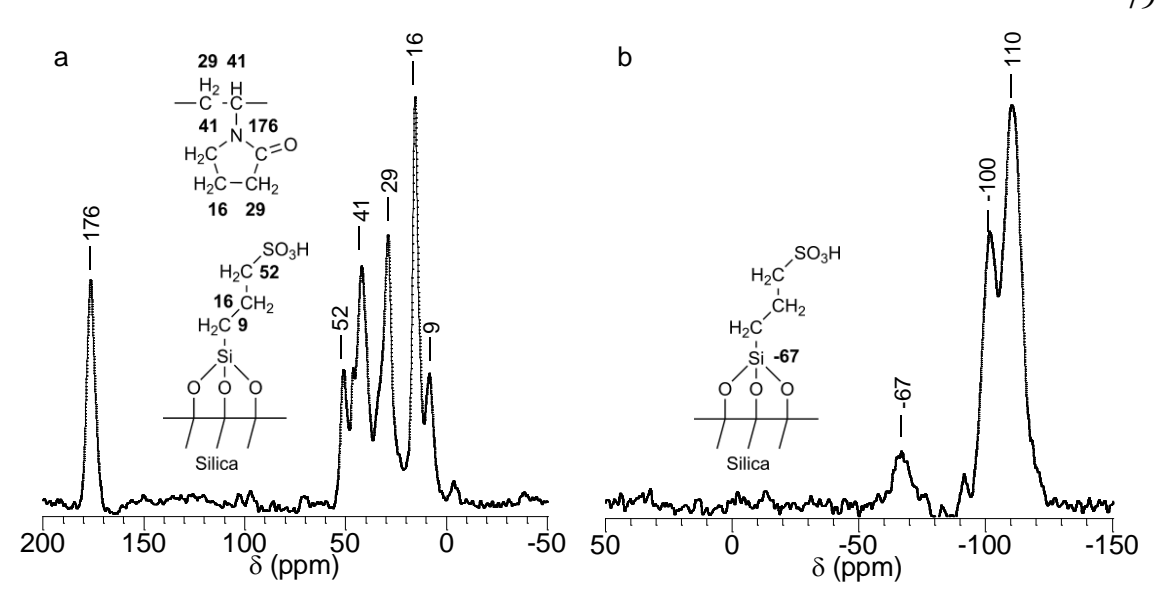


Figure 5.1. Solid-state NMR spectra: (a) ¹³C CP/MAS; and (b) ²⁹Si MAS NMR. for PVP-pSO₃H-SBA-15.

Intercalation of PVP caused the surface area, pore diameter, and pore volume of SBA-15 to decrease by ca. 50, 49 and 65%, respectively (Table 5.2), indicating a partial obstruction (but not collapse) of the ordered pores. ^{18, 19} This same trend is seen for both PVP- pSO₃H-SS and PVP- pSO₃H-MCM-41. If higher loadings we achieved, the surface area would dramatically drop, as well as the pore size and diameter, blocking the pores and not allowing reactanst to enter the active sites. The acid site density decreased by 45%, 28%, and 30% for the PVP- pSO₃H-SS, SBA-15, and MCM-41, respectively. This decrease in acid site density is expected for each material, as the PVP incorporation added to the mass of the catalysts without contributing to the acidity of the materials.

Table 5.2. Physicochemical properties of catalysts

Catalyst	Surface area m²/g	Pore size ^a	Pore volume	H ⁺ content ^b
		nm	cm³/g	mmol/g
pSO ₃ H-SS	315		0.44	0.65
PVP- pSO ₃ H-SS	288		0.38	0.36
pSO ₃ H-SBA-15	670	5.3	0.97	1.04
PVP-pSO ₃ H-SBA- 15	330	3.7	0.32	0.75
pSO ₃ H-MCM-41	747	2.9	0.37	0.79
PVP-pSO ₃ H-MCM- 41	237	-	0.12	0.55

^a B.J.H. pore diameter.

^bFor pSO₃H-SS, the acid content was reported by Silicycle, Inc. The acid contents of catalysts were calculated from elemental analysis (S). Previously, we showed by acid-base titration and XPS, we showed that oxidation of thiol groups to sulfonic acid groups during catalyst synthesis is quantitative.¹⁰

The *p6mm* pore structure of PVP-SBA-15 remains clearly visible by SEM (Figure 5.2), and by XRD (Figure 5.3). In addition, the particle morphology and surface texture of PVP-SBA-15 are indistinguishable from those of unmodified SBA-15, and no polymer aggregates were observed by SEM. In the STEM images, the pore channels become obscured upon polymer intercalation, due to the decrease in contrast relative to the unfilled pores (Figure 5.4). Similar results were obtained for pSO₃H-SBA-15 and pSO₃H-MCM-41.

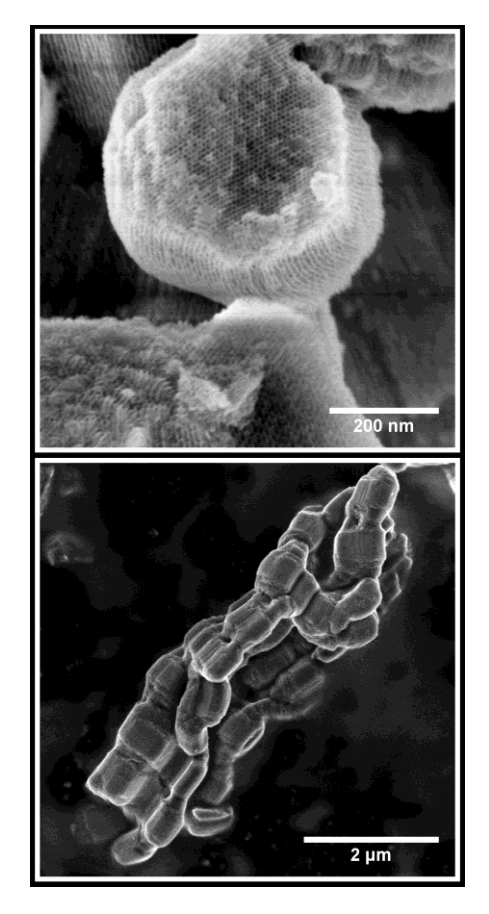


Figure 5.2. SEM Images of the PVP-pSO₃H-SBA-15 catalyst, at two different magnifications.

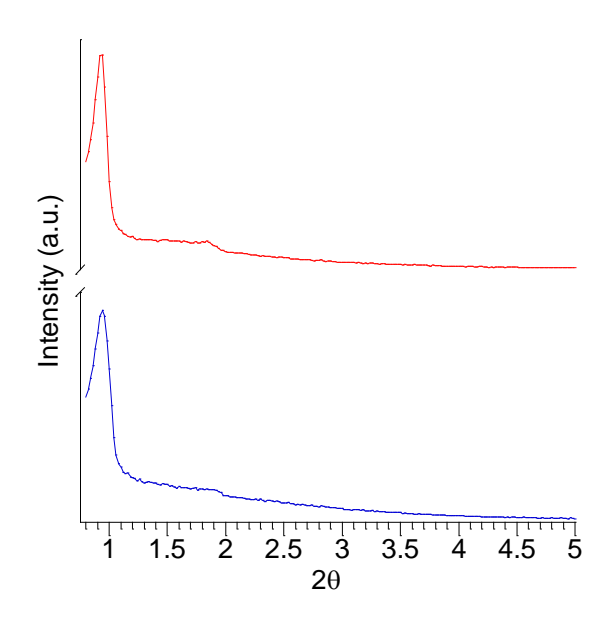


Figure 5.3. XRD reflection patterns for pSO_3H -SBA-15 prior to (blue) and after (red) the intercalation of PVP.

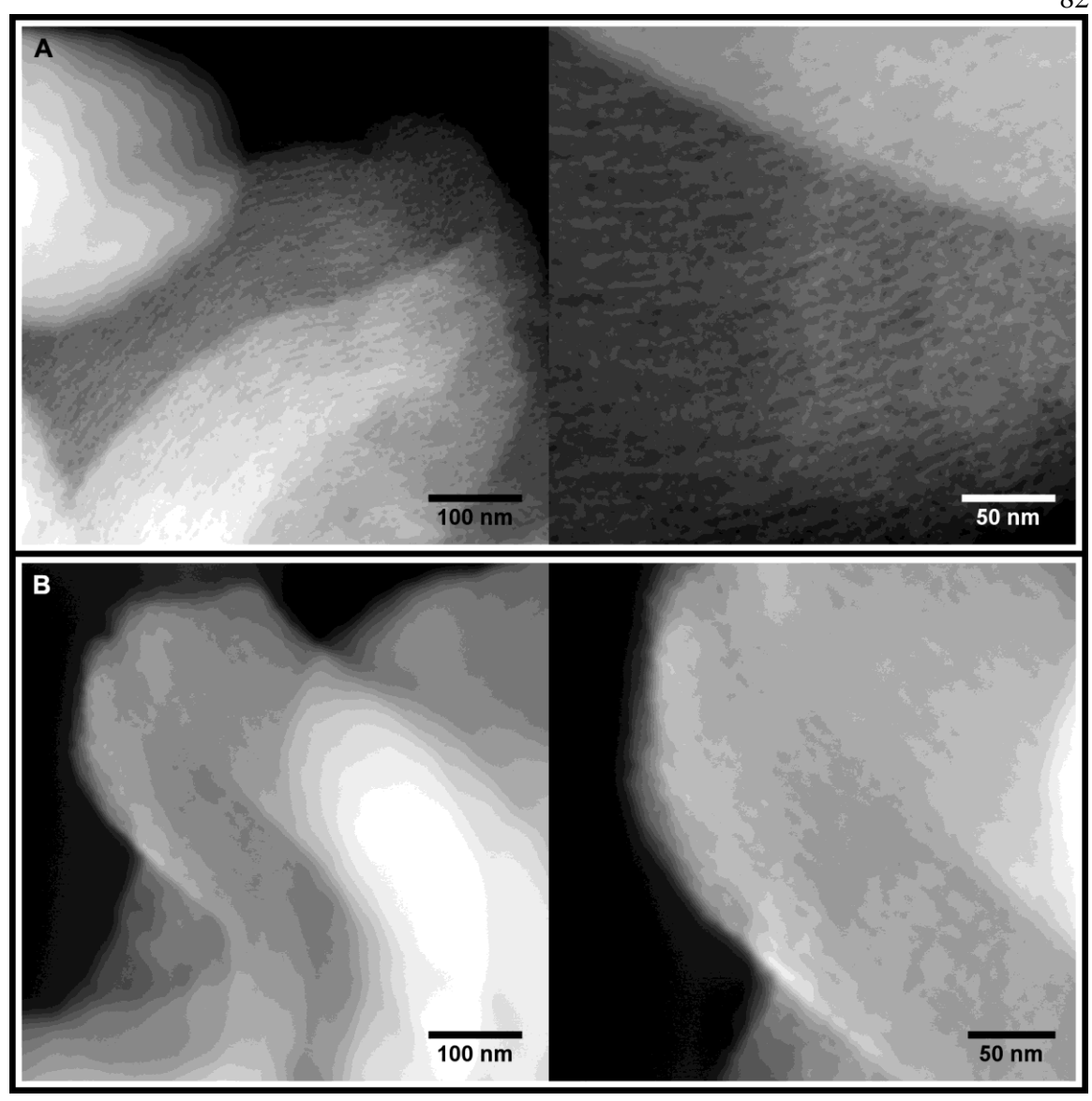


Figure 5.4. STEM images of (a) pSO₃H-SBA-15, (b) PVP-pSO₃H-SBA-15 at two different magnifications. Pore channels are visible for pSO₃H-SBA-15. However, the density increases and the contrast decreases when these channels are filled with polymer in PVP-pSO₃H-SBA-15. Consequently, the pore channels are no longer visible.

5.2.3 PVP-Catalyst Reactivity Studies

Catalytic activity in fructose dehydration was studied in batch mode at 403 K, both before and after impregnation of PVP, Table 5.3. Each reaction was allowed to proceed until the fructose conversion was ca. 50%, to enable direct comparisons of selectivity. For each of the PVP-modified catalysts, the HMF selectivity was significantly higher than for the corresponding unmodified catalysts, Table 1. Both of the PVP-modified ordered mesoporous silica catalysts (MCM-41 and SBA-15) achieved HMF selectivities above 80 %. Notably, these selectivities were retained even at high conversion (ca. 85 %). In addition, PVP-pSO₃H-SBA-15 operated in a flow reactor (403 K and weight-hourly space velocity of 0.11 h⁻¹) at 50 % conversion achieved 78% selectivity after 120 hours on stream (versus 60% selectivity to HMF for pSO₃H-SBA-15 under similar conditions at the same conversion levels).

Table 5.3. Batch fructose dehydration catalyzed by unmodified and PVP-modified silica-based materials^[a]

Catalyst	PVP Loading (wt%) ^[b]	Fructose Conv. (%)	HMF Select. (%)	10 ⁵ Rate (mol g-cat ⁻¹ min ⁻¹)
pSO₃H-SS	-	43	36	4.3
PVP-pSO ₃ H-SS	8	48	64	2.0
pSO₃H-SBA-15	-	48	68	4.0
PVP-pSO ₃ H-SBA-15	17	52	87	3.1
pSO ₃ H-MCM-41	-	45	63	1.5
PVP-pSO ₃ H-MCM-41	16	57	85	1.4

[a] Reaction conditions: 50 mg unmodified catalyst or 100 mg PVP-modified catalyst, 1.5 g 2 wt% fructose solution in THF:H₂O (4:1 w:w) at 403 K. [b] Determined by thermogravimetric analysis (TGA).

Despite the accompanying reduction in accessible surface area, intercalation of PVP does not dramatically impede access to the active sites, since HMF production rates decrease only modestly. We also note that HMF selectivity is unaffected by changes in acid site accessibility and/or density: catalysts partially neutralized with NH₄OH achieved the same selectivity as unmodified catalysts, albeit with longer reaction times required to reach similar conversions.

5.2.4 Catalyst-Surface Localization and Functionality Effects

Both the *nature* of the functional groups and their *location* (in relation to the acid sites) are critical to the observed increases in HMF selectivity. Thus, the increase in HMF selectivity relative to unmodified pSO₃H-SS was much larger for PVP-pSO₃H-SS (28%) than for unmodified pSO₃H-SS in the presence of soluble PVP (8 wt%) (Figure 5.5). Even at increasing amounts of PVP in solution there were no significant increase in the HMF selectivities observed. Similarly, when pSO₃H-SS was intercalated by cross-linked poly(vinyl alcohol) (PVA) instead of PVP, HMF selectivity increased was 25% lower than that of that of the PVP overcoat. We infer that the pyrrolidone functionality, confined within the silica pores, is responsible for the dramatic increase in HMF selectivity.

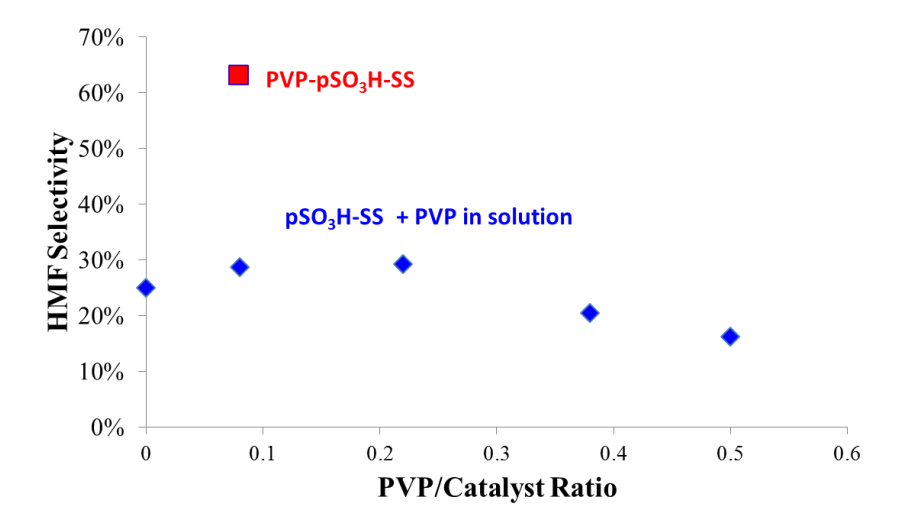


Figure 5.5. The effect of PVP intercalated (red) versus that in free solution (blue) for various ratios of PVP to catalyst ratios on the selectivity to HMF at 50% fructose conversion.

Table 5.4. The effect of changing the polymer type on HMF selectivity.

Catalyst	Fructose Conversion %	HMF Selectivity %
PVP-pSO ₃ H-SS	46	73
PVA-pSO ₃ H-SS	52	48

5.2.5 Catalyst-Surface Effects on Fructose Tautomer Distributions

HMF is formed preferentially from the fructofuranose tautomers (α - and β -),²⁰ which are favored over the pyranose forms in polar aprotic solvents. For example, in water at 303 K, 29% of the fructose exists in the furanose forms,²⁰ while in *N*-methylpyrrolidone (NMP, a molecular analog of PVP), this fraction increases to 69% (Table 5.5). The influence of NMP (and, presumably, by analogy, PVP) on the fructose tautomer distribution also depends on the pyrrolidone concentration. For aqueous fructose solutions (2 wt%), the presence of either 10 wt% NMP or 10 wt% PVP had no observable effect on the tautomer distribution at RT, as judged by 13 C NMR. (We note that 10 wt% is the maximum solubility of NMP and PVP in the 4:1 THF:H₂O solvent selected a single-phase solvent system for use in our flow reactor¹⁰).

The tautomer distribution of pore-confined fructose was assessed for PVP-SBA-15. The modified silica was saturated with a 2 wt% fructose solution in 4:1 THF:H₂O at 298 K, and the furanose fraction was observed by solid-state ¹³C HR-MAS NMR. Relative to 33 % in solution, an increase to 44 % was observed for the PVP-modified silica. The furanose fraction is expected to be even higher at elevated temperature. In contrast, unmodified SBA-15 had no discernible effect on the tautomer distribution. We infer that PVP acts like a polar aprotic solvent in the confined micro-environment of the mesopores, increasing the stability of the furanose tautomers and resulting in increased HMF selectivity relative to catalysts without PVP modification.

Table 5.5. Fructose tautomer composition determined by ¹³C NMR^a

Solvent/solid system	Total furanose %	Total pyranose %
H ₂ O	29	70
10 wt% PVP in H ₂ O	29	70
4:1 THF:H ₂ O	33	66
NMP	69	27
10% NMP in H ₂ O	30	69
SBA-15 ^b	35	64
PVP-SBA-15 ^b	44	55

^a Temperature: 303 K. ^b Determined by solid-state HR-MAS NMR with 2 wt.% fructose solution in THF:H₂O (4:1 w:w) at 298 K.

5.2.6 Catalyst-Surface Effects on Catalyst Stability

To assess the stability of the new catalysts, cross-linked PVP-SBA-15 was exposed to batch reaction conditions, but in the absence of fructose. The solid was then recovered, washed, dried and re-exposed. After four cycles, the PVP loading remained constant, as determined by TGA (Figure 5.6). Conversely, PVP intercalated without cross-linking leached quickly into solution, and was lost after just one cycle. The amount of PVP lost without crosslinking corresponds to the amount of PVP introduced via incipient wetness. In the presence of fructose under batch reaction conditions, recycled pSO₃H-SS lost activity with each reuse, while PVP-pSO₃H-SS showed stable activity, Figure 5.7. The PVP-modified catalyst experienced only a minor decrease in selectivity after the first use, Figure 5.8.

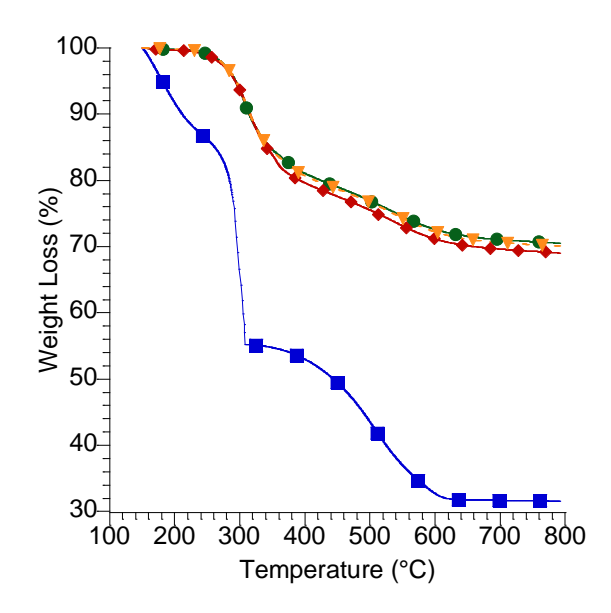


Figure 5.6. Thermogravimetric analysis of PVP-SBA-15 prior to (blue squares) and after (red diamonds) Soxhlet extraction of soluble PVP with ethanol. Post-extraction, PVP-SBA-15 was subjected to simulated reaction conditions by treatment in 4:1 THF-H₂O at 403 K for 30 min. The solid was recycled (recovered, washed with ethanol and dried) and again subjected to simulated reaction conditions. A portion of the solid from each cycle was examined by TGA: cycle 1 – orange triangles, and cycle 2 – green circles.

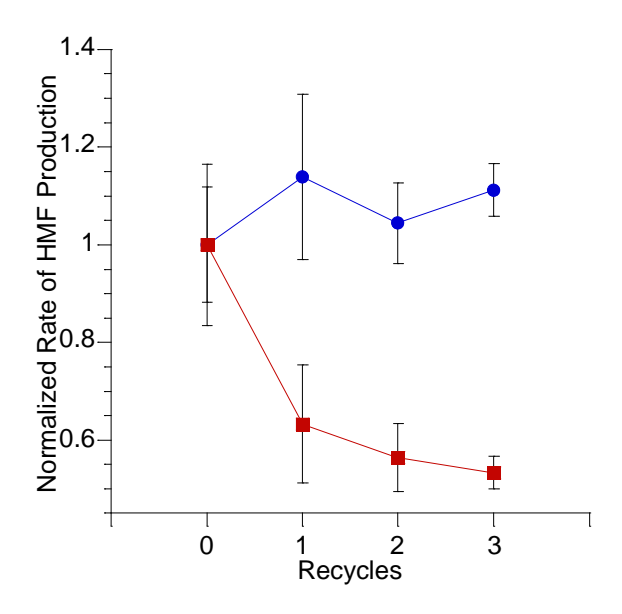


Figure 5.7. Effect of pSO₃H-SS (red) and PVP-pSO₃H-SS (blue) catalyst recycle on HMF production rate at 403 K in 4:1 THF:H₂O (w:w). After each reaction, the catalyst was recovered, washed, dried and reused.

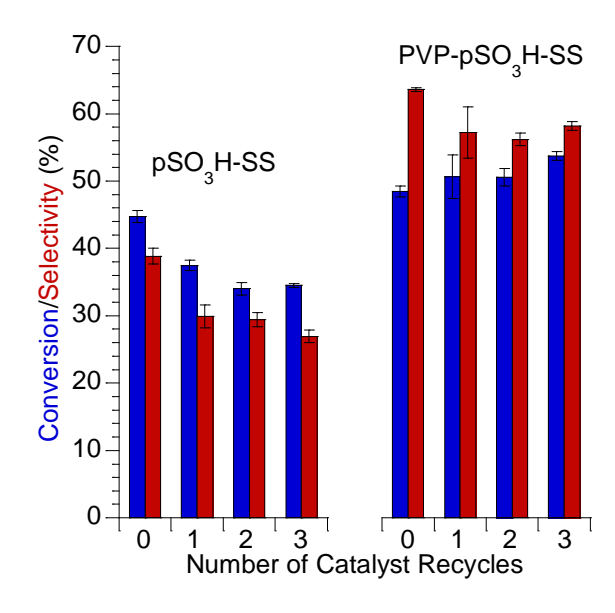
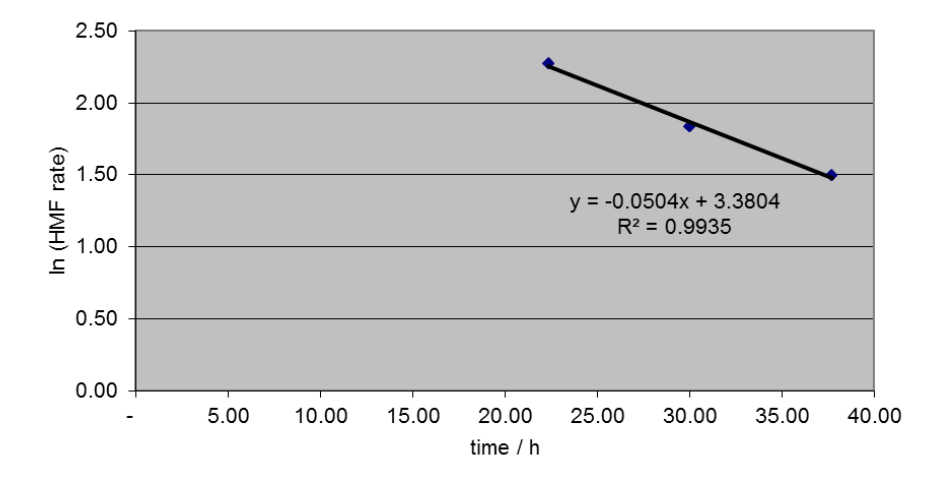
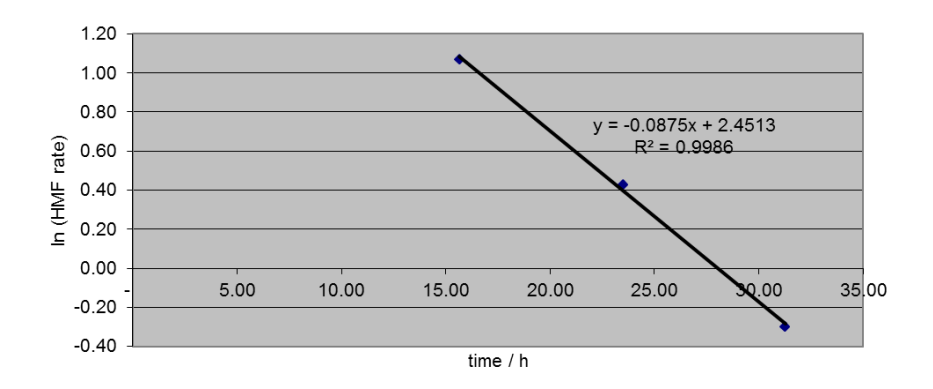


Figure 5.8. Effect of catalyst recycle on fructose conversion and HMF selectivity at 403 K in 4:1 THF:H₂O (w:w). After each batch reaction, the catalysts were recovered, washed, dried and reused.

Based on our prior studies, silica-based catalysts deactivate by hydrolysis and subsequent leaching of the propylsulfonic acid sites. Deactivation rates were quantified by measuring catalytic activity continuously in a flow reactor. (Figure 5.9) Pseudo-first-order deactivation rate coefficients for pSO₃H-SS and pSO₃H-SBA-15 were previously measured to be 0.152 and 0.124 h⁻¹, respectively, at 403 K. Under similar conditions, the deactivation rate coefficients for PVP-pSO₃H-SS and PVP-pSO₃H-SBA-15 are 0.088 and 0.050 h⁻¹, respectively. Thus intercalation of PVP into the pores of SBA-15-based catalysts leads to significant stabilization. (Figure 5.10)



(a)



(b)

Figure 5.9. Determination of the first-order deactivation rate coefficient for the (a) $PVP-pSO_3H-SBA-15$ and (b) $PVP-pSO_3H-SS$ catalysts.

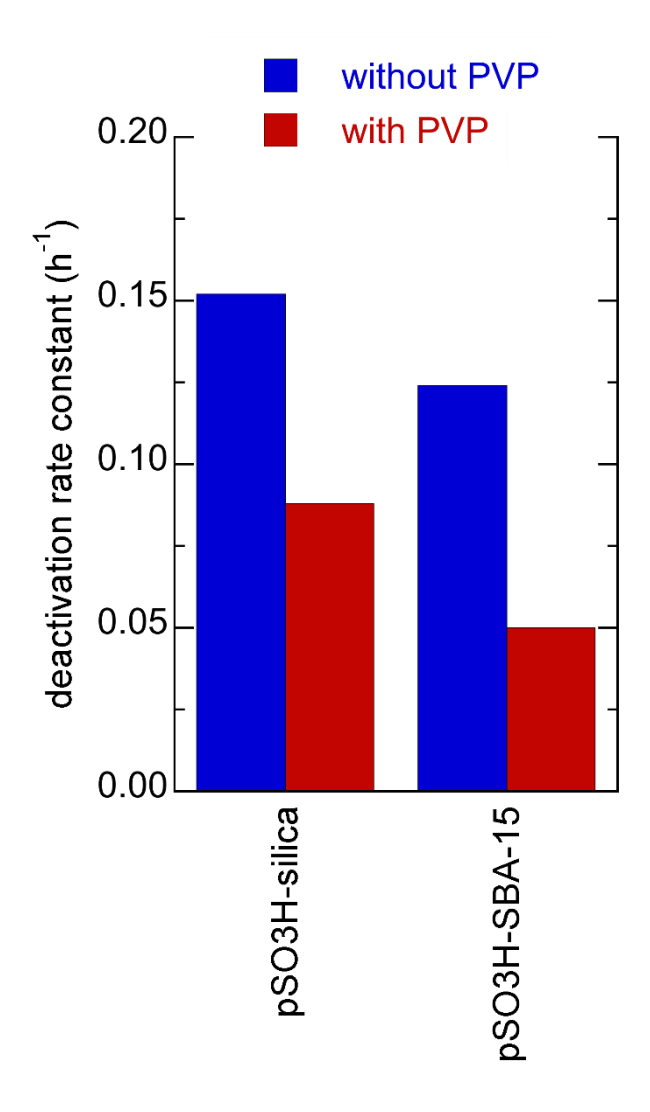


Figure 5.10. Comparison of the first-order deactivation rate coefficient for the (a) PVP-pSO₃H-SBA-15 and (b) PVP-pSO₃H-SS catalysts.

5.3 Acid Functionalized Mesoporous Carbon for the Continuous Production of HMF

5.3.1 Introduction

The major challenge in the long-term stability of sulfonic/sulfated silica or metal oxides is the oxygen that mediates the anchoring of the functional group in the support, making the material susceptible to hydrolysis. ^{21, 22} Carbon can be a robust alternative for these supports, since

functional groups can be anchored through C-C and C-S bonds that are not easily hydrolyzed. In this work, we study the activity and deactivation of periodic mesoporous carbons modified with sulfonic and organosulfonic acid groups for the continuous production of HMF from fructose, using 4:1 THF:water (w:w) as a solvent. Shanks et. al. have reported hydrothermal stability of carbon based acid catalysts previously with extensive focus on the solid state NMR characterization of the carbon catalysts and its' hydrothermal deactivation. ²³ However, there are few reports that investigate both the continuous production of HMF and quantify catalyst deactivation. ²²

5.3.2 Catalyst Characterization Studies

The X-ray diffactograms (XRD) for the functionalized CMK-3 and CMK-5 are presented in Figure 2. Similar to their parent material (SBA-15), CMK3 and CMK-5 contain both the hexagonal pores array and the associated XRD patterns. The expected peaks are assigned to the (100) (most intense), (110), and (200) Miller indices which appear at relative 2θ values of X, ($\sqrt{3}$)X, and 2X, respectively. CMK-3 and CMK-5 modified with PSA (Figure 5.11 a and d) and CMK-3-NSA (Figure 5.11 b) present the three expected XRD peaks, which indicates good organization of the pores and long range ordering. On the other hand, the CMK-3-SA XRD diffractogram (Figure 5.11 c) presents only a broader peak related to the (100) Miller index, indicating a large range of unit cell sizes.

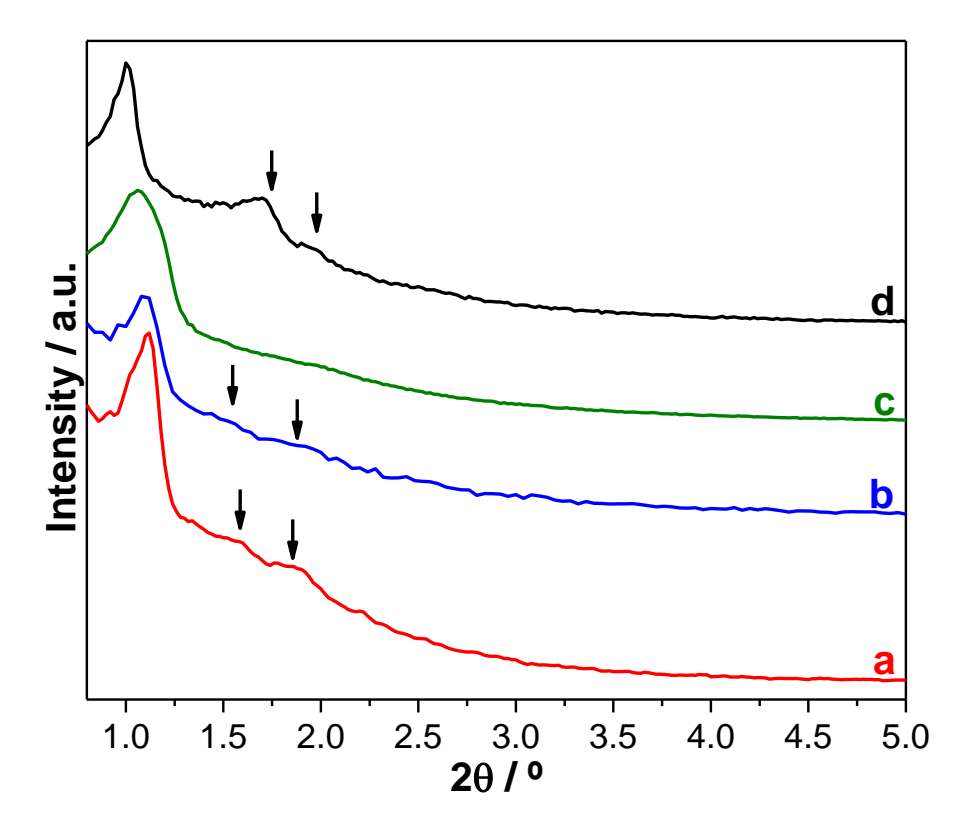


Figure 5.11. X-ray diffractograms for (a) CMK-3-PSA, (B) CMK-3-NSA, (C) CMK-3-SA, (d) CMK-5-PSA. Arrows indicate peaks assigned to (110) and (200) planes.

The acid sites loading in the samples were determined by potentiometric titration using a $0.01 \text{ mol } L^{-1}$ sodium hydroxide solution,²⁴ and the results are shown in Table 5.6. The samples had an acid site loading between 0.90 and 1.25 mmol g⁻¹.

Table 5.6. Acids site loading, surface area, and pore sizes for CMK-3 and CMK-5 catalysts.

Catalyst	[H ⁺] ^a / mmol g ⁻¹	S_{BET}^{b}/m^2g^{-1}	W _{BJH} ^c / nm
CMK-3-PSA	1.21	480	2.80
	1.21	100	2.00
CMK-3-NSA	0.97	420	2.58
CMK-3-SA	1.25	1368	3.72
CMK-5-PSA	0.90	616	2.67 & 3.38

^a determined by potentiometric titration; ^b surface area obtained by BET method; ^c pore size obtained by BJH method using KJS correction, except for CMK-5, in which no correction was used, as recommended in literature ²⁵.

The surface area and porosity of the samples were determined by nitrogen physisorption at 77 K and are shown in Table 5.6. CMK-3-NSA presents a slightly lower surface area and smaller pore sizes than CMK-3-PSA, which is expected since NSA is a bulkier functional group. Due to the absence of bulk functional groups, CMK-3-SA has the highest surface area and largest pore sizes of the above mentioned CMK-3 materials. CMK-5-PSA displays a surface area higher than CMK-3-PSA, since its structure is formed by pipes, which have internal and external surfaces. CMK-5 has a bimodal pore structure, in which the larger pores are assigned to the voids inside the nanopipes, whereas the smaller pores are due to the voids between the nanopipes (similar to CMK-3).^{25, 26}

5.3.3 Catalyst Reaction Kinetic Studies

A comparison of catalyst performance at higher fructose conversions is shown in Figure 5.12. The CMK-3 and CMK-5 based catalysts demonstrated comparable selectivities to HMF (71-74 %) at similar conversions. The results are similar to the mesoporous silica pSO₃H-SBA-15 but higher than that obtained for the commercial Nafion SAC-13 (53 %). For the mesoporous

carbon catalysts studied, the functional group and support structure do not seem to affect the HMF selectivity. On the other hand, the HMF production turnover frequency (TOF) is affected by the catalyst nature. As shown in Table 5.7, CMK-3-PSA, CMK-3-NSA, and pSO₃H-SBA-15 displayed comparable TOF values, which were higher than the TOF obtained for CMK-3-SA and Nafion SAC-13. CMK-5-PSA is the catalyst with highest TOF, being approximately 1.5 and 2 times higher than the TOF obtained for CMK-3-PSA and Nafion SAC-13, respectively.

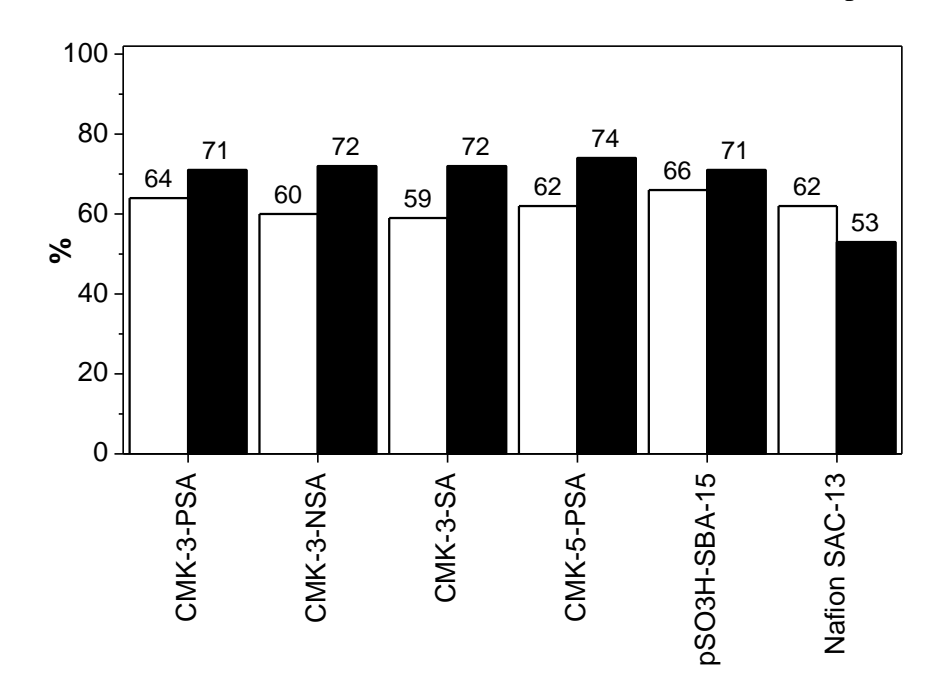


Figure 5.12. Conversion (white bars) and selectivity (black bars) for the CMK-3 and CMK-5 based catalysts, pSO₃H-SBA-15, and SAC-13.

Table 5.7. Initial HMF production TOF and first order deactivation rate coefficient for CMK-3 and CMK-5 based catalysts, pSO₃H-SBA-15, and SAC-13.

Catalyst	HMF TOF ^a / min ⁻¹	Deactivation Rate Coefficient ^b / h ⁻¹
CMK-3-PSA	0.045	0.006
CMK-3-NSA	0.052	0.009
CMK-3-SA	0.028	0.014
CMK-5-PSA	0.069	0.002
pSO ₃ H-SBA-15	0.048	0.120
Nafion SAC-13	0.033	0.008

^a Initial TOF obtained at X=0 obtained from the extrapolation of the curve ln(TOF) for HMF production as a function of time on stream; ^b First order deactivation rate coefficient is the slope of the curves shown in Figure 4.

5.3.4 Catalyst Deactivation Studies

The deactivation of the CMK-3 and CMK-5 based catalysts was studied in ½ inch diameter downflow reactor at a high flow rate in the kinetic regime, as previously reported. ^{22, 27} By using a broader reactor than the one used for the activity studies, the bed length decreases, which results in a lower pressure drop and a decreased driving force for liquid channeling ²². The first order deactivation rate coefficient for each catalyst was obtained by plotting the log of the TOF as a function of the time on stream (Figure 5.13 and Table 5.7). Deactivation of the acid mesoporous carbons can take place mainly due to coking or leaching of the active sites ^{28, 29}. As reported previously ²², at the reaction conditions used, the extent of carbon deposition is minimized and the deactivation is primarily due to leaching of the active sites. In the case of the mesoporous carbons studied, the leaching mechanism is similar to that observed for sulfonated polystyrene resins ^{28, 29}, in which the sulfonic acid moiety bonded to the aromatic ring is hydrolyzed to sulfuric acid.

The first order deactivation rate coefficients for all catalysts studied are shown in Table 2.

Comparing the CMK-3 based materials, the stability of the functional groups in the reaction

conditions follows the order $PSA > NSA > -SO_3H$. When comparing the different supports, CMK-5-PSA is more stable than CMK-3-PSA, even though CMK-3 structure is more robust.

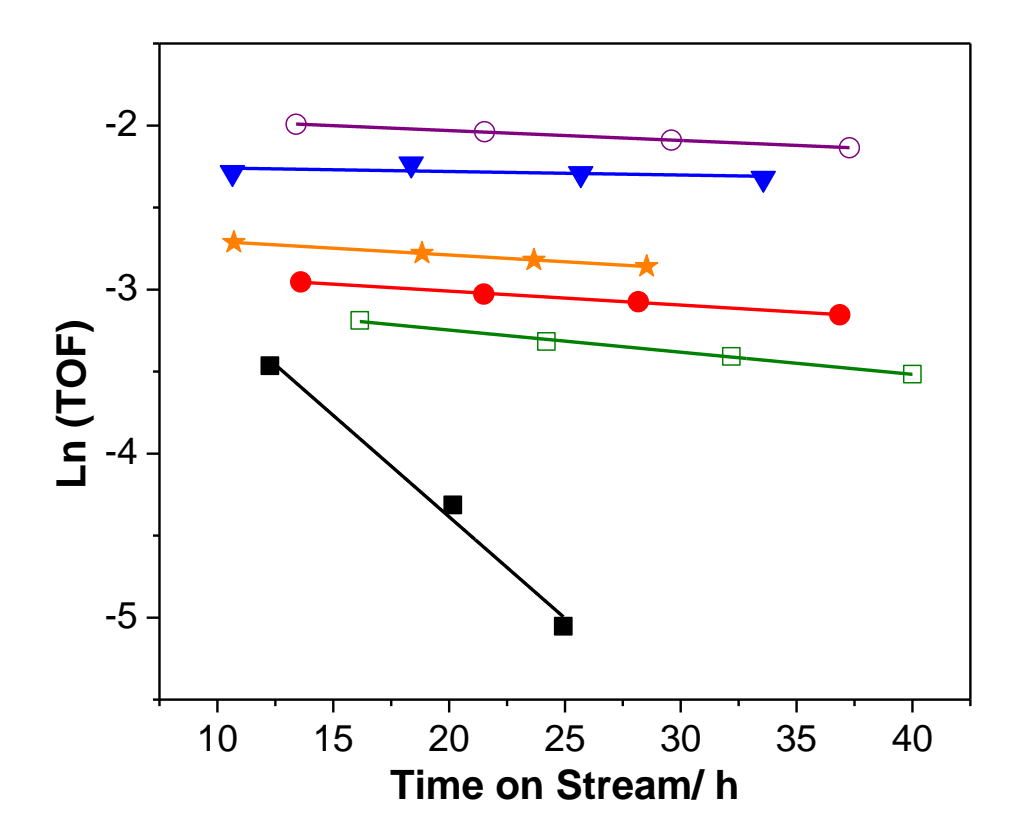


Figure 5.13. Natural logarithm of the HMF production TOF as a function of the time on stream. (open purple circles) CMK-3-PSA, (full red circles) CMK-3-NSA, (open green squares) CMK-3-SA, (full blue triangles) CMK-5-PSA, (full black squares) SBA-15-pSO₃H, and (full orange stars) Nafion SAC-13.

The deactivation rate coefficients for CMK-3-PSA, CMK-3-NSA, CMK-3-SA, and CMK-5-PSA were, respectively, 20, 13.3, 8.5, and 60 times lower than pSO₃H-SBA-15. The deactivation of pSO₃H-SBA-15 is due primarily to leaching of the whole functional group [(OH)₃Si(CH2)₃SO₃H] by hydrolysis of the support surface, which is easier than the hydrolysis of the C-SO₃H bond ²². Comparing the acid mesoporous carbons with the commercial Nafion SAC-13, known for its remarkable stability, we observed that the deactivation rate constant for the

Nafion catalyst is similar to CMK-3-NSA, and 1.5 and 3 times higher than for CMK-3-PSA and CMK-5-PSA.

5.4 Rh-Re Bimetallics for Fructose Dehydration

5.4.1 Introduction

We recently proposed that the combination of an oxophilic promoter and a highly reducible metal results in the formation of a bifunctional catalyst possessing both acid and metal sites ³⁰. We demonstrated this concept using results from experimental studies and first-principle density functional theory (DFT) calculations, where the reactivity trends over the RhRe/C catalyst were consistent with a bifunctional mechanism in which selective C-O hydrogenolysis proceeds through initial acid-catalyzed ring-opening or dehydration followed by metal-catalyzed hydrogenation ³⁰. Temperature-programmed desorption (TPD) of NH₃ was used as a means to quantify these active sites over RhRe/C, and the apparent Brønsted acidity of this catalyst was proposed to arise from the deprotonation of hydroxyl groups on rhenium atoms associated with rhodium. Similarly, recent work by Zhang et al. has reported the presence of acid sites on a PtRe catalyst under glycerol reforming conditions using NH₃ TPD analysis and examination of product distributions ³¹; their work provides further evidence of the general bifunctional nature of this unique class of catalysts. In the present paper we show that the reduction temperature used to pretreat a RhRe/C (molar ratio Rh:Re = 1:0.5) catalyst prior to exposure to continuous-flow reaction conditions has a significant effect on the catalytic activity and the number of active sites quantified by NH₃ TPD. Additionally, we have studied this catalyst for an acid- catalyzed reaction that is important in biomass conversion processes: the dehydration of biomass-derived fructose to 5-hydroxymethylfurfural (HMF). 8, 32-34

5.4.2 Catalyst Reactivity Studies for Fructose Dehydration

To further probe the apparent of acidity of RhRe/C, we employed an acid-catalyzed probe reaction, namely fructose dehydration to HMF 8, 32-34, a reaction of relevance to biomass conversion. Results from DFT calculations presented in previous work 30 showed that the deprotonation energies of Re-OH species in contact with metallic Rh were in the range comparable to that for typical solid acid catalysts such as zeolites and heteropolyacids. Figure shows results for the dehydration of fructose over RhRe/C that was pretreated at 523 K in flowing hydrogen prior to initiation of liquid feed flow. A pretreatment temperature of 523 K was informed by our results for C-O hydrogenolysis of HMTHP showing that this pretreatment temperature leads to stable catalytic activity under continuous flow conditions.³⁵ A single-phase reaction solvent consisting of a mixture of tetrahydrofuran (THF) and water (mass ratio of THF: water = 4:1) was employed, because this solvent system was previously shown to be effective for fructose dehydration to HMF under continuous flow reaction conditions ¹⁰. Interestingly, the RhRe/C catalyst displayed high activity for conversion of fructose to HMF, with selectivity to HMF maintained at approximately 50% at a conversion level of 30% (5.14). While the selectivity to HMF was low for the first 24 h TOS, the selectivity increased and stabilized thereafter. The initial low selectivity to HMF is consistent with results previously reported by Tucker et al. 10 and Ordomsky et al. ^{36, 37} for a wide range of conventional solid acid catalysts such as zeolites, ZrPO₄, sulfonated polystyrene and silica-based catalysts. Significantly, the RhRe/C catalyst here was stable with TOS and specific formation rates of HMF were maintained at approximately 1.8 µmolg⁻¹min⁻¹ for up to 250 h TOS. The formation of HMF from fructose here provides further evidence of Brønsted acid sites over RhRe/C.

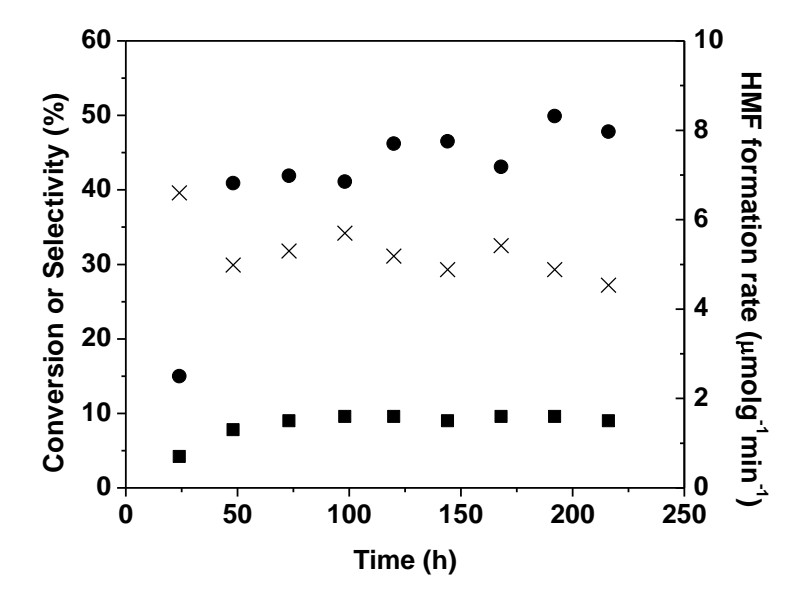


Figure 5.14. Conversion of fructose (×), selectivity to 5-hydroxymethylfurfural (\bullet), and specific formation rate of HMF (\blacksquare) as a function of time on stream over RhRe/C catalyst pretreated at 523 K. Reaction conditions: 300 psi He, 403 K, 2 wt% fructose in THF/water (mass ratio of THF: water = 4:1) as feed, WHSV =0.1h⁻¹.

The effect of the reduction temperatures on the catalytic activity for fructose dehydration was investigated, and these results are shown in 5.15. The RhRe/C catalyst was pretreated in flowing hydrogen at 523 and 723 K, and fructose dehydration was conducted in the presence of an inert sweep gas (i.e., He). The lower pretreatment temperature of 393 K was not used here due to the instability of the catalyst for C-O hydrogenolysis. During the initial stages of the experiment (i.e., 48-72 h TOS), it is evident that the catalyst pretreated at the higher temperature is significantly less active, consistent with observations for C-O hydrogenolysis. Interestingly, it was observed that the activity of the catalyst pretreated at 723 K increased after 100 h TOS, and eventually reached a similar rate of HMF formation rates as the catalyst that was pretreated at a lower temperature (i.e., 523 K). This increase in catalytic activity with TOS suggests that surface Re species, although significantly reduced in number after a high temperature reduction pretreatment

step (i.e., over-reduced), may repopulate the catalyst after prolonged exposure to liquid water and in the absence of a reducing environment. It is notable that this increase in catalytic activity with TOS for the catalyst pretreated at 723 K was not observed for experiments in the C-O hydrogenolysis of HMTHP, presumably due to the reducing environment these experiments were conducted under. The fructose conversion and HMF selectivity levels for the catalyst pretreated at 723 K from 120-215 h TOS were 30% and 45%, respectively.

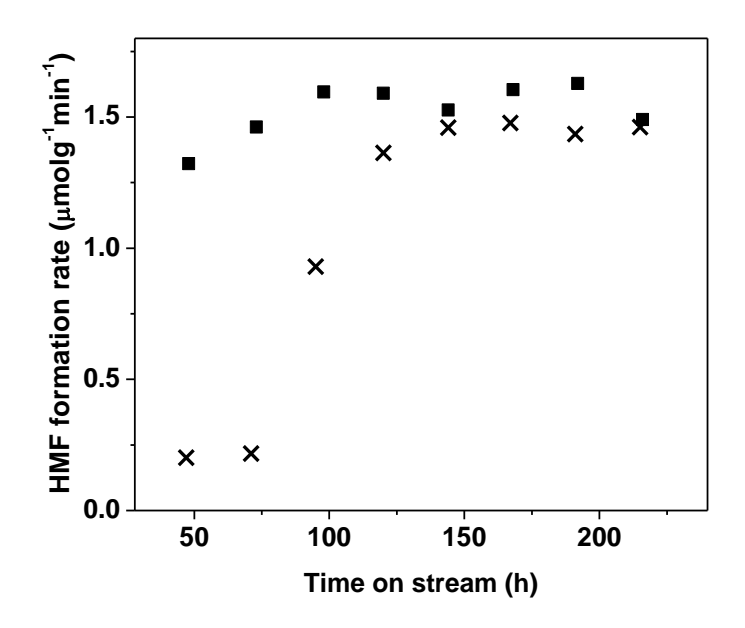


Figure 5.15. Fructose dehydration in a continuous flow reaction system over RhRe/C catalyst pretreated at different reduction temperatures of 523 K (\blacksquare) and 723 K (\times). Reaction conditions: 300 psi He, 403 K, 2 wt% fructose in THF/water (mass ratio of THF: water = 4:1) as feed, WHSV =0.1h⁻¹.

ZSM-5 was used as a benchmark catalyst for fructose dehydration, for comparison with the dehydration activity of RhRe/C. Figure 5.16 shows the results for the dehydration of fructose to HMF over ZSM-5, using the same number of sites, as titrated by NH₃ TPD, that were used as for RhRe/C in the previous continuous flow experiments (5.15). The selectivity for production of HMF over ZSM-5 was similar to that over RhRe/C (i.e., approximately 40% selectivity at 20%

conversion). Also, similar to what was observed for RhRe/C, the selectivity to HMF was low initially, and then increased and stabilized thereafter. The HMF selectivity has been suggested to correlate with the strength and availability of Bronsted acid sites over solid acid catalysts ^{36, 37}, and our results for RhRe/C and ZSM-5 thus suggest that the strength of Brønsted acid sites over these two catalysts are similar. The turnover frequencies for production of HMF over RhRe/C and ZSM-5 are plotted versus TOS in 5.17, using the number of sites titrated by NH₃ TPD. On a rate-persite basis, Figure 5.17 shows that RhRe/C displays HMF formation rates that are approximately twice as high as ZSM-5. This behavior is in agreement with the results from DFT calculations which indicate similar deprotonation energies for these catalysts.

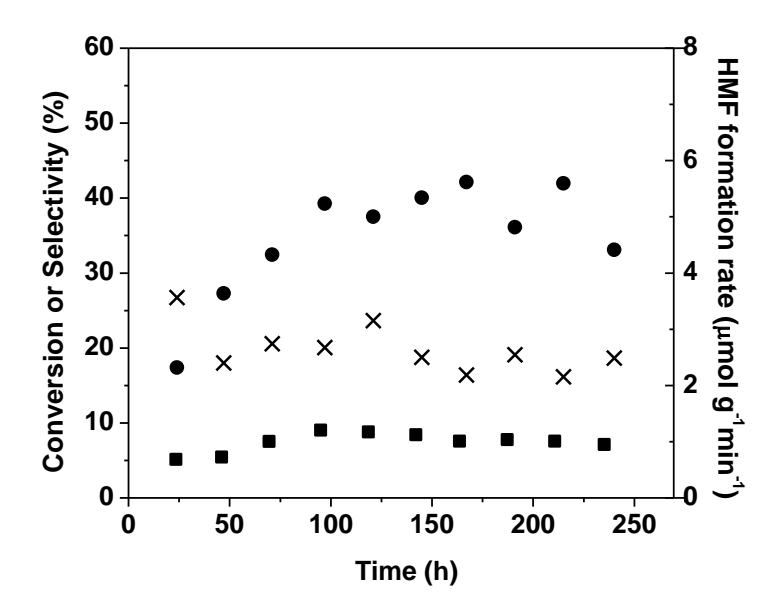


Figure 1.16. Conversion of fructose (×), selectivity to HMF (\bullet), and specific formation rate of HMF (\blacksquare) as a function of time on stream over ZSM-5. Reaction conditions: 300 psi He, 403 K, 2 wt% fructose in THF/water (mass ratio of THF: water = 4:1) as feed, WHSV =1.4 h⁻¹.

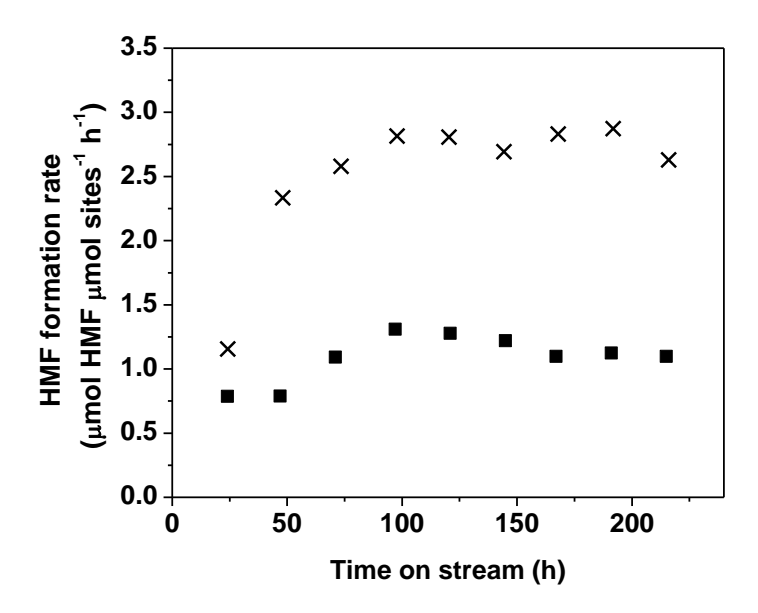


Figure 5.17 Specific formation rates of HMF over RhRe/C pretreated at 523 K (\times) and ZSM-5 (\blacksquare). Reaction conditions: 300 psi He, 403 K, 2 wt% fructose in THF/water (mass ratio of THF: water = 4:1) as feed.

5.5 Conclusions

Three different solid Brønsted acid catalysts were investigated. While acid-functionalized ordered mesoporous silica catalysts show high selectivity for HMF in the absence of PVP, 9, 10 incorporation of PVP causes the selectivity to approach levels previously achieved only with ionic liquids and high-boiling aprotic organic solvents. The high concentration of pyrrolidone groups in the confined space of the nanochannels favors the furanose tautomers of fructose. Since HMF is derived from these tautomers, a corresponding increase in selectivity occurs. Unlike other selective methods for HMF production, the solid catalyst is both easily recovered from the reaction mixture, and the product is readily isolated from the low-boiling, single-phase solvent system. Thus, the reaction environment within the catalyst has been designed to favor the desired product. Modification of inexpensive solid catalysts with functional polymers may have more general applications as reported in subsequent reports.³⁸

Acid mesoporous carbon based catalysts presented comparable performance to silica based catalysts in the conversion of fructose to HMF in the presence of water. However, acid mesoporous carbon had a significantly lower deactivation rate coefficient, being up to 60 more stable than pSO₃H-SBA-15, and up to three times more stable than the commercial Nafion SAC-13. From the catalysts studied, CMK-5-PSA is the most promising material, since it not only presents the lowest deactivation, but also the highest TOF for HMF production. Acid mesoporous carbons have potential to substitute the well-known and well characterized mesoporous silica and organosilica based catalysts, as well as the commercial Nafion SAC-13, for biomass conversion in the presence of water.

We show for the first time that a bimetallic catalyst displays substantial activity and selectivity for fructose dehydration to HMF (i.e., 50% selectivity to HMF at 30% conversion of fructose), providing evidence for Brønsted acidity over this RhRe/C catalyst in liquid water. The turnover frequency for production of HMF (with acid sites titrated by temperature programmed desorption of NH₃) was found to be two-times higher over RhRe/C compared to ZSM-5.

5.6 References

- [1] R. Alamillo, A.J. Crisci, J.M.R. Gallo, S.L. Scott, J.A. Dumesic, Angewandte Chemie International Edition, 52 (2013) 10349-10351.
- [2] J.J. Bozell, G.R. Petersen, Green Chem., 12 (2010) 539-554.
- [3] A. Aden, J. Bozell, J. Holladay, J. White, A. Manheim, G. Petersen, T. Werpy, in: T. Werpy, G. Petersen (Eds.), U.S. Department of Energy, Oak Ridge, 2004.
- [4] H.E. Van Dam, A.P.G. Kieboom, H. Van Bekkum, Starch, 38 (1986) 95-101.
- [5] A.S. Amarasekara, L.D. Williams, C.C. Ebede, Carbohydrate Research, 343 (2008) 3021-3024.
- [6] K. Shimizu, R. Uozumi, A. Satsuma, Catal. Commun., 10 (2009) 1849-1853.
- [7] H. Zhao, J.E. Holladay, H. Brown, Z.C. Zhang, Science, 316 (2007) 1597-1600.
- [8] Y. Román-Leshkov, J.N. Chheda, J.A. Dumesic, Science, 312 (2006) 1933-1937.
- [9] A.J. Crisci, M.H. Tucker, M.-Y. Lee, S.G. Jang, J.A. Dumesic, S.L. Scott, ACS Catal., 1 (2011) 719-728.
- [10] M.H. Tucker, A.J. Crisci, B.N. Wigington, N. Phadke, R. Alamillo, J. Zhang, S.L. Scott, J.A. Dumesic, ACS Catal., 2 (2012) 1865-1876.
- [11] B.H. Lipshutz, A.R. Abela, Org. Lett., 10 (2008) 5329-5332.

- [12] C.H. Kim, S.S. Kim, F. Guo, T.P. Hogan, T.J. Pinnavaia, Adv. Mater., 16 (2004) 736-739.
- [13] H. Takahashi, B. Li, T. Sasaki, C. Miyazaki, T. Kajino, S. Inagaki, Chem. Mater., 12 (2000) 3301-3305.
- [14] V.M. Gun'ko, E.F. Voronin, V.I. Zarko, E.V. Goncharuk, V.V. Turov, S.V. Pakhovchishin, E.M. Pakhlov, N.V. Guzenko, R. Leboda, J. Skubiszewska-Zięba, W. Janusz, S. Chibowski, E.
- E.M. Pakhlov, N.V. Guzenko, R. Leboda, J. Skubiszewska-Zięba, W. Janusz, S. Chibowski, E. Chibowski, A.A. Chuiko, Colloids Surf., A, 233 (2004) 63-78.
- [15] E.M. Kampouris, A.G. Andreopoulos, J. Appl. Polym. Sci., 34 (1987) 1209-1216.
- [16] C.C. Anderson, F. Rodriguez, D.A. Thurston, J. Appl. Polym. Sci., 23 (1979) 2453-2462.
- [17] S. Zheng, Q. Guo, Y. Mi, J. Polym. Sci., Part B: Polym. Phys., 37 (1999) 2412-2419.
- [18] F. Zhang, Yan, H. Yang, Y. YanMeng, C. Yu, B. Tu, D. Zhao, J. Phys. Chem. B, 109 (2005) 8723-8732.
- [19] M. Kruk, M. Jaroniec, C.H. Ko, R. Ryoo, Chem. Mater., 12 (2000) 1961-1968.
- [20] M. Tucker, R. Alamillo, A. Crisci, G. Gonzalez, S. Scott, J. Dumesic, ACS Sustainable Chem. Eng, 1 (2013) 554–560.
- [21] K. Suwannakarn, E. Lotero, J.G. Goodwin, C.Q. Lu, J. Catal., 255 (2008) 279-286.
- [22] M.H. Tucker, A.J. Crisci, B.N. Wigington, N. Phadke, R. Alamillo, J.P. Zhang, S.L. Scott, J.A. Dumesic, ACS Catal., 2 (2012) 1865-1876.
- [23] J.M. Anderson, R.L. Johnson, K. Schmidt-Rohr, B.H. Shanks, Carbon, 74 (2014) 333-345.
- [24] L.M. Yang, Y.J. Wang, G.S. Luo, Y.Y. Dai, Microporous Mesoporous Mater., 84 (2005) 275-282.
- [25] H. Darmstadt, C. Roy, S. Kaliaguine, T.W. Kim, R. Ryoo, Chem. Mater., 15 (2003) 3300-3307.
- [26] S.H. Joo, S.J. Choi, I. Oh, J. Kwak, Z. Liu, O. Terasaki, R. Ryoo, Nature, 412 (2001) 169-172.
- [27] M.H. Tucker, in: Department of Chemical & Biological Engineering, University of Wisconsin-Madison, Madison, 2011.
- [28] J.M. Aragon, J.M.R. Vegas, L.G. Jodra, Ind. Eng. Chem. Res., 33 (1994) 592-599.
- [29] L. Petrus, E.J. Stamhuis, G.E.H. Joosten, Industrial & Engineering Chemistry Product Research and Development, 20 (1981) 366-371.
- [30] M. Chia, Y.J. Pagan-Torres, D. Hibbitts, Q. Tan, H.N. Pham, A.K. Datye, M. Neurock, R.J. Davis, J.A. Dumesic, Journal of the American Chemical Society, 133 (2011) 12675-12689.
- [31] L. Zhang, A.M. Karim, M.H. Engelhard, Z. Wei, D.L. King, Y. Wang, J. Catal., 287 (2012) 37-43.
- [32] B.F.M. Kuster, H.M.G. Temmink, Carbohydrate Research, 54 (1977) 185-191.
- [33] B.F.M. Kuster, H. S. van der Baan, Carbohydrate Research, 54 (1977) 165-176.
- [34] J.N. Chheda, Y. Roman-Leshkov, J.A. Dumesic, Green Chemistry, 9 (2007) 342-350.
- [35] M. Chia, B.J. O'Neill, R. Alamillo, P.J. Dietrich, F.H. Ribeiro, J.T. Miller, J.A. Dumesic, Journal of Catalysis, 308 (2013) 226-236.
- [36] V.V. Ordomsky, J. van der Schaaf, J.C. Schouten, T.A. Nijhuis, Journal of Catalysis, 287 (2012) 68-75.
- [37] V.V. Ordomsky, J. van der Schaaf, J.C. Schouten, T.A. Nijhuis, ChemSusChem, 5 (2012) 1812-1819.
- [38] T.J. Schwartz, R.L. Johnson, J. Cardenas, A. Okerlund, N.A. Da Silva, K. Schmidt-Rohr, J.A. Dumesic, Angewandte Chemie International Edition, 53 (2014) 12718-12722.

Chapter 6: The Design of Catalytic Systems for the Selective Isomerization of Glucose to Fructose

6.1 Introduction

The efficient and selective conversion of biomass-derived renewable feedstocks to chemicals and fuels remains a major techno-economic challenge.^{1, 2} Fructose, a simple carbohydrate that can be obtained from cellulose, can be dehydrated to a potential platform chemical, 5-hydroxymethylfurfural (HMF).³ Glucose, the more abundant hexose sugar, is not selectively dehydrated to HMF and must undergo isomerization to fructose, before dehydration, to achieve higher HMF yields as reported in previous chapters.

6.2 Homogenous Base-catalyzed Glucose Isomerization

There are few reports on the use of organic Brønsted base catalysts for glucose isomerization and even fewer that report high fructose yield in aqueous environments. Recent work by Tessonnier, et. al. investigated the kinetics and product distribution under high fructose yield conditions in an aqueous system.⁴ The base-catalyzed isomerization of glucose to fructose proceeds via the Lobry de Bruyn-Alberda van Ekenstein (LdB-AvE) mechanism.⁵ Both ring and open chain forms of glucose coexist in aqueous solution where the base reacts with glucose to promote the formation of the 1,2 enediol intermediate (Scheme 6.1).

There was a lack of dependence on the initial pH of the solution in the range of 10.7 to 11.3, no glucose conversion below pH 9, and an observed decrease in the pH with time. Glucose is converted to fructose which degrades to acidic by-products (e.g. lactic acid, formic acid, and levulinic acid) that neutralizes the base and stopping the reaction. This is apparent at low NaOH

concentrations and/or high temperatures where after 30 min the reaction plateaus for both glucose conversion and fructose production (Figure 6.1). No HMF or other products were detected.

Scheme 6.1. Reaction mechanism for the base-catalyzed isomerization of glucose to fructose.⁴

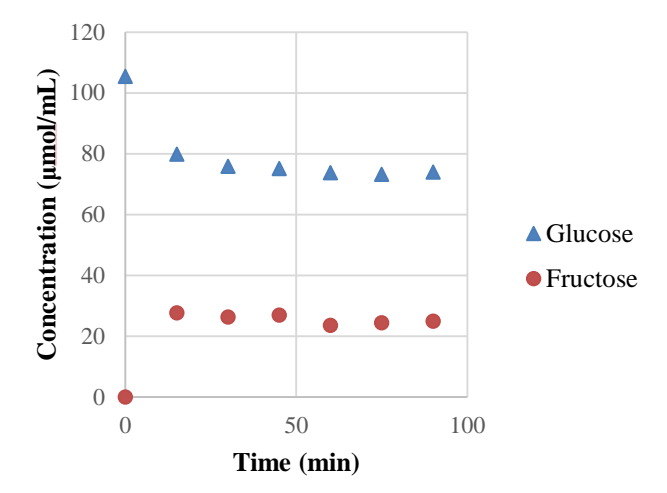


Figure 6.1. Glucose isomerization in water. Reactions were carried out at 403 K using 1.5 mL solutions of 2 wt% glucose and 5 mM NaOH.

Catalyst deactivation was apparent even at changing THF co-solvent concentrations, NaOH concentrations, and temperature (Table 6.1). Increasing the concentration of THF at higher temperatures increased the glucose conversion, however had no effect on selectivity to fructose. However, increasing the initial NaOH concentration had a major increase in the glucose conversion, but lowered the selectivity to fructose. This is in agreement that highly basic environment enhances degradation pathways of ring fructose and acyclic forms of both sugars⁴ which also increases glucose conversion past equilibrium values. The degradation effects were minimized with temperatures reaching calculated equilibrium conversion based on previous literature values.⁶ When GVL was used as the organic co-solvent, no activity for glucose conversion was observed, most likely due to trace acid neutralizing the solution.

Table 6.1. Glucose isomerization in different solvents mixtures of THF and water, and varied NaOH concentrations. Reactions were carried out at varied temperatures using 1.5 mL solutions of 2 wt% glucose. Reported values are average of points after reaching a steady-state value.

THF	[NaOH]		Glucose	Fructose
weight %	(mM)	T (K)	Conversion	Selectivity
0%		403	30%	81%
25%		403	32%	79%
67%	5	403	39%	78%
0%		403	63%	61%
25%		403	68%	58%
67%	25	403	74%	53%
0%		368	52%	90%
25%		368	50%	89%
67%	25	368	47%	91%
0%		323	47%	93%
25%		323	47%	94%
67%	25	323	48%	88%

To determine initial turnover frequencies (TOF), the initial concentration of NaOH was increased to minimize deactivation. The organic co-solvent, THF, concentration was varied (Table 6.2) showing both an increase in the glucose consumption and fructose production with increasing THF concentrations. It has been proposed that the isomerization in basic solution most likely occurs via the Lobry de Bruyn-Alberda van Ekenstein (LdB-AvE) mechanism where the C-2 proton on the acyclic glucose is removed by a Brønsted base that forms an enediol intermediate, followed by a hydrogen transfer from the O-2 to O-1 and protonation of C-1.⁴

Table 6.2. Initial Turnover Frequency (TOF) for glucose isomerization in different solvents mixtures of THF and water. Reactions were carried out at 323 K using 1.5 mL solutions of 2 wt% glucose and 25 mM NaOH.

THF weight %	Glucose Consumption (min ⁻¹)	TOF * 10 ²	Fructose Production TOF * 10 ² (min ⁻¹)
0%	7.8		6.2
25%	9.6		7.1
67%	10.8		7.8

6.3 Homogenous Lewis Acid-Catalyzed Glucose Isomerization

In addition to Brønsted bases, homogenous Lewis acids are common catalyst for the glucose isomerization. Previous work focused on the production of HMF from glucose in a biphasic reactor with an alkyl phenol solvent as the organic extracting phase.⁷ This was accomplished by using a combination of Lewis and Brønsted acids for glucose isomerization and fructose dehydration, respectively. A selectivity to desired products (fructose and HMF) of 68% at 91% glucose conversion was achieved. We report the use of AlCl₃ as a Lewis acid for glucose isomerization in monophasic co-solvent systems, however one complexity that needs to be considered in this systems is the hydrolysis of AlCl₃ (Equation 1) that leads to the formation of HCl (Equation 2), a Brønsted acid in solution, which in turn catalyzes the dehydration of fructose formed to HMF (Scheme 6.2).

$$AlCl_3(aq) + 6H_2O(l) \rightarrow [Al(H_2O)_6]^{3+}(aq) + 3Cl^-(aq)$$
 (1)

$$[Al(H_2O)_6]^{3+}(aq) + Cl^{-}(aq) \rightarrow [Al(H_2O)_5(OH)]^{2+}(aq) + HCl(aq)$$
 (2)

Scheme 6.2. Tandem glucose isomerization to fructose and subsequent fructose dehydration to HMF

6.3.1 Cellobiose Hydrolysis by a Brønsted Acid

Fructose in the presence of a Lewis acid, can be isomerized back to glucose, but also be subjected to degradation pathways. Cellobiose (CB), a dimer of glucose linked via a $\beta(1\rightarrow 4)$ bond, was studied as a model reaction as it only hydrolyzed to glucose via Brønsted acids. There was no CB conversion detected in the presence of a purely solid Lewis acid, Sn-Beta zeolite. The initial rate of reaction for CB hydrolysis was linear with increasing HCl concentration in both water and a monophasic 2:1 (w:w) THF:water solvent system. An increase in the rate of reaction when going from a water to THF water systems is agreement with previous work. However, when AlCl₃ concentration is varied the initial rate of reaction has a linear increase from 0-4 mM, but after that plateaus. The AlCl₃ hydrolysis to HCl at higher concentration can be limited by the oligomerization of AlCl₃ therefore limiting the amount of HCl in solution. Future solvent students were done at 2 mM AlCl₃ to be in the linear regime for Brønsted acidity.

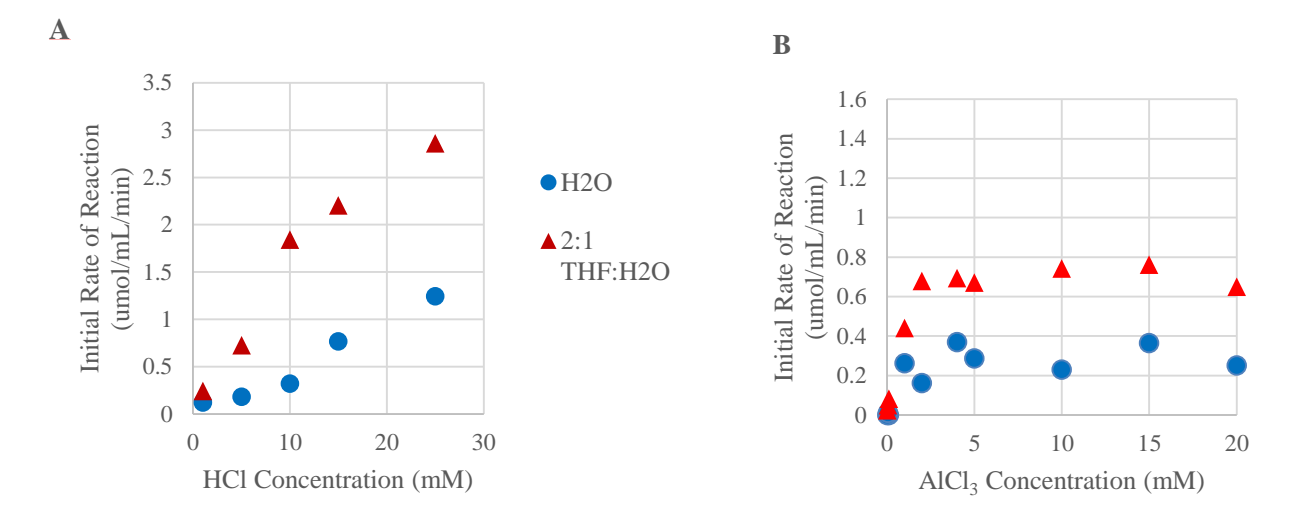


Figure 6.2 Cellobiose hydrolysis at varied acid concentrations in water (circles) and 2:1 (w:w) THF:water (triangles). Reactions were carried out at 403 K using 1.5 mL solutions of 2 wt% glucose and varied HCl and AlCl₃ concentrations.

6.3.2 Solvent Studies using Homogenous Lewis Acids

The initial glucose conversion TOF increased with increasing amount of THF until 66% THF, where the TOF stabilized (Figure 6.3). Subsequently, the fructose production TOF increased with increasing THF amounts with no plateau. When fructose is used as the initial substrate, at lower THF concentrations, the AlCl₃ has a higher production rate to HMF, most likely due to higher acid concentrations of HCl, since one mole of AlCl₃ can produce up to 3 mol of HCl (Figure 6.4). At 2 mM of HCl in pure water the fructose consumption and HMF productions are undetectable. But as the amount of THF increases an increased in HMF production rate by HCl surpasses that of the AlCl₃. At longer reactions times the selectivity to HMF from fructose is significantly higher at higher THF concentrations for the Brønsted acid versus the Lewis acid, most likely due to minimized degradation reactions.

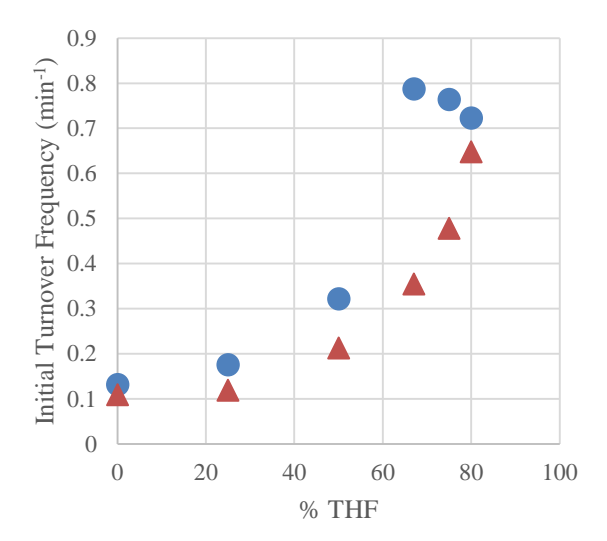


Figure 6.3. Glucose isomerization at varied THF concentrations. Reactions were carried out at 403 K using 1.5 mL solutions of 2 wt% glucose and 2 mM AlCl₃. Initial glucose consumption TOF (circle) and initial fructose product TOF (triangle)

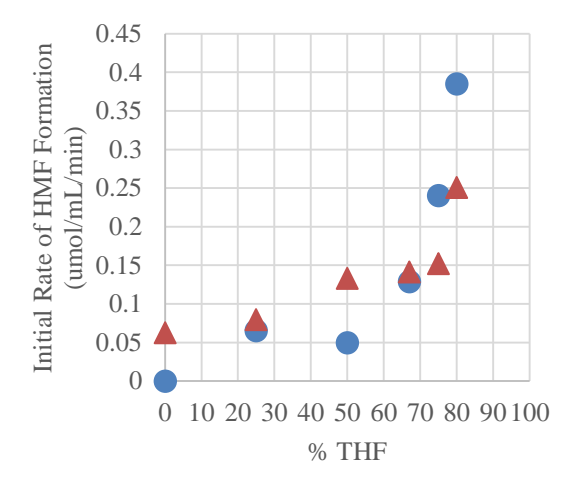


Figure 6.4. Initial rate of HMF formation for fructose dehydration reactions at varied THF concentrations using 2 mM AlCl3 (triangle) and 2 mM HCl (circle). Reactions were carried out at 403 K using 1.5 mL solutions of 2 wt% fructose and respective acid.

From these experiments we can conclude that glucose is converted to fructose via an intramolecular hydride shift only through a Lewis acid. Fructose, however, can be converted by both Lewis and Brønsted acids, with higher selectivity to HMF for Brønsted acid catalysts compared to Lewis acid catalysts. Rates of reaction and selectivity to HMF is also increased with increasing amounts of THF in the solvent. HMF was also seen to only be converted with Brønsted acids under the reaction conditions. It should be noted that no retro-aldol condensation products, such as glycoaldehyde, were detected.

6.4 Solid Base-Catalyzed Reactions

Microporous zeolites have been widely studied and well elaborated as solid catalysts in petroleum refineries, and have recently been investigated for biomass processing in liquid phase, e.g. carbohydrate isomerization, dehydration, upgrading, *etc*. The ability of zeolites to take up glucose from aqueous solutions selectively relative to fructose and sucrose has been reported ¹⁰, though the effect on the adsorption of glucose or HMF in the presence of a co-solvent (particularly GVL) was not clear.

FAU zeolites are typical large-pore microporous solids, with supercages 11.24 Å in diameter and 12 atom-ring apertures of 7.35 Å. This is large enough to accommodate glucose allow for its internal diffusion since glucose exists mostly in the form of pyranoses, representing 99.7 % of glucose tautomers in water at 25 °C ¹¹, with calculated dimensions of ca. 7 Å with an explicit water model. Thus, three catalysts from FAU family, NaX, NaY, and HY, were tested, of which the corresponding SiO₂/Al₂O₃ ratio are 2.8:1, 5.1:1, and 5.1:1, respectively.

6.4.1 Adsorption on FAU Zeolites

The microporous zeolites (200 mg) were mixed with a semi-aqueous solution of glucose or HMF (1 ml 0.1 mol L⁻¹) at room temperature, allowing the adsorption to reach equilibrium. After solid-liquid separation by centrifuge, the glucose concentration in the supernatant was analyzed. For NaX, the concentration decreased by just 7 %, Figure 6.5. Interestingly, glucose adsorption increases dramatically when raising the GVL content. When the GVL:water ratio reached 46:54 mol:mol (close to the solubility limit of for this concentration of glucose), the drop in concentration is 63 %. The extraframework cation ($Na^+ > H^+$ in Y) dictates the adsorption capacity while the impact of SiO₂/Al₂O₃ in NaX and NaY becomes insignificant. Consequently, ex situ analysis of post-reaction solutions may be highly misleading if it does not account for the amount of adsorbed material. Glucose uptake by the zeolite suggests differential stabilization by the bulk GVL-water mixture compared to internal pore environment of the zeolite. The latter may be influenced by the pore confinement, the nature of the extra-framework cations, and interactions with adsorbed solvent. In particular, coordination of glucose by Na⁺ (the extra-framework cations in NaX) has the potential to further contribute to the adsorption of glucose (especially α -Glcp).¹² Thus replacing Na⁺ by H⁺ lowers the adsorption of glucose significantly, in both aqueous and GVL-water mixtures.

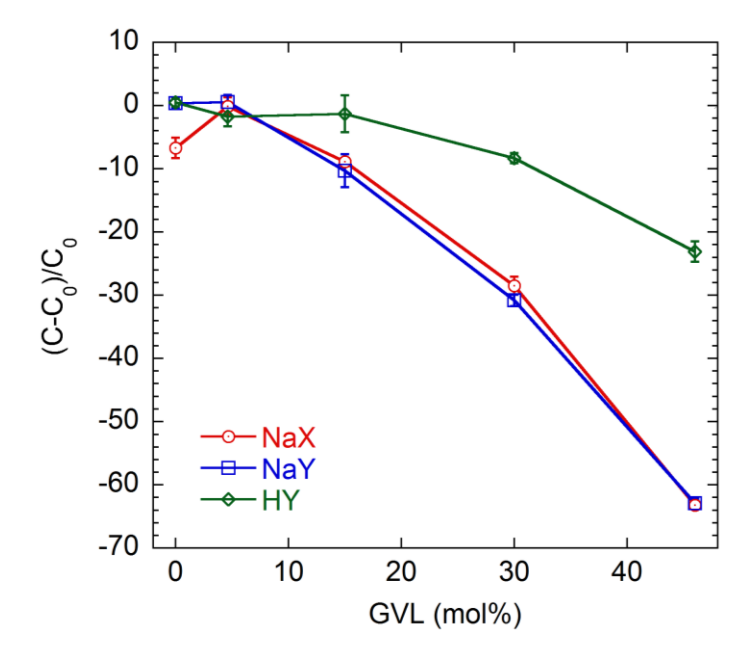


Figure 6.5. Change in liquid phase concentration of glucose (C), upon combining 1.0 mL of a 0.100 mol L⁻¹ solution of glucose in a GVL/water mixture with various zeolites (200 mg), as measured by quantitative solution-state ¹H NMR. Each result is the average of three independent experiments; error bars show the standard deviation.

As another interesting family of zeolites as the catalysts for carbohydrate processing, H-BEA zeolites have also been studied. H-BEA does not adsorb a significant amount of glucose at any of the five solvent compositions studied. Indeed, in the presence of GVL, the glucose concentration in the liquid phase actually increases because the dimensions of the largest H-BEA channel, 6.6×6.7 Å, are of comparable dimensions as the glucose tautomers, and only solvent uptake occurs. Thus further experiments were conducted with NaX zeolite, allowing appreciable and fine-tuning adsorption by solvent composition.

Solvents and solutes populate not only the micropores of zeolites but also the inter-particle spaces and external surfaces and the definition of the interface (Gibbs Divided Surfaces)¹³ for the surface excess extends is rather challenging for solid-liquid interface. Solid-state NMR with magic-angle spinning (MAS) was used to resolve such issues. For example, the spectrum of the

NaX slurry with 1^{-13} C-glucose in GVL:water (46:54 mol:mol) contains four distinct signals for highly mobile glucopyranose isomers (α -Glcp and β -Glcp) in the bulk solution (sharp, 92.7 and 96.8 ppm), and less mobile isomers confined in the zeolite pores (broad, 92.2 and 96.4 ppm), in Figure 2. The differences in chemical shift presumably arise as the result of changes in solvation of the sugar, and/or its interactions with the negatively-charged zeolite framework and extra-framework Na $^{+}$ ions. Deconvolution/integration of the NMR spectrum in Figure 6.6 reveals that 65 % of the glucopyranose tautomers are confined in the micropores. The α -Glcp: β -Glcp tautomer ratio is very close in the solution phase (45:55) and the adsorbed phase (43:57). Since both the exact distribution of glucose and the concentration of glucose in bulk liquid phase were determined, the decrease in volume of the liquid phase can be estimated to be (0.24 \pm 0.06) mL g^{-1} , which is close to but less than the pore volume determined by N₂ adsorption. The smaller value obtained is due to the fractal internal surface of zeolites and significantly larger molecular sizes of glucose and GVL compared to N₂. 14

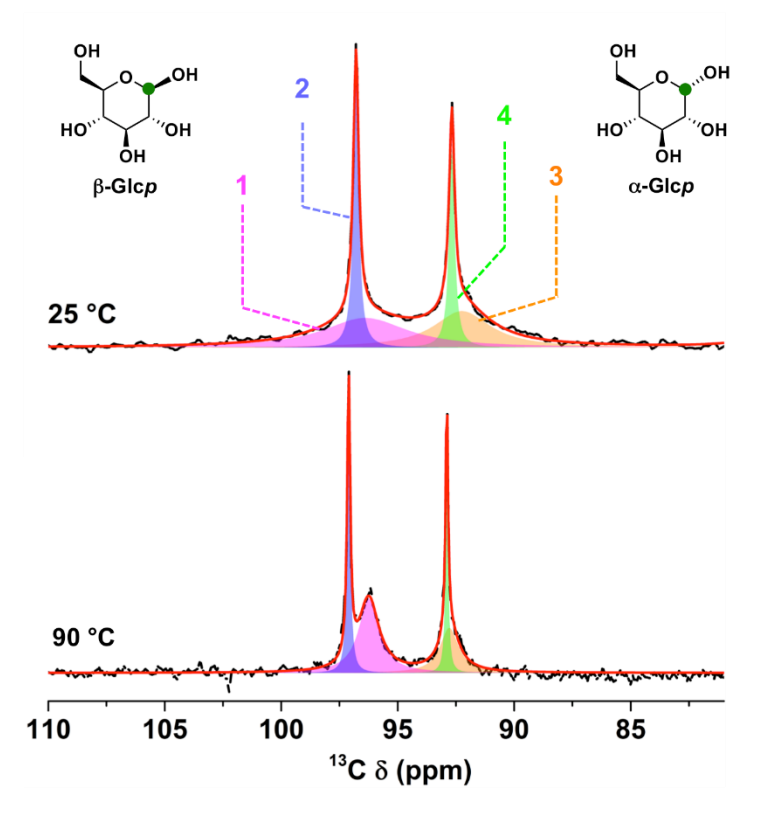


Figure 6.6. Direct polarization solid-state MAS ¹³C NMR spectra of NaX slurry with 0.10 mol/L 1-¹³C glucose in GVL:water (46:54 mol:mol), recorded *in situ* at 25 °C and 90 °C. A long relaxation delay (30 s) was used to ensure quantitative analyses in both cases.

At elevated temperatures, such as 130 °C (typical of reaction temperatures used for glucose isomerization), increased mobility of the adsorbed glucose molecules results in motional narrowing of the broad signals. The α -Glcp: β -Glcp tautomer ratio does not change significantly in the solution (43:57), while the ratio in the adsorbed phase changes to 35:65 (Figure 6.7). This indicates that the pore environment is even more different from the bulk solution under reaction conditions because the tautomer distribution is dictated only by the temperature and solvent composition.

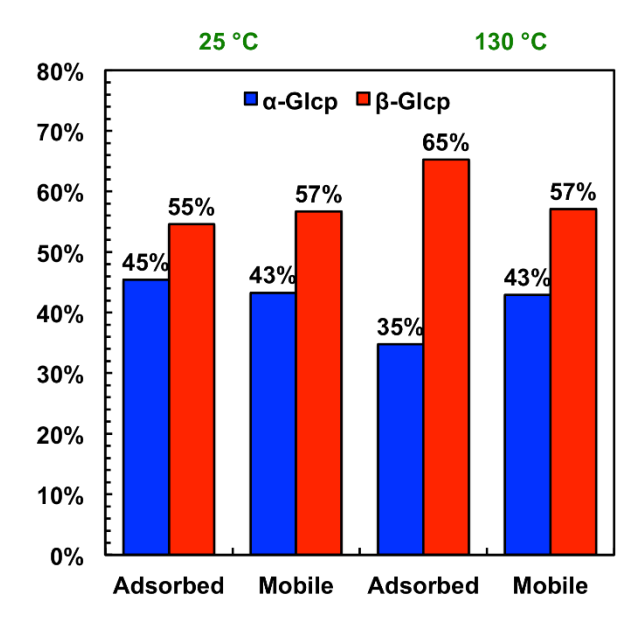
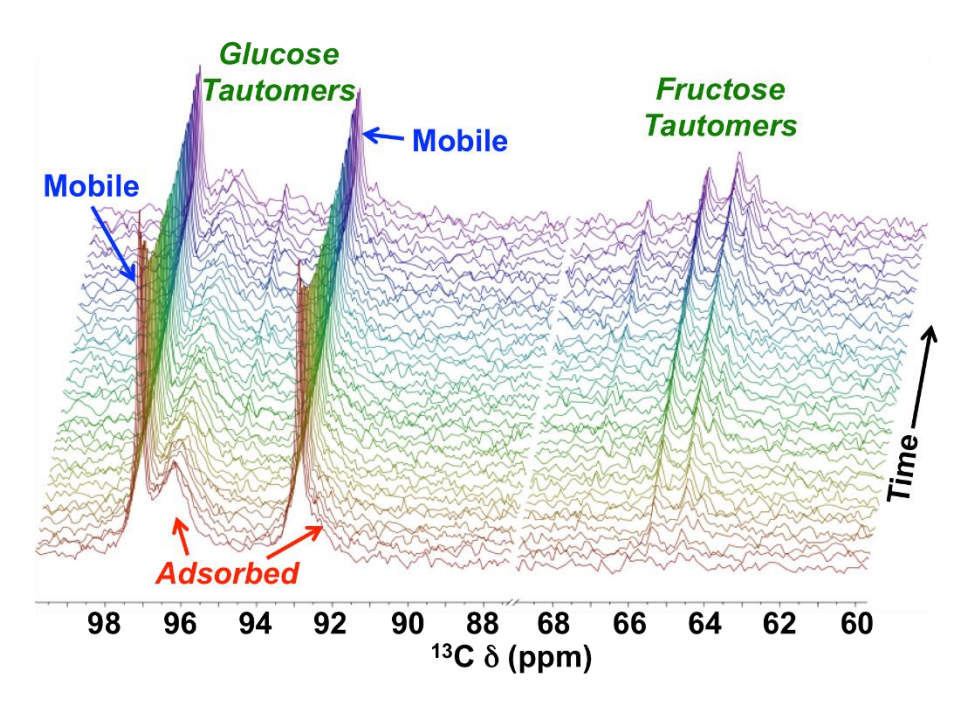


Figure 6.7. Ratio of α-Glc*p*:β-Glc*p* adsorbed in zeolite and in the bulk solution at 25 °C and 130 °C. NaX zeolite with 1 mL 1- 13 C-glucose solution (0.1 mol L- 1) in GVL:water mixture (46:54 by mole).

NaX was studied for glucose isomerization to fructose at reaction temperatures and followed *in situ*, by recording the direct polarization solid-state NMR spectra over the course of 20 h. Fructose signals at ca. 65 ppm (one for each of the four cyclic tautomers of 1-¹³C-fructose) are visible starting with the first spectrum (acquired 10-15 min after heating commenced) and their intensity increases gradually with time, Figure 6.8a. The absence of sugar signals at other chemical shifts rules out ¹³C scrambling during isomerization. Kinetic profiles extracted from these spectra are shown in Figure 6.8b.

A.



B.

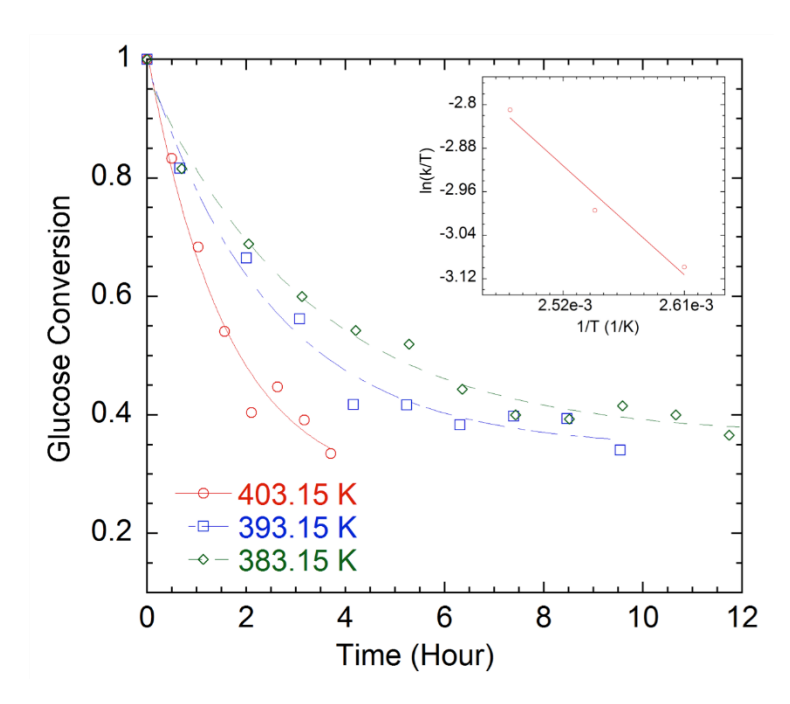


Figure 6.8. (A) Conversion of 1^{-13} C-glucose catalyzed by NaX in GVL-H₂O (46:54 mol:mol) in a high T/P solid-state NMR rotor, recorded at 130 °C (total of 20 h) and spin rate 5 kHz. (B) Variable temperature kinetic profiles for glucose conversion to fructose. The inset shows an Arrhenius plot, from which the activation energy was estimated.

The total amount of glucose declines as it reacts, while the fraction of glucopyranoses that are adsorbed increases slightly over time (Figure 6.9). Thus more dissolved glucose is taken up by the zeolite as the adsorbed glucose is converted. The α -Glcp: β -Glcp ratio in the solid phase is stable over the entire 24 h reaction time (Figure 6.10), confirming that the rotor environment is stable, *i.e.*, there is no significant temperature fluctuation or change in solvent composition due to evaporation. A small amount of mannose (overall yield < 3 %) is evident as signals at 94.9 and 94.5 ppm for the two mannopyranose tautomers. They appear after fructose signals are visible, suggesting that mannose is produced by isomerization of fructose rather than directly from glucose, as expected. In a separate experiment starting with fructose instead of glucose, equimolar amounts of glucose and mannose were formed (Figure 6.11), demonstrating that reversion of fructose is unselective.

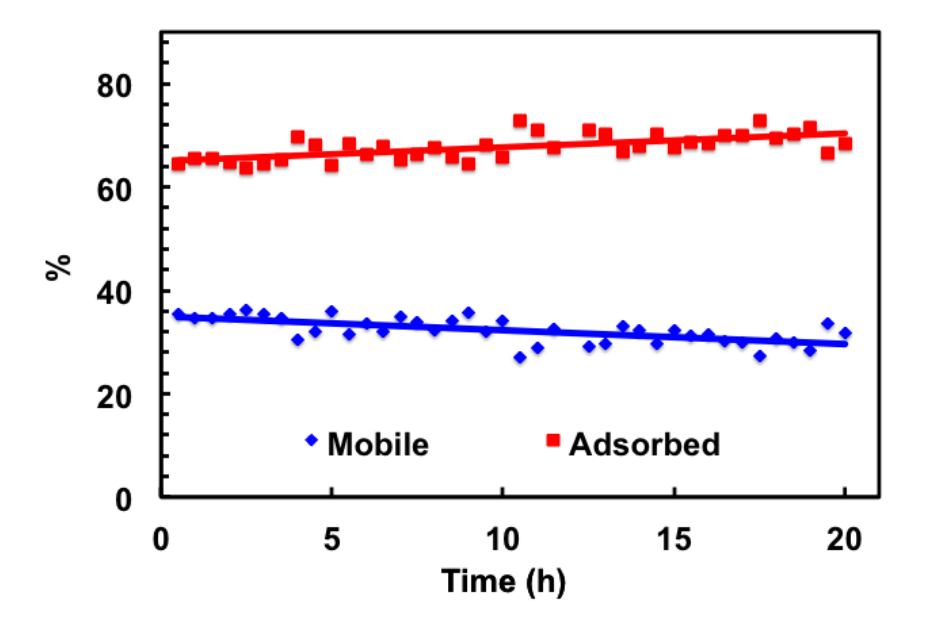


Figure 6.9 Ratio of mobile and adsorbed β-Glc*p* during the conversion of 1^{-13} C-glucose to 1^{-13} C-fructose by NaX in a GVL-H₂O mixture (46:54 by mole) in a high T/P solid-state NMR rotor, recorded at 130 °C (total of 20 h) and spin rate 5 kHz.

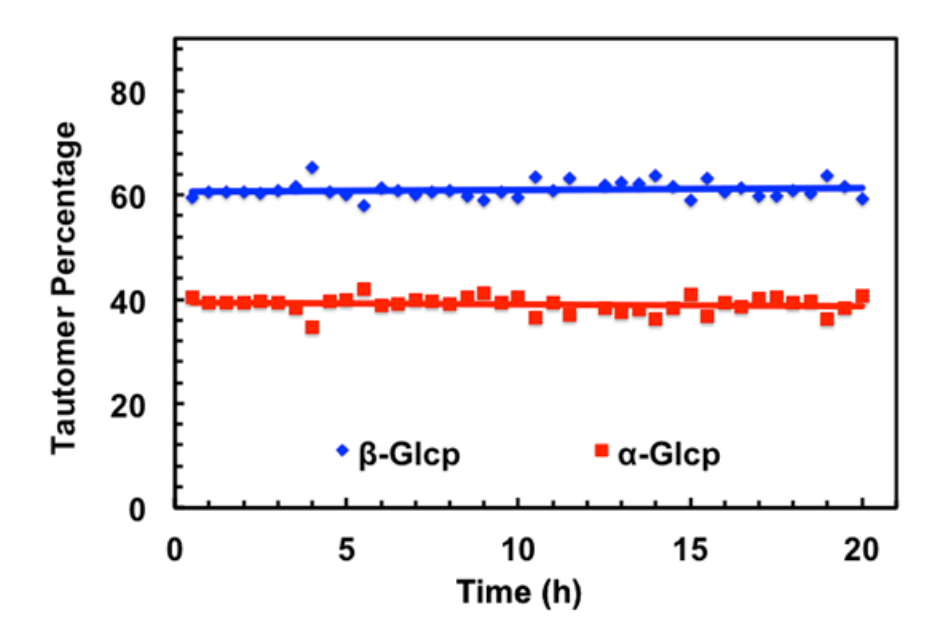


Figure 6.10 Ratio of combined α-Glcp:β-Glc during the conversion of 1- 13 C-glucose to 1- 13 C-fructose by NaX in a GVL-H₂O mixture (46:54 by mole) in a high T/P solid-state NMR rotor, recorded at 130 °C (total of 20 h) and spin rate 5 kHz.

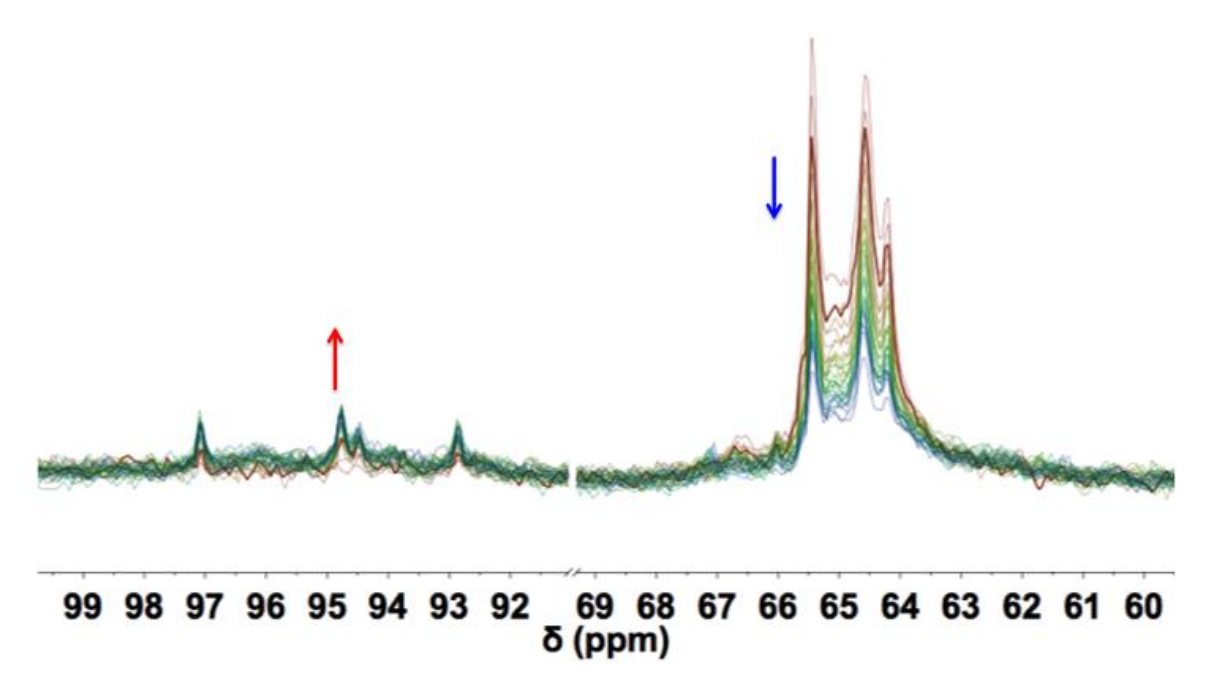


Figure 6.11. Conversion of 1^{-13} C-fructose by NaX in a GVL-H₂O mixture (46:54 by mole) in a high T/P solid-state NMR rotor, recorded at 130 °C (total of 20 h) and spin rate 5 kHz.

6.4.2 Solvent Studies on FAU Zeolites

6.4.3.1 Mass Transfer Considerations

With the small pore sizes of the FAU zeolites, internal and external mass transfer limitations were taken into account for the reactivity studies to be able to rule them out. In order to determine if external mass transfer limitations were present, the Mear's Criterion was calculated.¹⁵ The Mear's criterion is given by Equation 3:

$$\frac{r'''R_P}{C_Rk_C} < \frac{0.15}{n} \tag{3}$$

Where r''' is the reaction rate per volume of catalyst, R_p is the catalyst particle radius, C_b is the bulk phase reactant concentration, k_c is the mass transfer coefficient, and n in the reaction order. The reaction rate, catalyst radius (2 μ m), and bulk phase concentration (0.1 M) were taken from the reaction and characterization data. The reaction order is one. A dimensionless relationship applicable at low Reynold's numbers was used by relating the Sherwood, Reynolds, and Schmidt numbers as stated in Equation 4.16

$$Sh_{part} = \frac{1.13}{\epsilon} Re_{part}^{1/3} Sc^{1/3}$$
 (4)

The Sh_{part} and Re_{part} were determined from the particle diameter. A void fraction (ϵ) of 40% was assumed. The diffusivity of glucose in was determined to be 5.07 x 10-8 cm²s⁻¹.¹⁷ This resulted in a Mear's Criterion for NaX of about 3 x 10⁻³ indicating negligible external mass transfer limitations.

The Weisz-Prater number ($N_{W\text{-P}}$) was calculated to determine if internal (pore diffusion) was limiting the reaction.¹⁸

$$N_{W-P} = \frac{\Re R_p^2}{C_S D_{eff}} \tag{5}$$

Where \Re is the reaction rate, R_p is the catalyst particle radius, C_s is the reactant concentration at the external surface of the particle, and D_{eff} is the effective diffusivity in the pores of the catalyst. If the N_{W-P} is less than 0.3 this indicates negligible internal mass transfer limitations. The surface concentration was estimated to be that of the bulk solution. The pore diameter of the NaX was determined to be 10 Å and using a reduced pore diameter the effective diffusivity was estimated to be 10^{-3} . This resulted in a N_{W-P} of 1 x 10^{-8} indicating negligible internal mass transfer limitations.

6.4.3.2 Reactivity Studies

The adsorption of sugars and its products in varied solvent systems has major effects on reactivity trends. Therefore, packed-bed flow reaction studies were conducted for NaX and NaY zeolites to elucidate solvent effects for glucose isomerization studies (Figure 6.12). NaX has a higher fructose production TOF than that of NaY, but both follow similar trends. When water is used as the solvent, the fructose production TOF is the about high, but the small addition of GVL using a 1:4.5 GVL:H₂O co-solvent mixture, significantly drops the reactivity of both the NaX and NaY catalyst. When the GVL content is increased the fructose production TOF also increases, over 50% of that of pure water for NaX and about the same for NaY.

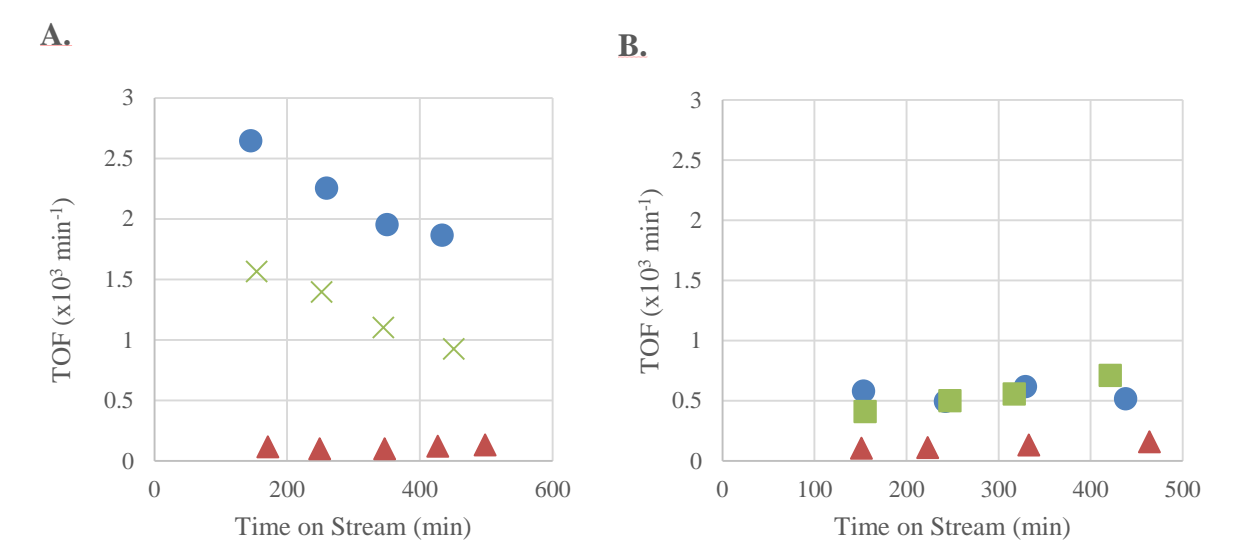


Figure 6.12. Fructose production TOF for glucose isomerization flow studies using NaX (A) and NaY (B) using H₂O (circle), 1:4.5 (v:v) GVL: H₂O (triangle), and 4.5:1 (v:v) GVL: H₂O. Reactions were carried out using 100 mg of NaX or NaY zeolite at 403 K using a feed of 2 wt% glucose flowed in at 0.04 mL min⁻¹.

For pure water NaX system, after 400 minutes on stream the glucose conversion remains at 29% with a selectivity to fructose of 74%. When 4 mol% GVL is present in the solvent system, the glucose conversion level is steady at 9% with a selectivity to fructose of about 30%. With an increase to 46 mol% of GVL in the systems, the system had a higher activity than that of the 4 mol% system, but less than that of pure water, with a glucose conversion of 22% with a selectivity to fructose of 59%.

Further flow reaction studies were carried out with solvents of different GVL- H₂O. The presence of just 4 mol% GVL causes the reactivity of NaX to drop dramatically compared to tests with only water as the solvent (Figure 6.13). When the GVL content is increased, the initial fructose production TOF also increases. Adsorption of sugars and reaction products in various solvent systems has a major effect on reactivity trends.

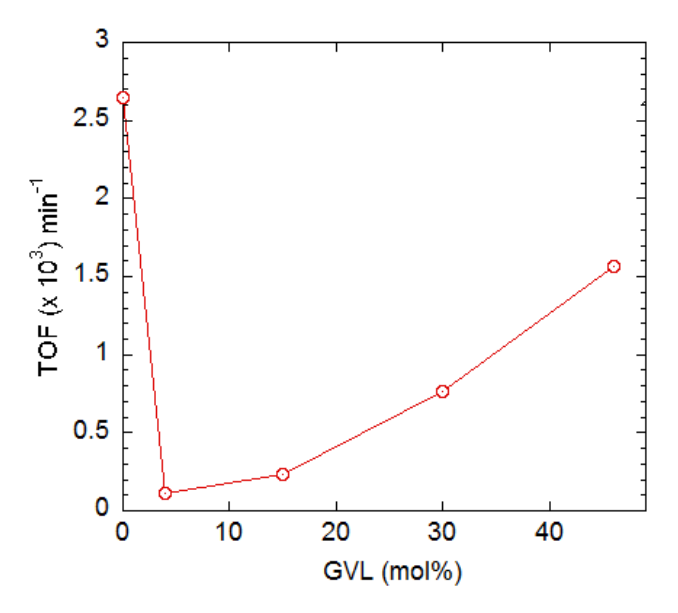


Figure 6.13. Initial fructose production TOF for glucose isomerization flow studies using NaX using varying GVL:H₂O ratios. Reactions were carried out using 100 mg of NaX at 130 °C using a feed of 0.1 mol L⁻¹ glucose flowed in at 0.04 mL min⁻¹.

FAU zeolites exchanged with alkali metal cations possess basicity rather than acidity, owing to the partially negatively charged oxygen sites on the surface. ^{19, 20} Since no HMF was formed from glucose or fructose during the isomerization, the possibility of Brønsted acids as the active sites was ruled out. GVL promotes the Brønsted acidity of both homogeneous and heterogeneous acids, however such activity enhancement was not observed when comparing to water as the solvent. The Lewis acidity of zeolites originates from its Al content, mostly in the form of extra-framework alumina. Since the activity of NaX decreases upon heating, and such deactivation is accompanied by formation of more extra-framework alumina, the latter can be ruled out as the source of the glucose isomerization activity. Since glucose isomerization can be promoted not only by acids but also by bases (e.g., hydrotalcites²¹), it can be speculated that the reaction may be catalyzed by interaction of carbohydrates with basic framework oxygens.

Furthermore, the activity of NaY is much lower than that of NaX and such difference is attributed to lowered surface negative charge.

6.4.3.2 Catalyst Regeneration Studies

The NaX reaction run was run under similar conditions as previously mentioned with a regeneration solvent to determine the feasibility of catalyst regeneration using a solvent to remove any possible humin formation. After the catalyst run, the feed was stopped via the HPLC pump and system cooled while continuing the flow of helium. Once at room temperature, 50% acetone/water (v/v) mixture was primed through the inlet and then the mixture was flowed through the reactor at 0.04 mL/min for 10 hours at RT. After the gas-liquid separator was drained, the separator was re-pressurized to system pressure, and the system was heated back to reaction temperature of 130°C under flowing He. The system was heated for 12 hours under flowing helium with occasional draining of the separator to remove any regeneration solvent. The feed solvent was then primed through the inlet before Run 2 was started, and after collecting a transient point, steady-state data was collected for Run 2.

The catalyst in the flow reactor underwent a recycle wash to determine catalyst regeneration and long-term stability. With NaX, when the solvent composition was 46 mol% GVL, an initial deactivation was noticed but stabilized after 350 minutes on stream. After the regeneration step, an initial increase in the first steady-state point was observed, but after that a steady-state fructose production was observed (Figure 6.14). When the solvent was composed of pure water, similar observations to that of the 46 mol% GVL for the first run was observed, but he regeneration step led to a steady-state fructose production rate slightly lower than that of the first run (Figure 6.15).

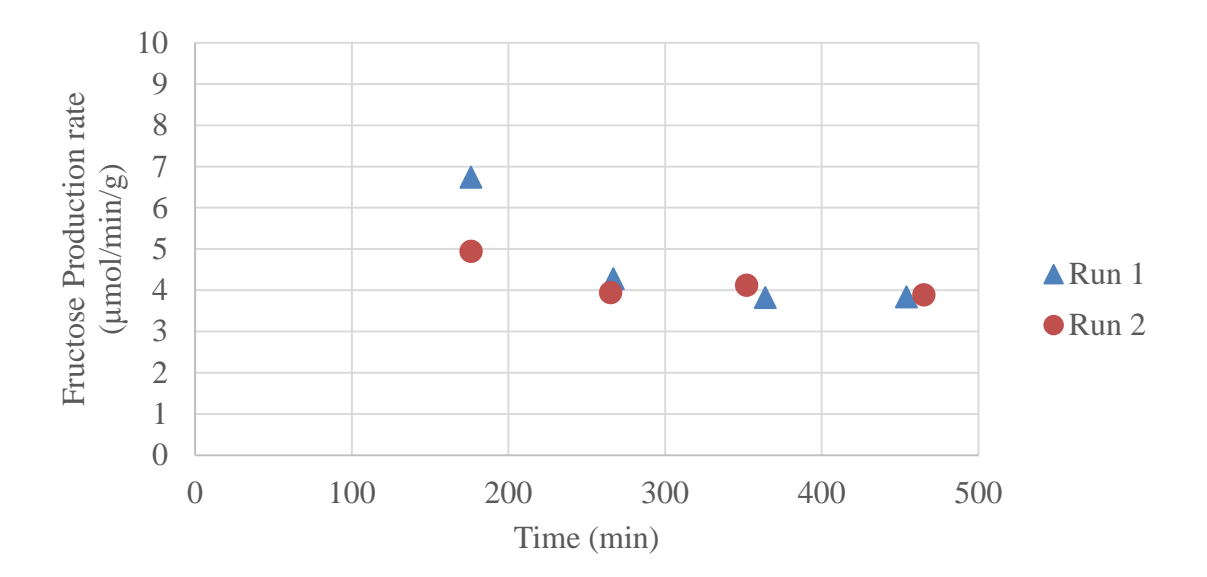


Figure 6.14. Fructose Production Rate flowing in 0.04 mL/min 0.1 M glucose in 46 mol% GVL at 130°C in packed reactor with 100 mg of NaX. Triangles represent Run 1 and Circles Run 2 after regeneration step.

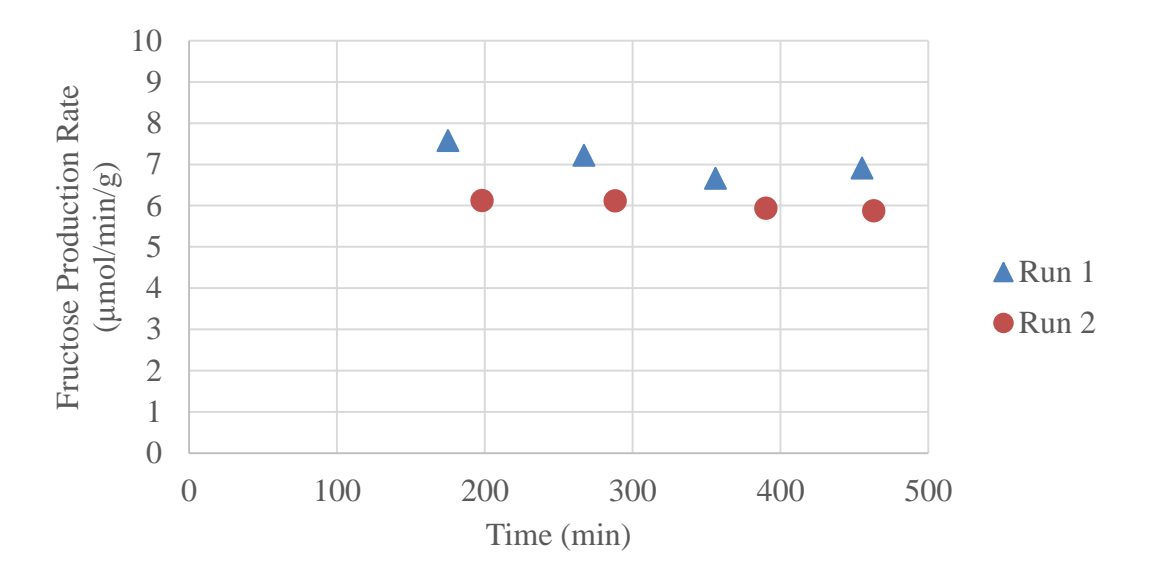


Figure 6.15. Fructose Production Rate flowing in 0.04 mL/min 0.1 M glucose in H₂O at 130°C in packed reactor with 100 mg of NaX. Triangles represent Run 1 and Circles Run 2 after regeneration step.

Nitrogen physisorption was conducted on NaX (control) and on the zeolite after reaction in water (0%), 4 mol% GVL, and 46 mol% GVL (Figure 6.16). The largest reduction in surface area and pore volume (t-plot) is observed for the sample conducted in water. The higher concentration of GVL leads to minimal reduction in surface area and pore volume, which could account for the stability of NaX even after two reaction runs, whereas in water, the second run is slightly lower than that of the first run.

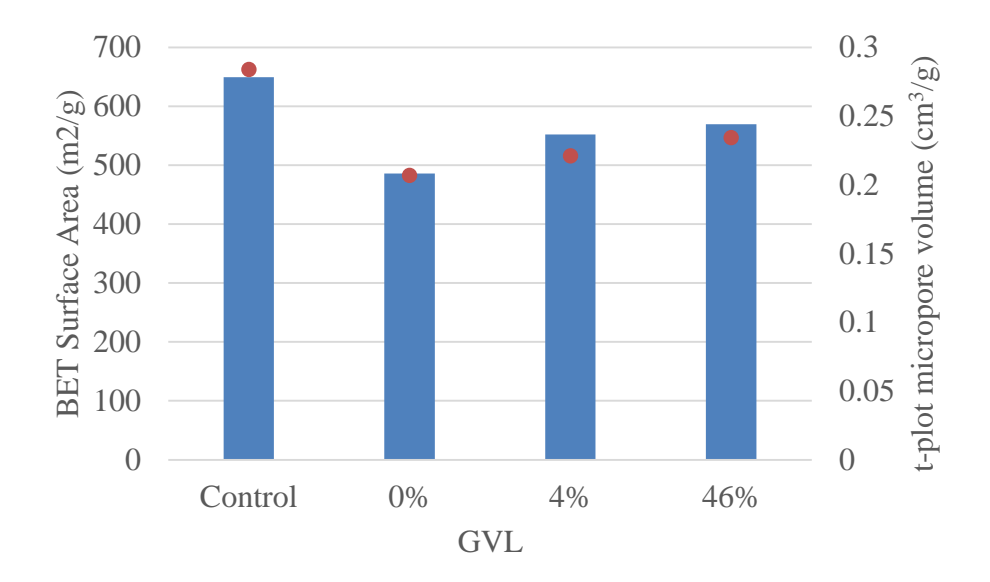


Figure 6.16. BET surface area and t-plot micropore volume as determined by nitrogen physisorption for varied NaX reaction conditions. Bars represent surface area and dots micropore volume.

6.4.3 Tandem Isomerization and Dehydration using FAU Zeolites

NaX was partially exchanged with protons to study the feasibility of tandem glucose isomerization and fructose dehydration to HMF. No HMF was detected in the NaX or NAHX catalyst in the presence of pure water. In water, the specific production to desired products decreased when going from NaX to NaHX, which correlates with a lower amount of Na present in NaHX relative to NaX (Figure 6.17). When the same catalytic systems are introduced to a 46 mol% GVL:water system, HMF is observed in the NaHX system, but only accounts for 2% of total products. With NaHX, when going from a pure water to GVL system increases the glucose conversion levels increases from 12% to 40% while maintaining similar selectivity levels of 69%.

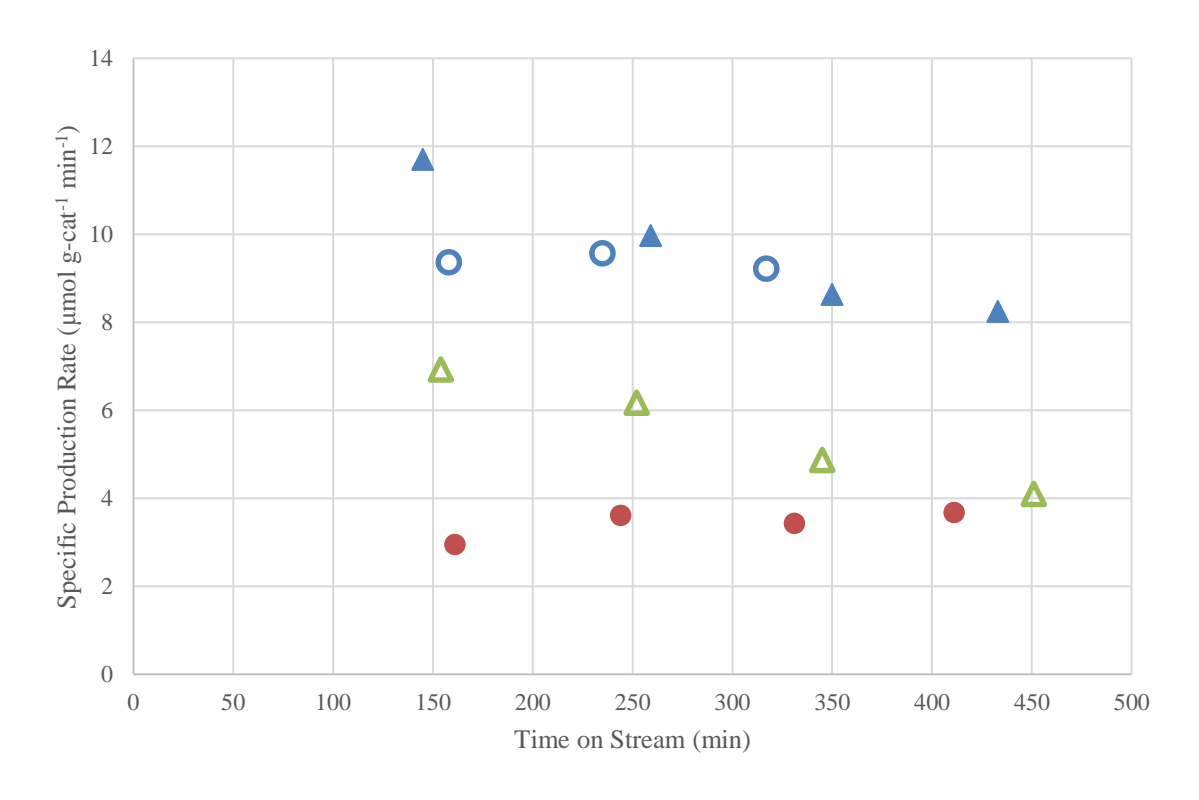


Figure 6.17. Combined fructose and HMF specific production rate for tandem glucose isomerization and fructose dehydration flow studies using NaX (triangles) using H₂O (solid) and 46 mol% GVL: H₂O (hollow). Reactions were carried out using 100 mg of catalysts at 403 K using a feed of 2 wt% glucose flowed in at 0.04 mL min⁻¹.

6.4.4 Glucose Isomerization using Sn-Beta Zeolite in a Flow Reactor

Sn-Beta zeolite has been of studied extensively as a solid Lewis acid catalyst for glucose isomerization to fructose. Catalyst loading and temperature were adjusted to exclude any mass transfer limitations and keep conversion levels to less than a third below equilibrium conversion. Similar to that of NaX and NaY, Sn-Beta shows the same reactivity trends when a small addition of GVL is added in the solvent, the fructose production TOF has a significant decrease compared to that of the pure water system. The TOF increased with the increase of GVL in the solvent system again. (Figure 6.18)

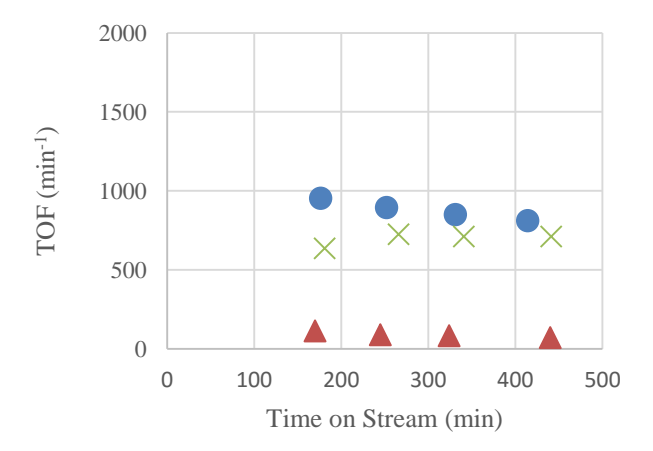


Figure 6.18. Fructose production TOF for glucose isomerization flow studies using Sn-Beta zeolite using H₂O (circle), 1:4.5 (v:v) GVL: H₂O (triangle), and 4.5:1 (v:v) GVL: H₂O. Reactions were carried out using 10 mg of Sn-Beta zeolite at 368 K using a feed of 2 wt% glucose flowed in at 0.04 mL min⁻¹.

6.5 Sn-substituted Periodic Ordered Mesoporous Materials for Tandem Glucose Isomerization and Fructose Dehydration

Some efforts to convert glucose²²⁻²⁴ (or even cellulose)²⁵ directly to HMF in a high-boiling solvent (e.g., DMSO, ionic liquids) using a metal chloride catalyst (e.g., CrCl₂, PrCl₃, NdCl₃,

DyCl₃, YbCl₃) have resulted in high yields, but catalyst toxicity and the difficulty of product isolation are major challenges that complicate scale-up. To generate HMF efficiently, tandem glucose isomerization/fructose dehydration should be conducted in a reaction medium from which the catalysts, products and unconverted reactants are easily separated. Previously, we reported a family of silica-based solid acid dehydration catalysts that are effective for the selective conversion of fructose to HMF with a low-boiling, single-phase mixed solvent (4:1 w:w THF:H₂O) in a continuous flow reactor.^{26, 27} Robust attachment of the propylsulfonic acid sites to the silica framework through co-condensation in an ordered mesopore structure was found to suppress catalyst deactivation via acid site leaching. Hydrophobic versions of these catalysts based on periodic mesoporous organosilicas (PMOs) showed both greater resistance to deactivation and improved activity for HMF production.²⁶ The THF/H₂O reaction medium causes the fructose tautomer equilibrium to shift (relative to water alone) in favor of the fructofuranoses, which are the direct precursors of HMF.²⁸ Thus, performing glucose isomerization in the mixed solvent system should promote the tandem reaction, eventually enabling a more sustainable production of HMF from glucose.

While the success of Sn-Beta as a glucose isomerization catalyst is undisputed,⁶ the traditional zeolite synthesis is time-consuming, involving a 40-day hydrothermal treatment.²⁹ In addition, highly crystalline materials are obtained only when the reagent ratios in the sol-gel mixture are extremely precise.³⁰ Recently, efforts have been made to reduce synthesis time,³¹⁻³⁴ but with uncertain consequences for Sn loading and/or reactivity. Operation of Sn-Beta in tandem with a second catalyst for carbohydrate dehydration has been reported.³⁵⁻³⁸ However, functionalization of Sn-Beta itself with Brønsted acid sites to create a single, bifunctional catalyst could be achieved via post-synthesis graft modification. Such reactions are limited by the small

number of silanols associated with crystal defects. While the zeolite can be etched or dealuminated to create more grafting-site silanols,³⁹ this may cause loss of the incorporated Sn sites, impacting pore hydrophobicity and structural integrity, as well as catalytic activity. In addition, grafted functional groups are usually sensitive to hydrothermal cleavage.²⁶

In contrast, the hydrophobic Sn-doped PMOs can be readily tailored to accommodate additional functionality. Relative to Sn-Beta, the preparation of the Sn-doped PMOs is rapid and readily scalable. They can be synthesized in hours (via microwave-assisted synthesis)⁴⁰ or a few days (via traditional hydrothermal synthesis). 41 The materials are not crystalline, and the synthesis conditions required to induce mesopore ordering are very tolerant of varying reagent ratios and/or the addition of heteroatom dopants. 42 Like other ordered mesoporous silicas (e.g., MCM-41, SBA-15, KIT-6), the PMOs are prepared by hydrolysis and condensation of a silane in the presence of a templating surfactant. 43 Similar to Sn-Beta, the pores of the PMOs are highly hydrophobic. 44, 45 Their physicochemical properties may be altered in a variety of ways: (1) by varying the bridging organic group R' of the disilane precursors, (RO)₃Si-R'-Si(OR)₃ during synthesis; (2) by postsynthetic modification of the bridging R´ groups or the residual, unreacted surface silanols; or (3) co-condensation of the disilane with functional silane 3by (e.g., (mercaptopropyl)trimethoxysilane or 3-(aminopropyl)triethoxysilane). 43

In this section (6.5), the Sn-PMO's performance as glucose isomerization catalysts are explored, comparing them directly to Sn-Beta. A bifunctional PMO catalyst containing both Lewis acid (Sn^{4+}) and Brønsted acid (propylsulfonic) sites was also synthesized, to explore the single-pot conversion of glucose to HMF.

6.5.1 Synthesis and structural characterization of Sn-containing Periodic Mesoporous Organosilicas (Sn-PMOs).

These materials were synthesized by hydrolysis of 1,4-bis(triethoxysilyl)benzene in the presence of a templating surfactant, followed by a mild calcination to remove the template. Incorporation of Sn⁴⁺ sites was achieved by co-condensation, via addition of SnCl₄·5H₂O to the synthesis mixture. The nominal Sn loading varied from ca. 0.5 to 6 wt%. In addition, an undoped PMO was modified with Sn⁴⁺ post-synthesis (Sn-PMO-2PS), via incipient wetness impregnation (IWI). The actual amount of Sn incorporated in each material, determined by elemental analysis after surfactant removal, was always within 20 % of the expected loading, Table 6.3.

Table 6.3. Physico-chemical characteristics of PMO catalysts

Nominal Sn Loading wt%	Actual Sn Loading wt%	Surface Area m ² g ⁻¹	Pore Diameter nm	Total Pore Volume cm ³ g ⁻¹	Micropore Volume cm ³ g ⁻¹
-	-	928	5.5	0.92	0.121
0.5	0.4	753	4.9	0.72	0.090
1.0	1.1	819	5.3	0.74	0.124
2.5	2.9	1268	5.9	1.30	0.132
5.0	4.6	691	5.1	0.62	0.084
5.0	5.4	875	6.9	1.31	0.060
7.5	5.8	858	5.7	0.89	0.096
1.0	1.2	742	5.1	0.74	0.076
	Sn Loading wt% - 0.5 1.0 2.5 5.0 7.5	Sn Loading wt% Loading wt% - - 0.5 0.4 1.0 1.1 2.5 2.9 5.0 4.6 5.0 5.4 7.5 5.8	Sn Loading wt% Loading wt% Area m² g⁻¹ - - 928 0.5 0.4 753 1.0 1.1 819 2.5 2.9 1268 5.0 4.6 691 5.0 5.4 875 7.5 5.8 858	Sn Loading wt% Loading wt% Area m² g⁻¹ nm Diameter nm - - 928 5.5 0.5 0.4 753 4.9 1.0 1.1 819 5.3 2.5 2.9 1268 5.9 5.0 4.6 691 5.1 5.0 5.4 875 6.9 7.5 5.8 858 5.7	Sn Loading wt% Loading wt% Area m² g⁻¹ Diameter nm Volume cm³ g⁻¹ - - 928 5.5 0.92 0.5 0.4 753 4.9 0.72 1.0 1.1 819 5.3 0.74 2.5 2.9 1268 5.9 1.30 5.0 4.6 691 5.1 0.62 5.0 5.4 875 6.9 1.31 7.5 5.8 858 5.7 0.89

All of the powder XRD patterns show the expected reflections near $2\theta = 1.0$, 1.6 and 1.8°, Figure 6.19. These features are attributed to the d_{100} , d_{200} and d_{210} reflections, respectively, of the p6mm pore structure, typical of an SBA-15-type silica. The parallel pore channels are visible by TEM, and the 2-D hexagonal pore arrangement is clearly evident by STEM, Figure 6.20. For each PMO, N₂ physisorption experiments yielded type IV isotherms, characteristic of materials with hexagonally-ordered mesopores, Figure 6.21. Overall, the presence of Sn(IV), at any of the loadings used in this study, does not appear to hinder the formation of ordered mesopores.

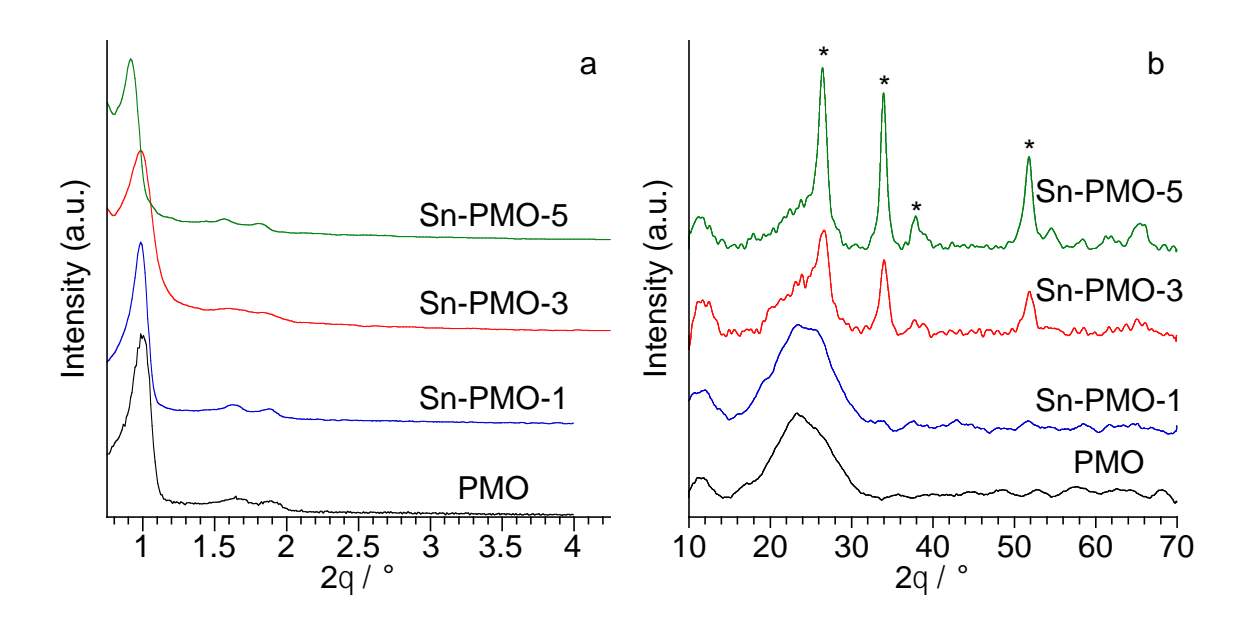


Figure 6.19. Powder X-ray diffraction patterns for PMO (containing no Sn) and various Sn-PMOs, in two different regions of 2θ ; (*) indicates major reflections for SnO₂ nanoparticles.

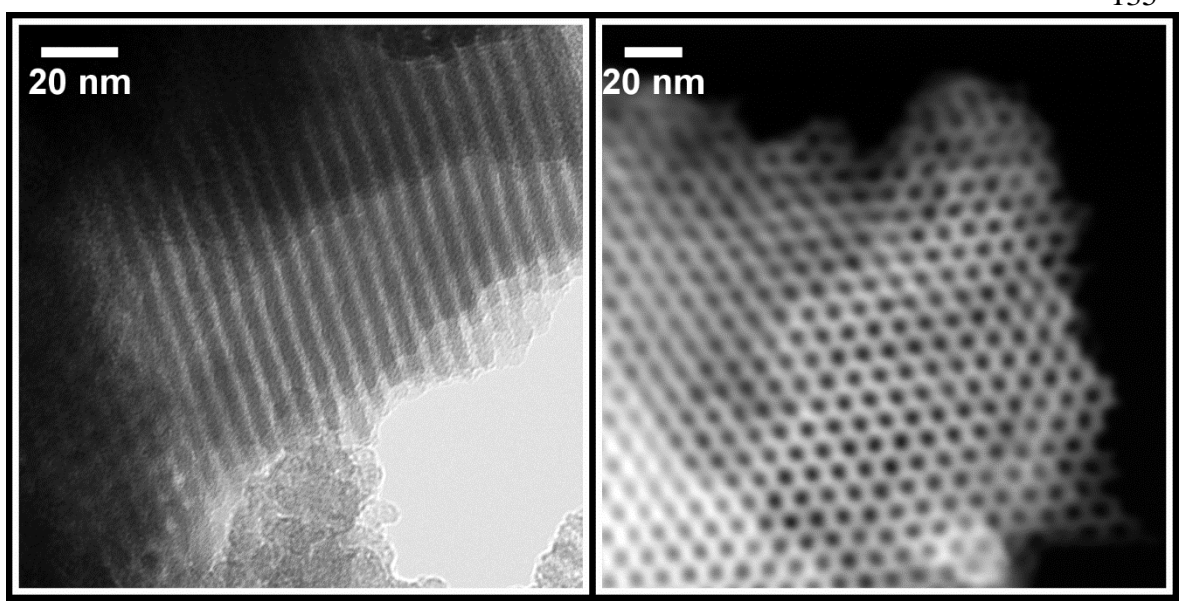


Figure 6.20. TEM (left) and STEM (right) images of Sn-PMO-1.

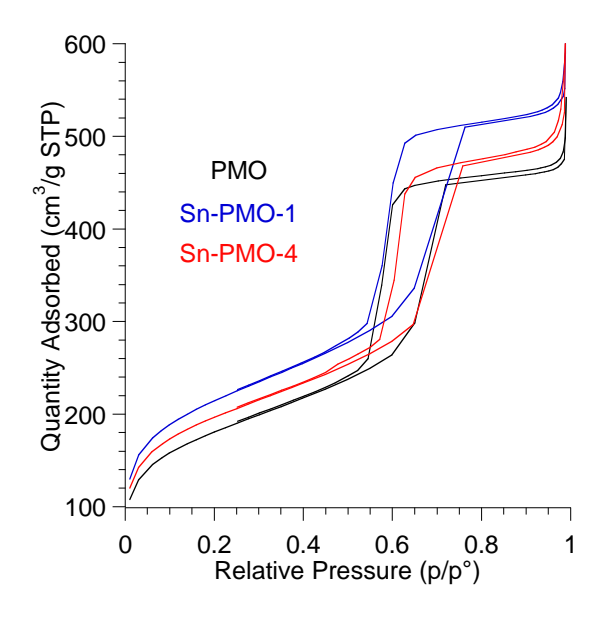


Figure 6.21. N₂ sorption isotherms typical of PMOs with low and high loading Sn-loading.

The solid-state NMR spectra shown in Figure 6.22 are typical⁴⁶ of benzene-bridged PMOs. The ¹³C CP/MAS spectra contain isotropic signals for the bridging benzene groups (134 ppm), as well as residual surfactant (ca. 75 ppm) and surface-bound ethoxy groups (59 and 16 ppm). In the

²⁹Si CP/MAS spectra, major signals for the T¹, T² and T³ sites associated with Si substituents on the benzene ring appear at 57, 65 and 75 ppm, respectively. Signals representing Q² and Q³ sites (i.e., Si atoms not associated with benzene) are also visible, but have low intensity. They may arise as a result of the calcination process, which disrupts a small fraction of Si-C bonds.⁴¹ The exceptional thermal stability of the Sn-free PMO⁴¹ is retained by the Sn-PMOs, as shown by the TGA profiles in Figure 6.23. All are relatively stable up to 723 K, at which temperature the materials begin to decompose rapidly.

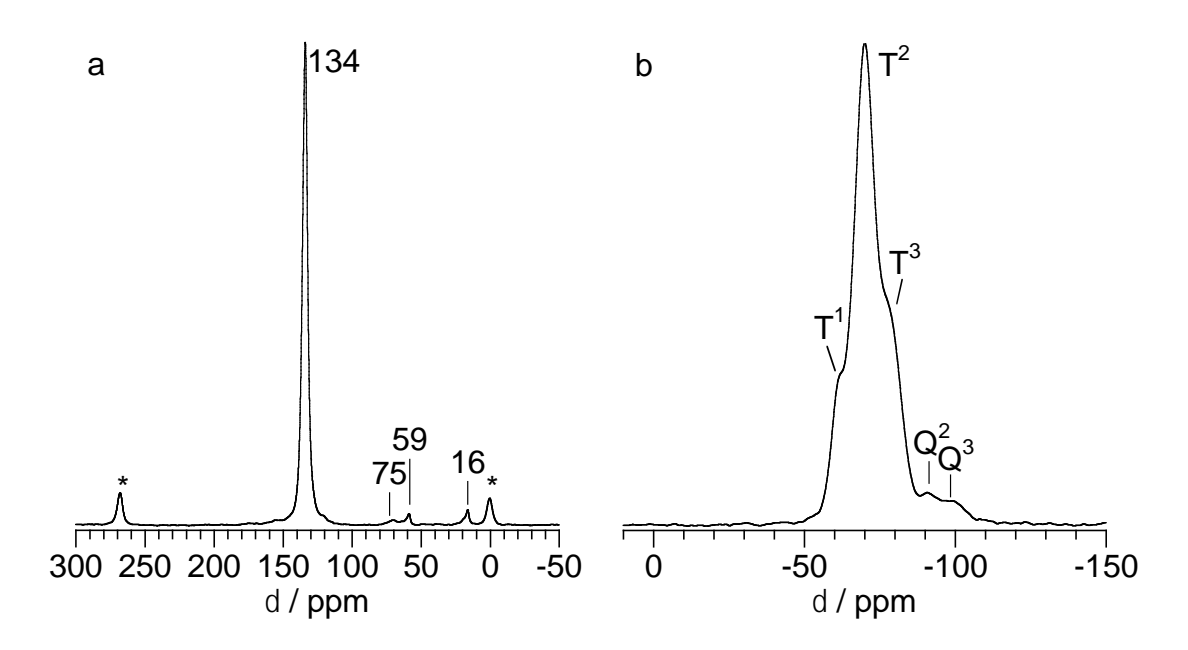


Figure 6.22. Solid-state NMR spectra of Sn-PMO-1: (a) ¹³C CP/MAS spectrum; and (b) ²⁹Si CP/MAS spectrum; (*) indicates a spinning sideband.

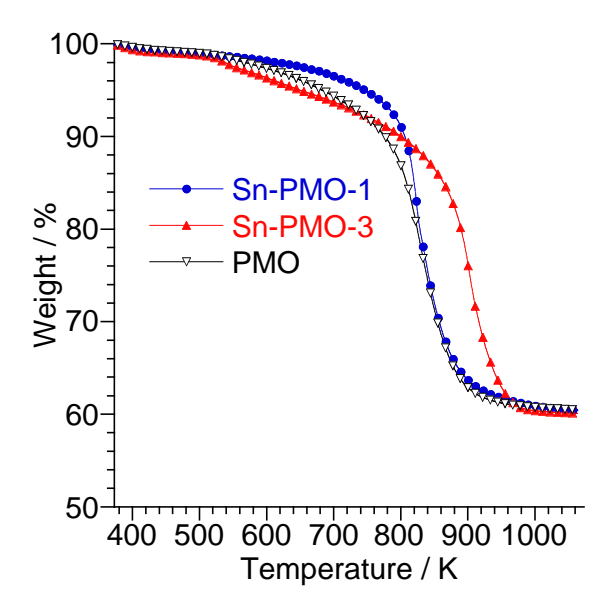


Figure 6.23. Thermogravimetric analyses of various PMOs, recorded in flowing O₂.

In the powder XRD patterns shown in Figure 6.19b, no reflections characteristic of SnO₂ nanoparticles are evident for Sn-PMO-1 or Sn-PMO-2 (with 0.4 and 1.1 wt% Sn, respectively), but they are present for Sn-PMO-3 and Sn-PMO-5 (with 2.9 and 5.4 wt% Sn, respectively). The intensity of these reflections increases with Sn loading. Using the Scherrer equation, the average diameters of the nanoparticles were calculated to be 6.8 and 9.2 nm for Sn-PMO-3 and Sn-PMO-5, respectively.

6.5.1.1 *Sn dispersion and framework incorporation*. The EXAFS at the Sn K-edge was recorded to explore whether smaller nanoparticles (i.e., those undetectable by pXRD) are present in the PMOs that have lower Sn loadings. The magnitudes of the Fourier-transformed EXAFS are compared for Sn-PMO-1, Sn-PMO-3 and Sn-Beta in Figure 6.24. The strongest peak in the FT magnitude, at ca. 1.6 Å, arises from the Sn-O single-scattering paths representing atoms in the first coordination sphere of the metal. Peaks at higher *R*-values involve next-nearest neighbors, such as the Sn-Sn paths of SnO₂. Their absence from the EXAFS of Sn-PMO-1 suggests that Sn is well-dispersed in the PMO framework. The EXAFS of Sn-Beta also shows no distinct features in this

region, consistent with a prior report of isolated Sn^{4+} sites in the zeolite. Bare and coworkers showed that Sn^{4+} ions dispersed in the framework of Sn-Beta zeolite were tetra-coordinated by oxygen, and that longer-range paths involving framework Si and/or O did not produce obvious features in R-space.⁴⁷

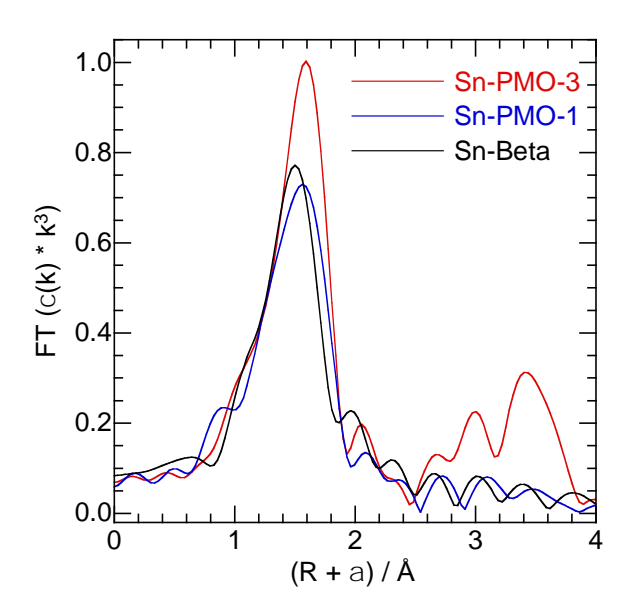


Figure 6.24. Comparison of the Sn K-edge EXAFS, as k^3 -weighted FT magnitudes (not phase-corrected), for Sn-Beta and two Sn-PMOs.

Sn-PMO-3 was chosen as representative of the PMO catalysts with high Sn-loading (2.9 wt%). Cassiterite (SnO₂) was used as a model to generate paths for curve-fitting. The fit is shown in Figure 6.25, and the fit parameters are given in Table 6.4. In Sn-PMO-3, each Sn ion has on average (4.6 \pm 0.1) O neighbors, at a distance of 2.05 Å. For comparison, each Sn atom in SnO₂ has 6 O neighbors at a distance of 2.05 Å.⁴⁷ Bulk SnO₂ also has Sn-Sn paths at 3.19 Å (N = 2) and 3.71 Å (N = 8). For Sn-PMO-3, these paths appear at 3.18 Å ($N = 0.9 \pm 0.2$) and 3.71 Å ($N = 1.8 \pm 0.2$), respectively. The low N values for the PMO relative to the bulk oxide are consistent with the presence of SnO₂ as nanoparticles.²⁸

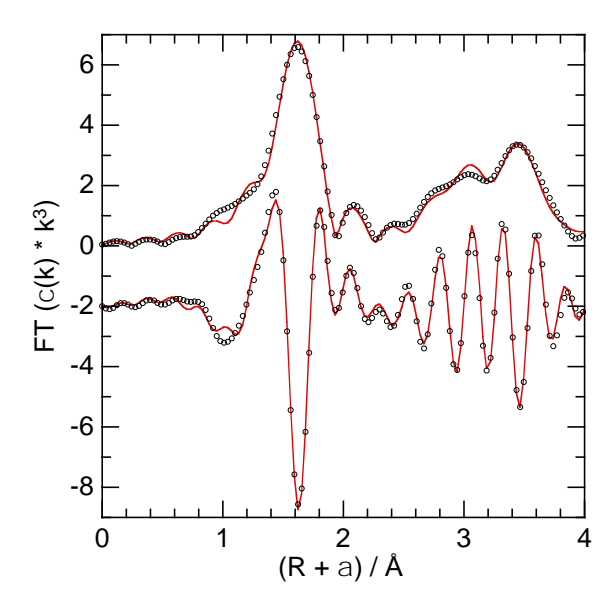


Figure 6.25. Sn K-edge EXAFS (points) for Sn-PMO-3, shown k^3 -weighted in R-space (not phase-corrected) as FT magnitude and its imaginary component. The curve-fit (lines) corresponds to the parameters in Table 6.4.

Table 6.4. EXAFS curvefit parameters^a from a first-shell analysis, for various Sn catalysts

Catalyst	Sn Loading	N	R	$10^3 \sigma^2$	S_0^2	ΔE_0
	wt%		Å	$\mathring{\mathbf{A}}^2$		eV
Sn-PMO-3	2.9	4.7 (0.1)	2.044 (0.005)	3.2 (0.4)	0.60	10.8 (0.7)
Sn-PMO-2PS	1.2	4.0 (0.3)	2.037 (0.007)	8.8 (0.5)	0.78	9.3 (1.2)
Sn-PMO-1	0.4	4.0 (0.3)	2.036 (0.009)	5.9 (0.6)	0.68	10.5 (1.1)
Sn-Beta	0.5	3.7 (0.2)	1.983 (0.013)	6.4 (0.9)	0.74	7.8 (1.7)

^a Analysis conducted using the data ranges 3.0 Å⁻¹ $\leq k \leq$ 12.0 Å⁻¹ and 1.2 Å $\leq R \leq$ 2.0 Å; N_{idp} = 4.3.

Similarly, Sn-PMO-1 was chosen as representative of the PMO catalysts that do not contain detectable SnO₂ nanoparticles, due to the absence of significant intensity in R-space beyond the first shell. We obtained values for the coordination number N and bond distance for the Sn-O path of (4.0 ± 0.3) and 2.04 Å, respectively, consistent with isomorphic substitution of Sn for Si in the PMO framework. While the Sn-O distance is slightly longer than that found in Sn-Beta (1.98 Å in our analysis), it is similar to that for SnO₂.

6.5.1.2 *Post-synthesis Sn incorporation into the PMO*. The addition of SnCl₄·5H₂O to the undoped PMO via incipient wetness impregnation is also an efficient method of Sn incorporation. Sn-PMO-2PS possesses a surface area and pore diameter of 742 m² g⁻¹ and 5.1 nm, respectively. Unlike Sn-PMO-2, the absence of higher peaks in the EXAFS FT magnitude suggests that the Sn⁴⁺ ions in Sn-PMO-2PS are well-dispersed in the PMO framework, resembling the coordination environment in Sn-PMO-1 despite the higher metal loading (1.2 wt%). No residual Cl was detected by elemental analysis.

6.5.1.3 *Synthesis of a bifunctional PMO*. PMOs have previously been functionalized with propylsulfonic acid groups via co-condensation. As a proof of concept, pSO₃H/Sn-PMO containing both Sn⁴⁺ and propylsulfonic acid sites was prepared by modifying the Sn-PMO-1 synthesis to co-condensed Brønsted acid sites. The bifunctional PMO has a Sn loading of 0.5 wt% and contains 0.6 mmol/g propylsulfonic acid groups (Sn:H⁺ = 0.7).

6.5.2 Reactivity Studies using Sn-PMO Materials

6.5.2.1 Reactivity in Glucose Isomerization Glucose isomerization tests were conducted in batch mode in 4:1 THF:H₂O containing 2 wt% glucose (Sn:glucose = 100). We developed this single-phase solvent system for use in the continuous production of HMF from fructose.²⁶ Another potential advantage is the compatibility with a dual-bed reactor in the tandem production of HMF

from the more abundant carbohydrate, glucose. Catalyst performance is compared in Figure 6.26. After 2 h at 140 °C in a batch reactor, the Sn-free PMO achieved a glucose conversion of 19 %, but with a fructose selectivity of only 5 %. When Sn was present even at 0.4 wt. % (Sn-PMO-1), glucose conversion increased moderately, to 28 %, while fructose selectivity increased significantly, to 47 %. With 1.1 wt. % Sn (Sn-PMO-2), the glucose conversion was similar, but the fructose selectivity declined to 27 %. At higher Sn loadings, both glucose conversion and fructose selectivity decreased, compared to Sn-PMO-1.

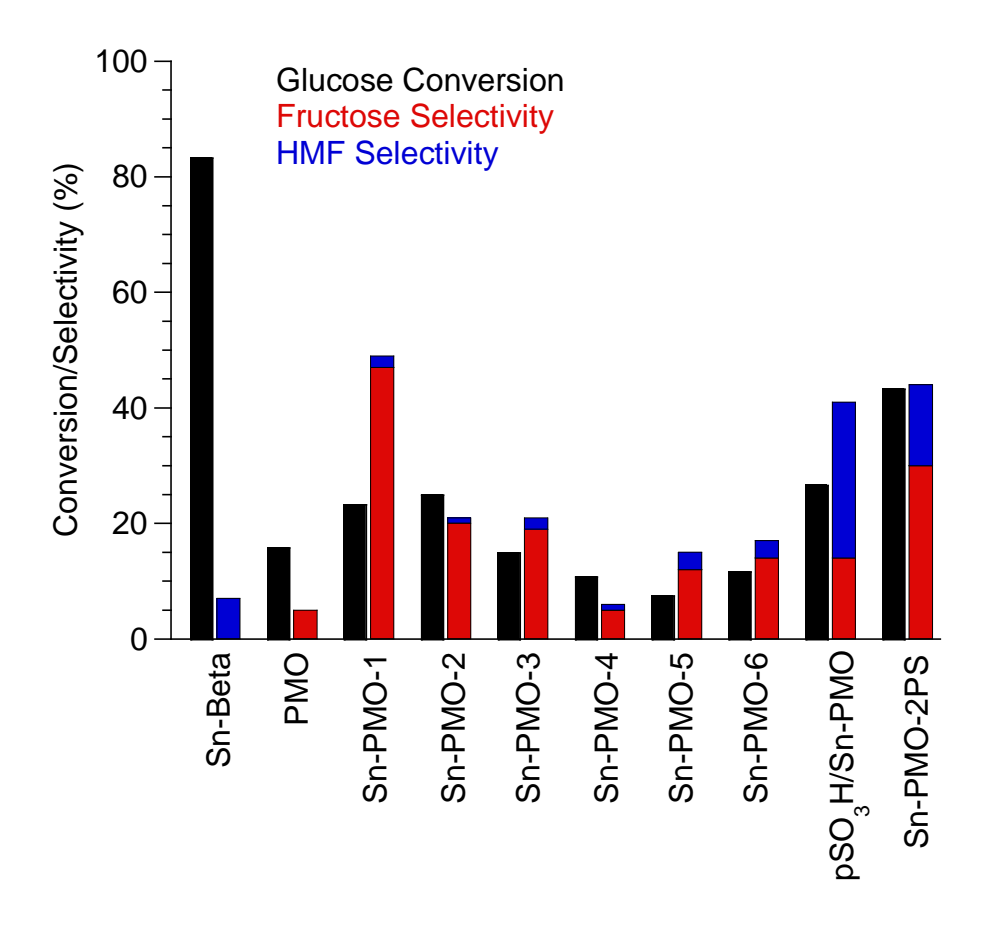


Figure 6.26. Effect of Sn loading on batch glucose isomerization/dehydration in 4:1 THF:H₂O. Reaction conditions: 2 h at 413 K with 2 wt% glucose in 4:1 (w:w) THF:water with a Sn: glucose molar ratio of 1:100.

For all of the Sn-PMO catalysts, the HMF selectivity is consistently just 2-3 %, at fructose conversions less than 50 %. However, Sn-PMO-2PS reached ca. 52 % conversion and gave fructose and HMF selectivities of 30 and 14 %, respectively. In addition to being more highly dispersed than in Sn-PMO-2, the Sn⁴⁺ sites of the post-synthesis-modified PMO are likely more accessible, accounting for the higher conversion observed. The origin of the surprising HMF selectivity is not currently known, although it is unlikely a consequence of HCl-catalyzed dehydration, since no residual chloride was detected. In general, unless paired with ionic liquids, Lewis acid catalysts are reported to give low HMF selectivity from fructose. 48, 49

Sn-Beta was also tested under the same conditions. After the standard reaction time (2 h), the glucose was fully converted, however, no fructose was present and the HMF selectivity was very low (7 %), Figure 6.26. Levulinic and formic acid were not among the observed products. Sn-Beta clearly catalyzes extensive, undesired reactions of the glucose isomerization products (fructose and/or mannose).

Product distributions were also measured at shorter reaction times, in order to compare the behavior of the zeolite with that of the Sn-PMOs at similar conversions. Achieving lower conversions with Sn-Beta required a different Sn:glucose ratio, 1:200 vs. 1:100 for the Sn-PMO catalysts and very short reaction times. Even after only 15 min, equilibrium conversion (55 %) was achieved, and a fructose selectivity of 78 % was observed for the zeolite. Using a Sn:glucose ratio of 1:100 at extended reactions times the desired products (fructose + HMF) react further, and the selectivity drops significantly, Figure 6.27a. In contrast, Sn-PMO-1 (Sn:glucose 1:100) maintains its selectivity (ca. 40 %) to the desired products (fructose + HMF) even at high conversion and long reaction times, Figure 6.27b. Sn-PMO-4, with its higher Sn loading, gives lower glucose

conversion and lower selectivity to the desired products compared to Sn-PMO-1, even at the same reaction times and conversion, Figure 6.27c.

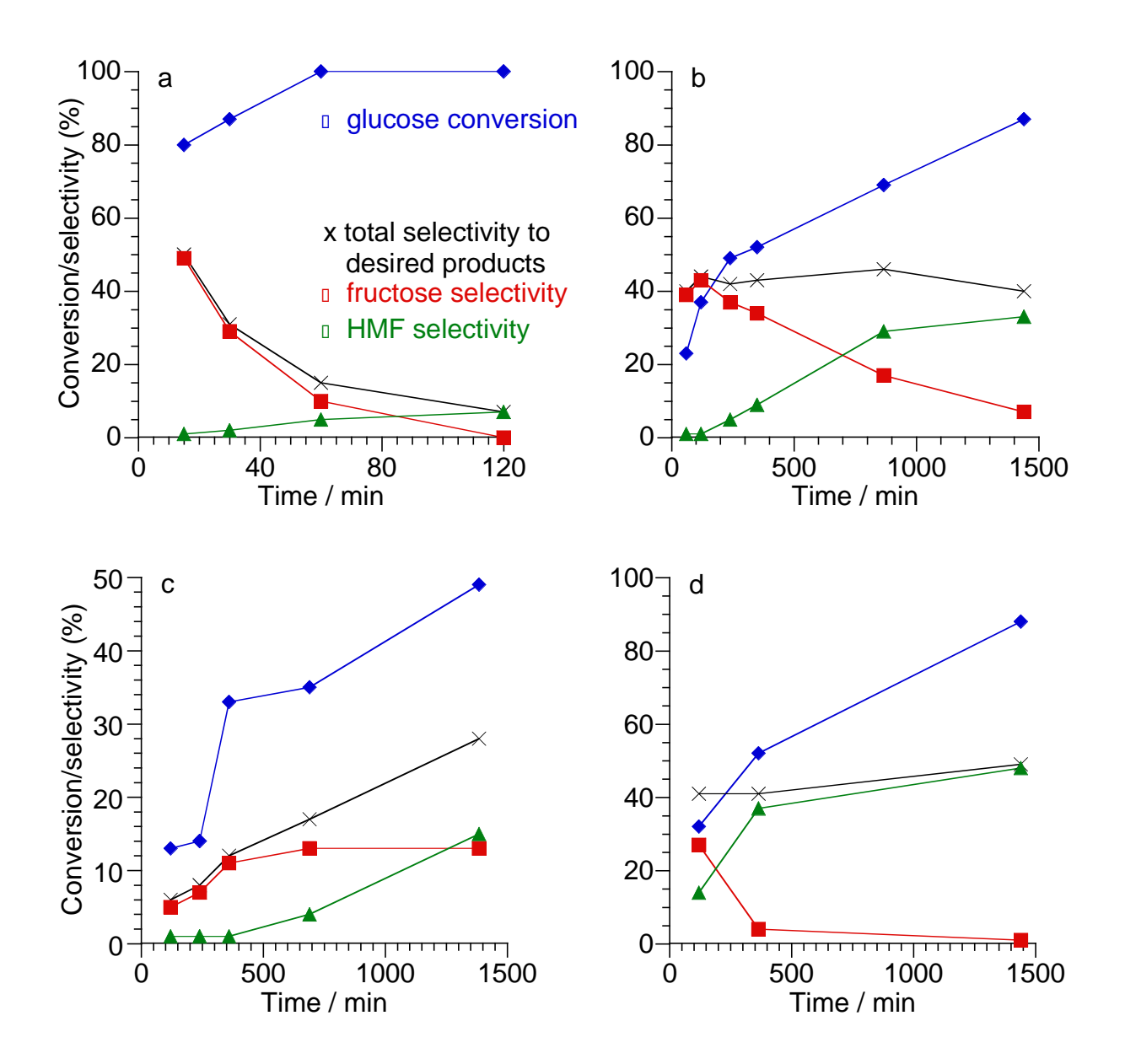


Figure 6.27. Comparison of batch glucose isomerization over various Sn-containing catalysts: (a) Sn-Beta; (b) Sn-PMO-1; (c) Sn-PMO-4; and (d) bifunctional pSO₃H-Sn-PMO. Reaction conditions: 1.5 g feed, comprised of 2 wt% glucose in 4:1 (w:w) THF:water at 413 K. For (a) – (c), the Sn:glucose molar ratio was 1:100. For (d), the Sn:glucose:H⁺ loading of (d) was 1:100:1.4.

6.5.2.2 Solvent Effects in Glucose Isomerization In addition to 4:1 THF:water, glucose isomerization was also studied in two other single-phase solvent systems: pure water, and a methanol/water mixture (Table 6.5). In water, Sn-Beta has been shown to isomerize glucose by a Lewis acid-catalyzed mechanism, while SnO₂ nanoparticles have been reported to isomerize glucose via a base-catalyzed mechanism.⁵⁰ The production rate of fructose production using Sn-Beta in 4:1 THF:water at 140 °C is $(4.0 \pm 0.2) \mu \text{mol} (g \text{ cat})^{-1} \text{ s}^{-1}$ with 2 wt% glucose (1:200 Sn:glucose; 55 % conversion with 78 % fructose selectivity). In pure water at the same reaction temperature but with 10 wt% glucose, a production rate of 3.6 $\mu \text{mol} (g \text{ cat})^{-1} \text{ s}^{-1} (56 \% \text{ glucose})$ conversion with 65 % fructose selectivity) was reported.⁶ For Sn-Beta, at reaction times of ≤ 15 min with a Sn:glucose ratio of 1:200, the rate of fructose production is unaffected by the THF/water solvent system. However, the fructose selectivity is higher in the semi-aqueous solvent, possibly due to the formation of difructose anhydrides that protect the product from further reaction at the Lewis acid sites.²⁷

In methanol, Sn-Beta was reported to preferentially epimerize glucose to mannose.⁵⁰ We observed that both Sn-Beta and Sn-PMO-1 (both of which lack detectable SnO₂ nanoparticles) show very low selectivity to either of the desired products fructose and HMF (less than 6 %) in methanol/water. SnO₂ has been reported to isomerize glucose to fructose in methanol.³⁹ Curiously, Sn-PMO-5 (with higher Sn loading, and containing SnO₂) showed 0 % fructose selectivity at 17 % glucose conversion.

In water, glucose conversion was 5 % in the absence of catalyst. A similar low conversion (4 %) was observed with Sn-PMO-1. It appears that the aqueous glucose solution does not diffuse into the hydrophobic pores of this catalyst. In contrast, the conversion in THF:water is 25 %, and the selectivity to desired products also increases significantly. Sn-Beta gives both higher glucose

conversion and selectivity to desired products in water, compared to THF:water. For the Sn-PMOs, both internal and external surfaces are hydrophobic,⁵¹ while only the internal surfaces of Sn-Beta are hydrophobic.⁵² In the case of the zeolite, limiting the hydrophobicity to only the internal surfaces may reduce the barrier for entry of glucose, relative to the PMO.⁵³

Table 6.5. Solvent effects on glucose isomerization/dehydration^a

Solvent	Catalyst	Conversion (%)	Selectivity (%)			
			Fructose	HMF	Total ^b	
Sn-Beta	H ₂ O	80	40	0	40	
	THF:H ₂ O (4:1)	55	28	0	28	
	MeOH:H ₂ O (9:1)	97	3	3	6	
Sn-PMO-1	H ₂ O	4	16	12	28	
	THF:H ₂ O (4:1)	25	45	0	45	
	MeOH:H ₂ O (9:1)	70	1	1	2	
Sn-PMO-5	H ₂ O	8	0	<1	<1	
	THF:H ₂ O (4:1)	9	12	3	15	
	MeOH:H ₂ O (9:1)	17	0	<1	<1	
No catalyst	H ₂ O	5	7	14	21	
	THF:H ₂ O (4:1)	7	16	5	21	
	MeOH:H ₂ O (9:1)	8	0	0	0	

^a Reaction conditions: 2 h at 413 K with 2 wt% glucose, at a molar ratio Sn:glucose of 1:100 (except where no catalyst was added). ^b Fructose + HMF.

6.5.2.3 Reactivity of Sn-PMOs towards fructose and HMF. A further benefit of the Sn-PMO catalysts are their lower reactivity towards the conversion of both fructose and HMF to undesired products, relative to Sn-Beta. The catalysts were tested with a 2 wt% fructose solution in 4:1 THF:water at a lower reaction temperature, 373 K, in order to maintain less than full conversion. After 18 h, Sn-PMO-1 converted only 20 % of the fructose, whereas Sn-Beta converted 82 %. Only for Sn-PMO-1 was a small amount of HMF detected, while the major products for both Sn-PMO-1 and Sn-Beta were not identified. In a similar experiment conducted using 2 wt% HMF in 4:1 THF:water at 413 K, Sn-PMO-1 gave 1.6 % HMF conversion, whereas Sn-Beta converted 4.1 %. Thus in the eventual design of a tandem isomerization/dehydration system, a lack of reactivity of the Lewis acid active sites towards fructose and/or HMF will be important in achieving high HMF yields.

6.5.3 Tandem Glucose Isomerization and Fructose Dehydration

To demonstrate the feasibility of a single, bifunctional catalyst for the production of HMF from glucose, the hybrid PMO containing both Lewis and Brønsted acid sites was first tested for its ability to catalyze fructose dehydration (2 wt%) at 413 K. After 2 h, the fructose conversion was 100 % with an HMF selectivity of 77 %, Figure 6.28. This HMF selectivity is slightly higher than that of other propylsulfonic acid-functionalized mesoporous ordered silicas we have reported.^{26,54} For comparison, Sn-PMO-1 and Sn-Beta were also tested under the same conditions. Both demonstrated low conversions and low HMF selectivities.

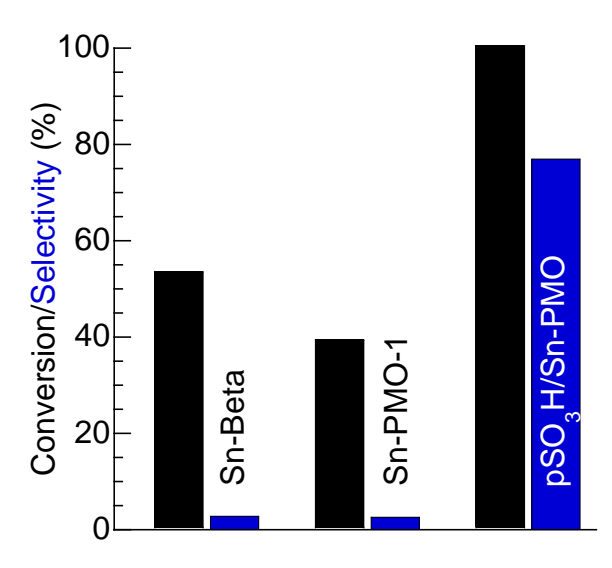


Figure 6.28. Comparison of catalyst performance in batch fructose dehydration to HMF. Reaction conditions: 2 h at 413 K with 1.5 g of 2 wt% fructose in 4:1 THF:water, at a molar ratio Sn:fructose of 1:100.

Finally, the reactivity of the bifunctional catalyst was studied in the tandem isomerization/dehydration of glucose in THF:H₂O at 413 K. After 2 h, the glucose conversion was 32 %, with selectivities to fructose and HMF of 27 and 14 %, respectively, Figure 6.27d. After 4 h, glucose conversion had increased to 52 %, with fructose and HMF selectivities of 4 % and 37 %, respectively. Thus the overall selectivity to desired products remains above 40 % over the entire range of conversion tested.

Recently, we showed that incorporating the reaction promoter poly(vinylpyrrolidone) (PVP) into the pores of propylsulfonic acid-functionalized mesoporous silicas caused their selectivity in fructose dehydration to HMF to increase significantly (Chapter 5). Applying this strategy to functionalized PMOs may further increase the yields of desired products starting from glucose. Instead of incorporating propylsulfonic acid sites, the Lewis acidic PMOs could be modified 3with **Brønsted** basic sites. via co-condensation with e.g., aminopropyl(trimethoxy)silane. Such materials may be useful in tandem reactions like Meinwald rearrangement–Knoevenagel condensations.⁵⁵

6.6 Conclusions

Solvent reactivity trends were observed for homogenous base catalyzed reactions when only using THF, as GVL led to no reactivity. When homogenous Lewis acids were used, the catalyst can be hydrolyzed to produce HCl in solution which led to formation of both fructose and HMF. Small of addition of miscible organic solvent led to a drop of reactivity compared to that of pure water. Upon the addition of GVL, the reactivity increased as well. Solid base catalyst, like NaX led to the adsorption of sugars and solvents that played a major factor in reactivity. Here the same solvent addition results were observed as well.

Benzene-bridged PMOs doped with Lewis acidic Sn sites are readily and rapidly synthesized. These thermally robust, hydrophobic materials catalyze the selective isomerization of glucose to fructose in THF/water at 413 K. While less active than Sn-Beta, they are more selective towards fructose and, surprisingly, yield appreciable amounts of HMF at long reaction times. The incorporation of propylsulfonic acid sites within the PMO further enables the rapid and selective conversion of fructose to HMF. Thus the efficient tandem conversion of glucose to HMF appears to be possible using a bifunctional PMO containing both Lewis and Brønsted acid sites. Since their ratio can be adjusted over a wide range during synthesis, there is considerable room for catalyst optimization.

6.7 References

- [1] J.J. Bozell, G.R. Petersen, Green Chem., 12 (2010) 539-554.
- [2] A. Aden, J. Bozell, J. Holladay, J. White, A. Manheim, G. Petersen, T. Werpy, in: T. Werpy, G. Petersen (Eds.), U.S. Department of Energy, Oak Ridge, 2004.
- [3] H.E. Van Dam, A.P.G. Kieboom, H. Van Bekkum, Starch, 38 (1986) 95-101.
- [4] C. Liu, J.M. Carraher, J.L. Swedberg, C.R. Herndon, C.N. Fleitman, J.-P. Tessonnier, Acs Catalysis, 4 (2014) 4295-4298.
- [5] C.L. De Bruyn, W.A. Van Ekenstein, Rec. trav. chim, 18 (1899) 147.
- [6] M. Moliner, Y. Román-Leshkov, M.E. Davis, Proc. Natl. Acad. Sci., 107 (2010) 6164-6168.
- [7] Y.J. Pagan-Torres, T. Wang, J.M.R. Gallo, B.H. Shanks, J.A. Dumesic, Acs Catalysis, 2 (2012) 930-934.
- [8] M.A. Mellmer, C. Sener, J.M.R. Gallo, J.S. Luterbacher, D.M. Alonso, J.A. Dumesic, Angewandte Chemie International Edition, 53 (2014) 11872-11875.
- [9] A. Singhal, K.D. Keefer, Journal of materials research, 9 (1994) 1973-1983.
- [10] H.J. Bieser, A.J. De Rosset, Starch Stärke, 29 (1977) 392-397.
- [11] S.R. Maple, A. Allerhand, J. Am. Chem. Soc., 109 (1987) 3168-3169.
- [12] Y. Cho, R.B. Honzatko, Acta Crystallographica Section C, 46 (1990) 587-590.
- [13] D.H. Everett, Pure Appl. Chem., 58 (1986) 967-984.
- [14] A.Y. Meyer, D. Farin, D. Avnir, J. Am. Chem. Soc., 108 (1986) 7897-7905.
- [15] J.A. Dumesic, The microkinetics of heterogeneous catalysis, An American Chemical Society Publication, 1993.
- [16] D. Seguin, A. Montillet, D. Brunjail, J. Comiti, The Chemical Engineering Journal and The Biochemical Engineering Journal, 63 (1996) 1-9.
- [17] R. Netrabukkana, K. Lourvanij, G.L. Rorrer, Industrial & engineering chemistry research, 35 (1996) 458-464.
- [18] M.A. Vannice, W.H. Joyce, Kinetics of catalytic reactions, Springer, 2005.
- [19] R.J. Davis, Res. Chem. Intermed., 26 (2000) 21-27.
- [20] D. Barthomeuf, Acidity and Basicity in Zeolites, in: H.P. G. Öhlmann, R. Fricke (Eds.) Stud. Surf. Sci. Catal., Elsevier, 1991, pp. 157-169.
- [21] C. Moreau, R. Durand, A. Roux, D. Tichit, Applied Catalysis A: General, 193 (2000) 257-264
- [22] H. Zhao, J.E. Holladay, H. Brown, Z.C. Zhang, Science, 316 (2007) 1597-1600.
- [23] T. Stahlberg, M.G. Sorensen, A. Riisager, Green Chem., 12 (2010) 321-325.
- [24] Y.J. Pagán-Torres, T. Wang, J.M.R. Gallo, B.H. Shanks, J.A. Dumesic, ACS Catal., 2 (2012) 930-934.
- [25] N. Shi, Q. Liu, Q. Zhang, T. Wang, L. Ma, Green Chem., 15 (2013) 1967-1974.
- [26] M.H. Tucker, A.J. Crisci, B.N. Wigington, N. Phadke, R. Alamillo, J. Zhang, S.L. Scott, J.A. Dumesic, ACS Catal., 2 (2012) 1865-1876.
- [27] M.H. Tucker, R. Alamillo, A.J. Crisci, G.M. Gonzalez, S.L. Scott, J.A. Dumesic, ACS Sustainable Chemistry & Engineering, 1 (2013) 554-560.
- [28] S.L.P. Savin, A.V. Chadwick, L.A. O'Dell, M.E. Smith, Solid State Ionics, 177 (2006) 2519-2526.
- [29] S. Valencia, A. Corma, in: US (Ed.), US, 1999.
- [30] C. Hammond, S. Conrad, I. Hermans, Angew. Chem. Int. Ed., 51 (2012) 11736-11739.

- [31] Z. Kang, X. Zhang, H. Liu, J. Qiu, K.L. Yeung, Chem. Eng. J., 218 (2013) 425-432.
- [32] C.-C. Chang, Z. Wang, P. Dornath, H. Je Cho, W. Fan, RSC Adv., 2 (2012) 10475-10477.
- [33] J. Dijkmans, D. Gabriels, M. Dusselier, F. de Clippel, P. Vanelderen, K. Houthoofd, A. Malfliet, Y. Pontikes, B.F. Sels, Green Chem., 15 (2013) 2777-2785.
- [34] Z. Kang, X. Zhang, H. Liu, J. Qiu, W. Han, K.L. Yeung, Mater. Chem. Phys., 141 (2013) 519-529.
- [35] E. Nikolla, Y. Román-Leshkov, M. Moliner, M.E. Davis, ACS Catal., 1 (2011) 408-410.
- [36] C.M. Lew, N. Rajabbeigi, M. Tsapatsis, Ind. Eng. Chem. Res., 51 (2012) 5364-5366.
- [37] V. Choudhary, A.B. Pinar, S.I. Sandler, D.G. Vlachos, R.F. Lobo, ACS Catal., 1 (2011) 1724-1728.
- [38] J.M.R. Gallo, D.M. Alonso, M.A. Mellmer, J.A. Dumesic, Green Chem., 15 (2013) 85-90.
- [39] Y. Román-Leshkov, M. Moliner, M.E. Davis, Chem. Mater., 22 (2010) 2646-2652.
- [40] E.B. Celer, M. Jaroniec, J. Am. Chem. Soc., 128 (2006) 14408-14414.
- [41] M. Kuroki, T. Asefa, W. Whitnal, M. Kruk, C. Yoshina-Ishii, M. Jaroniec, G.A. Ozin, J. Am. Chem. Soc., 124 (2002) 13886-13895.
- [42] Q. Wang, D.F. Shantz, J. Solid State Chem., 181 (2008) 1659-1669.
- [43] F. Hoffmann, M. Cornelius, J. Morell, M. Fröba, Angew. Chem. Int. Ed., 45 (2006) 3216-3251.
- [44] A. Corma, M.E. Domine, S. Valencia, J. Catal., 215 (2003) 294-304.
- [45] M.C. Burleigh, M.A. Markowitz, S. Jayasundera, M.S. Spector, C.W. Thomas, B.P. Gaber, J. Phys. Chem. B, 107 (2003) 12628-12634.
- [46] Y. Goto, S. Inagaki, Chem. Commun., (2002) 2410-2411.
- [47] S.R. Bare, S.D. Kelly, W. Sinkler, J.J. Low, F.S. Modica, S. Valencia, A. Corma, L.T. Nemeth, J. Am. Chem. Soc., 127 (2005) 12924-12932.
- [48] N. Mittal, G.M. Nisola, W.-J. Chung, Tetrahedron Lett., 53 (2012) 3149-3155.
- [49] V.V. Ordomsky, J. Van der Schaaf, J.C. Schouten, T.A. Nijhuis, ChemSusChem, 5 (2012) 1812-1819.
- [50] R. Bermejo-Deval, R. Gounder, M.E. Davis, ACS Catal., 2 (2012) 2705-2713.
- [51] J. Liu, Q. Yang, M.P. Kapoor, N. Setoyama, S. Inagaki, J. Yang, L. Zhang, J. Phys. Chem. B, 109 (2005) 12250-12256.
- [52] I. Batonneau-Gener, A. Yonli, S. Hazael-Pascal, J. Pedro Marques, J. Madeira Lopes, M. Guisnet, F. Ramôa Ribeiro, S. Mignard, Microporous Mesoporous Mater., 110 (2008) 480-487.
- [53] R. Gounder, M.E. Davis, AlChE J., 59 (2013) 3349-3358.
- [54] A.J. Crisci, M.H. Tucker, M.-Y. Lee, S.G. Jang, J.A. Dumesic, S.L. Scott, ACS Catal., 1 (2011) 719-728.
- [55] R. Srirambalaji, S. Hong, R. Natarajan, M. Yoon, R. Hota, Y. Kim, Y. Ho Ko, K. Kim, Chem. Commun., 48 (2012) 11650-11652.

Chapter 7: Summary of Conclusions and Future Directions

7.1 Conclusions

The use of heterogeneous catalysts, such as supported metals and acid-functionalized organosilicas, were used for biomass transformations for the potential use as a renewable carbon source for the production of fuels and chemicals. 5-hydroxymethylfurfural (HMF) and dihydroxymethyltetrahydrofuran (DHMTHF) were produced from cellulosic biomass and have been identified as important precursors and specialty chemicals. Cellulosic biomass can be hydrolyzed to its monomers, mainly glucose, via acid catalysis. Glucose can then be isomerized to its ketose form, fructose, by a Lewis acid or base. Fructose production is favored because it is more selective for its subsequent Brønsted acid catalyzed dehydration to HMF, an important platform chemical derived from biomass. HMF can further be hydrogenated to DHMTHF, a specialty chemical, or can undergo different chemistries to produce fuels and other value-added chemicals. From literature technoeconomic studies, the scale-up feasibility of bio-refineries is highly dependent of lowering capital and operating costs, starting from an abundant sugar source (i.e. glucose, instead of fructose), and obtaining high yields which could be accomplished by using solid catalysts.

In Chapter 3, we explore the hydrogenation of HMF to DHMTHF using ruthenium, palladium, and platinum supported catalysts prepared by incipient wetness techniques. From reaction studies in a Parr reactor in a biphasic system, it was determined that the selectivity for hydrogenation from HMF to DHMTHF is affected by the acidity of the aqueous solution containing HMF. This acidity could be from dilute acid in the feed from previous reaction steps or if HMF was further hydrolyzed to levulinic acid. The selectivity to DHMTHF drops sharply in the presence of any dilute acids (0.005 M) in solution or if the metal is supported on a low-isoelectric

point support (i.e. silica). The primary products observed when acid impurities are present include 1,2,5-hexanetriol(HT), 1,2,5,6-HT, and 1,2,6-HT, which are produced by series of ring-opening, rehydration, dehydration, and subsequent hydrogenations of dihydroxymethylfurfural (DMF), the intermediate hydrogenation product of HMF. High selectivities to DHMTHF can be achieved when the hydrogenation catalyst is comprised of ruthenium deposited on a support with a high isoelectric point oxide (e.g., ceria) and/or removing acid impurities with an ion-exchange resin.

The use of various single-phase solvent systems, including DHMTHF mixed with water, is explored for their use in acid-catalyzed fructose dehydration to HMF. The use of these miscible organic co-solvents saw a beneficial effect with increased rates of fructose dehydration and increased HMF selectivities over solid acid catalysts, relative to water. Fructose tautomerization favors the furanose form (five membered ring) versus the pyranose form (six membered ring) in the mixed solvent, relative to water alone, explaining at least part of the rate enhancement. The fructose tautomer distribution is a function of both temperature and solvent with increasing furanose fractions present with increasing temperatures and increasing concentration of polar aprotic solvents. The furanose form is expected to be more easily dehydrated to HMF as it is a five membered ring similar to that of HMF. The HMF selectivity was shown to also depend on both the fructose conversion and the amount of organic co-solvent present. With high levels of the co-solvent in water (e.g., ratios of 3:1 and 9:1), the HMF selectivity increases with fructose conversion. Thus a tandem approach may be feasible in the production of DHMTHF, based on the use of an inexpensive, easily-separable, non-corrosive solvent system. Other alcoholic co-solvents, including ethanol and THF-alcohol, showed similar, but less pronounced, selectivity enhancements. The use of polar, aprotic THF as the co-solvent also lead to the selective production of HMF. Due to its high volatility, this solvent facilitates isolation of HMF by simple evaporation, which is an advantage relative to high-boiling DMSO. Side-reactions involving the anomeric hydroxyl groups of fructose give rise to fructosides and difructose anhydrides in alcoholic and aprotic solvents, respectively. However, their formation is reversible, and high yields of HMF can be obtained at high fructose conversions.

Having developed monophasic co-solvent systems that lead to increases in HMF yields compared to that in pure water (Chapter 4), these reaction systems were applied for the use of novel solid acid catalysts for elucidating reaction networks to increase HMF yields, study the catalysts under continuous flow systems, and determine and quantify catalyst deactivation. In the first part of Chapter 5, a synthesis to intercalate polyvinylpyrrolidone (PVP) on the surface of acid-functionalized silica catalysts was presented. The PVP was stabilized on the surface by UVcrosslinking and polymer loading was determined using thermogravimetric analysis. Catalysts were fully characterized before and after intercalation and optimized for HMF yields. The incorporation of PVP led to increases in HMF selectivity previously achieved only with ionic liquids and high-boiling aprotic organic solvents. The high concentration of pyrrolidone groups in the confined space of the nanochannels favored the furanose tautomers of fructose. Since HMF is derived from these tautomers, a corresponding increase in selectivity occurs. Unlike other selective methods for HMF production, the solid catalyst is both easily recovered from the reaction mixture, and the product is readily isolated from the low-boiling, single-phase solvent system. Thus, the reaction environment within the catalyst has been designed to favor the desired product. In addition, benefits in catalyst stability was also observed. Modification of inexpensive solid catalysts with functional polymers may have more general applications.

Acid mesoporous carbon based catalysts (CMK-3 and CMK-5) studied in Chapter 5 showed comparable performance to silica based catalysts in the conversion of fructose to HMF in

the presence of water. However, acid mesoporous carbon had a significantly lower deactivation rate coefficient, being up to 60 more stable than pSO₃H-SBA-15, and up to three times more stable than the commercial Nafion SAC-13. From the catalysts studied, CMK-5-PSA is the most promising material, since it not only presents the lowest deactivation, but also the highest TOF for HMF production. Acid mesoporous carbons have potential to substitute the well-known and well characterized mesoporous silica and organosilica based catalysts, as well as the commercial Nafion SAC-13, for biomass conversion in the presence of water.

Starting from more abundant biomass feedstocks, such as glucose, are necessary to develop a more technoeconomic viable bio-refinery. Thus, glucose isomerization to fructose was studied in Chapter 6. Co-solvents studied and used in previous chapters were used to study their effect for homogenous and heterogeneous isomerization reactions. The systems here become more complicated, as a base catalyzes this reaction via an 1,2-enediol intermediate and hydrogen transfer and Lewis acid catalysts by an intramolecular hydride shift. For homogenous base catalyst were used, solvent reactivity trends showed reactivity only when sing THF, as GVL led to no reactivity, most likely dues to neutralization via trace acid in solution. When homogenous Lewis acids (AlCl₃) were used, the catalyst can be hydrolyzed to produce HCl in solution which led to formation of both fructose and HMF. The extent of aluminum hydration and oligomerization is a function of aluminum chloride concentration and temperature. For the reaction studies, a small of addition of miscible organic solvent led to a drop of reactivity compared to that of pure water. Upon the addition of GVL, the reactivity reversed with an increased fructose production rate as well as HMF production. Solid base catalyst, like NaX led to the adsorption of sugars and solvents that played a major factor in reactivity. Here the same solvent addition results were observed as well.

Novel catalyst based on Sn-Beta zeolites, which have similar performance to that of enzymes, were also synthesized. Hydrophobicity was introduced into the organosilicas during condensation to by a benzene bride and Lewis acidity by doping Sn into the materials. These thermally robust, hydrophobic materials were able to catalyze the selective isomerization of glucose to fructose in THF/water at 413 K. While less active than Sn-Beta, they are more selective towards fructose and, surprisingly, yield appreciable amounts of HMF at long reaction times. The incorporation of propylsulfonic acid sites within the PMO framework further enables the rapid and selective conversion of fructose to HMF. Thus the efficient tandem conversion of glucose to HMF appears to be possible using a bifunctional PMO containing both Lewis and Brønsted acid sites. Since their ratio can be adjusted over a wide range during synthesis, there is considerable room for catalyst optimization.

7.2 Future Directions

7.2.1 Increasing Catalyst Stability and Selectivity

Robust solid acid catalyst are important for the production of HMF, as well as other acid catalyzed transformations, such as transesterification and hydrolysis, important in many other biomass conversion processes. Ethane-bridged PMO materials were shown to be significantly more stable than purely siliceous supports at reaction conditions. The tethering siloxane bonds of the alkyl sulfonic acid sites are still prone to hydrolytic cleavage. Catalyst stability could be accomplished via dipodal silanes, which would have up to six siloxane bonds (compared to just three with current techniques). Organic bridging groups, such as that of the benzene PMO framework, could also be chemically modified to introduce acidity. This could be accomplished by reacting benzene PMOs with chlorosulfonic acid or oleum to produce the aryl sulfonic acid

sites. A second approach would be to further develop acid functionalized carbons for added hydrothermal stability. From here, studies can then focus on HMF selectivity.

PVP was seen in Chapter 5 to enhance HMF selectivity. PVP is an amphiphilic polymer soluble in water and other polar solvents synthesized from n-vinyl pyrrolidone (NVP) via free radical polymerization using azobisisobutyronitrile (AIBN) as an initiator in a range of different solvents such as diethylether and water. Literature reports the synthesis of polyvinylpyrollidone copolymers with vinylphoshonic acid² and a block copolymer with poly(ε-caprolactone) via a combination of ring opening polymerization and xanthate-mediated RAFT polymerization.³

A benchmark study with other acids and materials demonstrated sulfonic acid groups to be the most active and selective for HMF production.⁴ Sulfonic acid functionalized monomers have been selected as the catalytic acid site to be incorporated into the copolymer. A common monomer with sulfonic acid functionality is 2-acrylamido-2-methylpropanesulfonic acid (AMPS), which has been reported to be copolymerized with acryloyl chloride⁵, methacrylic acid⁶, and methyl methacrylate⁷ via controlled or free radical polymerization. The salt of AMPS (i.e. Na or K-AMPS) can be used in the preparation of copolymers if the acidic segment of AMPS hinders the copolymerization and be acidified via post-synthetic acid wash.

A possible strategy is to copolymerize AMPS with NVP (Figure 7.1) at different feed ratios and degree of polymerization to see the effect of PVP moieties on the selectivity to HMF. The reactivity ratio of NVP (r_1 =0.13) and Na-AMPS (r_2 =0.66) have previously been determined⁸ and since their product is less than one and is approaching zero, we can expect an alternating sequence. This provides insight into design parameters for the synthesis and characterization of these materials.

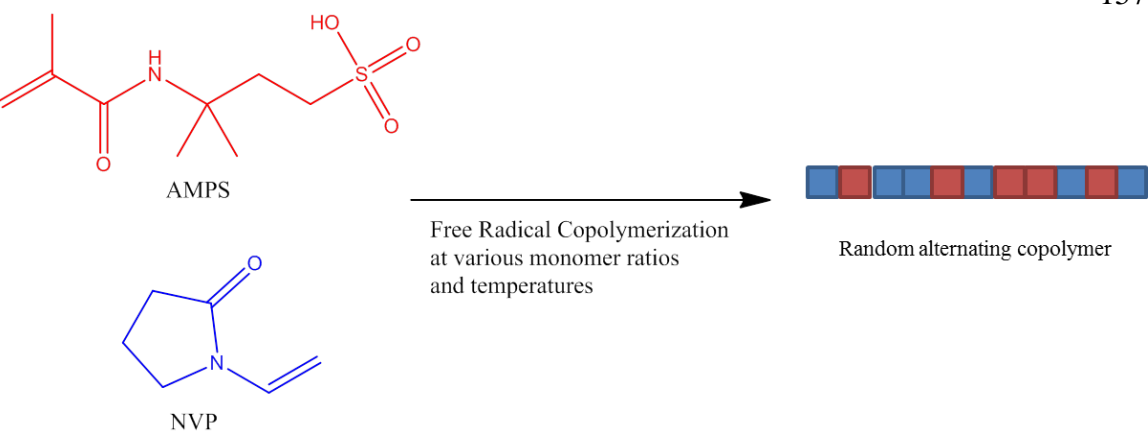


Figure 7.1. Monomers of interest for copolymerization including the acid site (red) and pyrrolidone functionality (blue)

An alternative approach would be to The PVP functionlized organosilane can be synthesized by 3-methacryloxypropyltrimethoxysilane will be reacted with NVP using AIBN as an initiator in a non-polar agent. Cyanomethyl methyl(phenyl)carbamodithioate can be as a chain transfer agent for a low PDI material, PSP. PSP can be co-condensed with tetraethylorthosilicate (TEOS) and 3-mercaptopropyl-trimethoxy-silane (MPTMS) around a template (Pluronic P123) to form an acid functionalized PVP PMO. (Figure 5) The success of the co-condensation of the novel PVP-silica hybrid can be monitored using solid state ¹³C CP/MAS NMR and ²⁹Si CP/MAS at the bridging siloxane bonds. Mesoporous order will be confirmed using x-ray diffraction. Materials will be tested at the same reaction conditions as those in this dissertation.

Figure 7.2. Synthesis approach for solid acid functionalized PVP PMOs for biomass conversion

7.2.2 Optimizing Tandem Glucose Isomerization and Fructose Dehydration

Tandem glucose isomerization and fructose dehydration has not been fully studied experimentally. Recent work by T. Swift, et al. 9 modeled glucose isomerization and fructose dehydration to HMF in a single catalyst/single pot and obtained intristic kinetic data for the bifunctional H-beta zeolite. An optimum HMF yield was modeled for a system with a Lewis acid to Brønsted acid ratio of about 0.3. Although this study was done in pure water, this same approach can be done for the Sn-PMOs in Chapter 6 for product optimization under mixed solvent conditions and packed-bed reactors. This could also elucidate solvent effects for glucose isomerization reactions which so far have been complicated. These same studies could be extended to hemicellulose, which accounts for about 25-35% of biomass, and has not been extensively studied as fructose dehydration. Hemicellulose is mainly composed of the pentose, xylose. The dehydration product of xylose is furfural, which may be converted to levulinic acid (LA). LA is a useful platform chemical for the production of fuels and chemicals. 10 Being able to process glucose

and xylose simultaneously would be a major step forward to the technoeconomic feasibility of bio-refineries.

7.2.3 Production of Higher Value Added Chemicals from HMF

In Chapter 3, the hydrogenation of HMF to DHMTHF was explored, however, it is also important to develop technologies that will efficiently convert HMF to other higher value products. Designing catalytic system that can be used in continuous operation in tandem with upstream or downstream catalysts would also be desirable. Understanding the oxidation of HMF to furandicarboxylic acid (FDCA) would be of potential interest. Gold on hydrotalcite and Au-Cu nanoparticles on titania have also been found to convert HMF to FDCA. 11, 12 Recent advances in controlled synthesis 3 of bimetallics could provide new insights into this oxidation chemistry and design of catalyst for use in tandem system.

7.3 References

- [1] M.H. Tucker, A.J. Crisci, B.N. Wigington, N. Phadke, R. Alamillo, J. Zhang, S.L. Scott, J.A. Dumesic, Acs Catalysis, 2 (2012) 1865-1876.
- [2] H. Erdemi, A. Bozkurt, European Polymer Journal, 40 (2004) 1925-1929.
- [3] A.K. Mishra, V.K. Patel, N.K. Vishwakarma, C.S. Biswas, M. Raula, A. Misra, T.K. Mandal, B. Ray, Macromolecules, 44 (2011) 2465-2473.
- [4] M. Tucker, in: Chemical and Biological Engineering, The University of Wisconsin-Madison, 2011, pp. 184.
- [5] Y.A. Aggour, European Polymer Journal, 36 (2000) 2231-2234.
- [6] B.L. Rivas, E. Martínez, E. Pereira, K.E. Geckeler Polymer International, 50 (2001) 456-462.
- [7] G. Masci, D. Bontempo, N. Tiso, M. Diociaiuti, L. Mannina, D. Capitani, V. Crescenzi, Macromolecules, 37 (2004) 4464-4473.
- [8] J. Brandrup, E.H. Immergut, E.A. Grulke, A. Abe, D.R. Bloch, in, John Wiley & Sons.
- [9] T.D. Swift, H. Nguyen, Z. Erdman, J.S. Kruger, V. Nikolakis, D.G. Vlachos, Journal of Catalysis, 333 (2016) 149-161.
- [10] D.M. Alonso, J.Q. Bond, J.A. Dumesic, Green Chemistry, 12 (2010) 1493-1513.
- [11] N.K. Gupta, S. Nishimura, A. Takagaki, K. Ebitani, Green Chemistry, 13 (2011) 824-827.
- [12] T. Pasini, M. Piccinini, M. Blosi, R. Bonelli, S. Albonetti, N. Dimitratos, J.A. Lopez-Sanchez, M. Sankar, Q. He, C.J. Kiely, Green Chemistry, 13 (2011) 2091-2099.
- [13] S.H. Hakim, C. Sener, A.C. Alba-Rubio, T.M. Gostanian, B.J. O'Neill, F.H. Ribeiro, J.T. Miller, J.A. Dumesic, Journal of Catalysis, 328 (2015) 75-90.